RICE UNIVERSITY

Two Stage Repair of Composite Craniofacial Defects with Antibiotic Releasing Porous Poly(methyl methacrylate) Space Maintainers and Bone Regeneration

by

Patrick Spicer

A THESIS SUBMITTED
IN PARTIAL FULFILLMENT OF THE
REQUIREMENTS FOR THE DEGREE

Doctor of Philosophy

APPROVED, THESIS COMMITTEE

Antonios G. Mikos, Chair
Professor, Bioengineering

George N. Bennett
Professor, Biochemistry and Cell Biology

K. Jane Grande-Allen
Associate Professor, Bioengineering

F. Kurtis Kasper
Faculty Fellow, Bioengineering

Mark E. Wong
Professor, Oral and Maxillofacial Surgery
University of Texas Health Science Center
at Houston

HOUSTON, TEXAS
December 2012

ABSTRACT

Two Stage Repair of Composite Craniofacial Defects with Antibiotic Releasing Porous Poly(methyl methacrylate) Space Maintainers and Bone Regeneration

by

Patrick Spicer

Craniofacial defects resulting from trauma and resection present many challenges to reconstruction due to the complex structure, combinations of tissues, and environment, with exposure to the oral, skin and nasal mucosal pathogens. Tissue engineering seeks to regenerate the tissues lost in these defects; however, the composite nature and proximity to colonizing bacteria remain difficult to overcome. Additionally, many tissue engineering approaches have further hurdles to overcome in the regulatory process to clinical translation. As such these studies investigated a two stage strategy employing an antibiotic-releasing porous polymethylmethacrylate space maintainer fabricated with materials currently part of products approved or cleared by the United States Food and Drug Administration, expediting the translation to the clinic. This porous space maintainer holds the bone defect open allowing soft tissue to heal around the defect. The space maintainer can then be removed and one regenerated in the defect. These studies investigated the individual components of this strategy. The porous space maintainer showed similar soft tissue healing and response to non-porous space maintainers in a rabbit composite tissue defect. The antibiotic-releasing space maintainers showed release of antibiotics from 1-5 weeks, which could be controlled by loading and fabrication

parameters. *In vivo*, space maintainers releasing a high dose of antibiotics for an extended period of time increased soft tissue healing over burst release space maintainers in an infected composite tissue defect model in a rabbit mandible. Finally, stabilization of bone defects and regeneration could be improved through scaffold structures and delivery of a bone forming growth factor. These studies illustrate the possibility of the two stage strategy for repair of composite tissue defects of the craniofacial complex.

Acknowledgments

First and foremost I would like to thank Dr. Mikos. He has mentored me for over 8 years as an undergraduate and a graduate student. I have learned countless lessons from him and I have grown as a researcher and as a person. None of the research in this thesis would be possible without his guidance and mentorship. Additionally, through laboratory environment he created I interacted with many people that helped me, taught me, and paved the way for my research, including Xinfeng (Charlie) Shi, Amit Mistry, Leda Klouda, Simon Young, Jim Kretlow, Diana Yoon, Manitha Nair, Ville Meretoja, Allan Henslee, Sean Piper, Brendan Watson, Lucas Kinard, Rebecca Dahlin, Sarita Shah, and Alex Tatara.

I was fortunate in my graduate school time to have multiple mentors. Another is Dr. Wong. He cultivated my clinical interests and aided in the development of several very important clinical collaborations with which I have benefited greatly. Additionally, Dr. Wong has taught me the joy of research and the excitement in translating an idea into clinical practice.

Dr. Kasper was an additional mentor to me as Co-director of the Mikos lab. He helped me hone my writing skills and encouraged me to step outside my comfort zone at conferences eventually leading to my appointment as the Tissue Engineering and Regenerative Medicine International Society Student and Young Investigator Meeting Chair for the 2011 North America meeting. This opportunity exposed me to many influential people in the field and was greatly appreciated. I am very thankful for Dr. Kasper's mentorship and friendship.

Additionally, my committee members, Dr. Jane Grande-Allen and Dr. Bennett provided me with expertise regarding study design and analysis for my thesis. Their guidance was crucial in the implementation of the research comprised in this thesis.

I was also fortunate to work with many collaborators at outside institutions and companies. Drs. Jansen, Both, Miller, Kontoyiannis, Kempen, Yaszemski, Murray, Mende, Yoo, Jackson, Ratcliffe, and Liu all helped me in my research through teaching of animal models, histology, bacterial culture, or product development.

The work in this thesis involved many animal studies, which would not have been possible without the help from personnel of the various animal facilities. Drs. Jensen and Smith helped with the planning and implementation of many of the studies and led the care team for the animals. Michele Pratt, Kelly Campbell, Peg Bek, Sarah Frazier, Amanda Sutton, Robin Work and Reinaldo Mendez helped tremendously through administrative support and animal care.

I would also like to thank the Armed Forces Institute of Medicine for not only funding much of this research but also providing valuable mentorship and development programs in which the students could participate. Additionally, I would like to thank Robert and Janice McNair and their foundation for their generous support of me in the Baylor College of Medicine Medical Scientist Training Program.

The Baylor College of Medicine Medical Scientist Training Program has also supported me through this thesis work, especially Drs. Plon, Brown and Wehrens as my MD/PhD advisors and Kathy Crawford, Vanessa Hatfield and Krista Defalco for

supporting me and providing immense help in navigating the path of the MD/PhD program.

I would also like to thank my family, my Mom and Dad and brother and sister, Nicolas and Amanda. My parents have always taught me to love school and learning and I can still say that I do love it. Nicolas has inspired me with his devout work ethic and desire to understand. Finally, Amanda was my initial inspiration to decide to go to medical school and I am constantly inspired by her devotion to and care of her patients.

Finally, I would like to thank Kristin. She has always supported me in my studies and I could not have done it without her. She is the best friend, wife and mother to our daughter, Ellis, I could ever ask for.

Contents

List of Figures

List of Tables

List of Equations

Abbreviations

ACS	Acellular collagen sponge
ANOVA	Analysis of variance
ASC	Adipose-derived stem cell
β-TCP	Beta-tricalcium phosphate
bmMNC	Bone marrow mononuclear cell
BMP	Bone morphogenetic protein
BMP-2	Bone morphogenetic protein-2
BMP-4	Bone morphogenetic protein-4
BSA	Bovine serum albumin
BUN	Blood urea nitrogen
CFU	Colony forming unit
CMC	Carboxymethylcellulose
CT	Computed Tomography
ddH_2O	Distilled deionized water
DISO	Distraction-assisted *in situ* osteogenesis
FDA	United States Food and Drug Administration
GMP	Gelatin microparticle
HPLC	High performance liquid chromatography
IM	Intramedullary
MIC	Minimum inhibitory concentration
MicroCT	Microcomputed tomography

MMA	Methylmethacrylate
MSC	Mesenchymal stem cell
OPF	Oligo(poly(ethylene glycol) fumarate)
PBS	Phosphate buffered saline
PCL	Poly(caprolactone)
PLGA	Poly(lactic-*co*-glycolic acid)
PMMA	Polymethylmethacrylate
PPF	Poly(propylene fumarate)
PRP	Platelet-rich plasma
PTFE	Poly(tetrafluoroethylene)
PVA	Poly(vinyl alcohol)
rhBMP-2	Recombinant human bone morphogenetic protein-2
rhBMP-7	Recombinant human bone morphogenetic protein-7
ROI	Region of interest
SEM	Scanning electron micrograph
TE	Tissue engineering
TGF-β	Transforming growth factor-beta
VOI	Volume of interest

Chapter 1

Introduction[‡]

The work described in this thesis covers biomaterial-based approaches for craniofacial reconstruction. As such, the following chapter will outline the clinical problems in craniofacial reconstruction, the current treatment modalities, advances in area and finally, some of the hurdles and pitfalls many of these advances have faced preempting their translation into clinical practice. This information will provide a basis for the work described and show relevance toward clinical translation.

[‡] This chapter will be published as a portion of Spicer PP, Young S, Kasper FK, Athanasiou KA, Mikos AG, Wong ME. Tissue Engineering in Oral and Maxillofacial Surgery. In Lanza R, Langer R, Vacanti J (Eds.), *Principles of Tissue Engineering.* Amsterdam: Elsevier (*in press*).

1.1. Craniofacial Reconstruction

The desire to reconstruct portions of the craniofacial complex have existed for centuries, and with the technological developments of the late 19th century, craniofacial reconstruction began to form a significant library of operative and technological repairs to craniofacial defects. This began in 1889, with C. Martin, who developed an artificial jaw to restore speech and mastication to a patient. This technology was refined through the following decades with better materials and constructions [1].

1.1.1. Craniofacial Anatomy

Virtually all tissue types of ectodermal, mesodermal and endodermal origin are candidates for tissue engineering strategies and are present in the oral and maxillofacial region. However, certain structures are more commonly impacted by disease, trauma and developmental failures and constitute the focus of our discussion, though the reconstructive methods described can be applied to more rare conditions.

A special concern in oral and maxillofacial reconstruction is the potential exposure of grafted tissue to the external environment. Constructs used to restore defects involving the jaws, orbits, nose and ears are potentially in direct contact with the mouth, sinuses (maxillary, ethmoidal and frontal), nasal passages and external environment. These areas are characterized by high moisture content, significant bacterial populations, and functional loads imposed by physiological activities such as chewing. If biological (i.e. tissue engineered) constructs are to survive under these conditions, modifications to account for the dilutional effects of moisture, presence of infective organisms, and mechanical loads, must be provided by the engineered tissue. For example, when *in vivo*

polymerization of materials is intended, the presence of fluid must be considered. Alternatively, pre-formed constructs can be used. Colonization of constructs with a mixed population of aerobic and anerobic bacteria is expected with reconstructions involving oral, nasal and sinus-related structures. Porous constructs, capable of harboring potentially pathological organisms might be modified to reduce either bacterial attachment or replication until lining tissue develops over the implant forming a barrier to the external environment. In addition to contaminated wound sites, tissue constructs may be exposed to complicated mechanical loads before anisotropy is restored with the regeneration of biological tissue. Both the mandible and temporomandibular joints are subject to a combination of compressive, shear and tensile loads depending on the type and degree of function [2, 3].

Another special feature of the maxillofacial region is the number of tissue types within a relatively small region. As a result of this proximity, traumatic, pathological and developmental events often lead to the creation of composite defects requiring reconstruction of multiple tissue types. This results in a special challenge not only to engineer composite tissues, but also to attach the various constructs to each other in their normal anatomical relationship.

Facial symmetry is an important consideration in oral and maxillofacial reconstruction. Since most structures are paired or contiguous (e.g. the orbits, zygomas, left and right maxillae and mandible), accurate reproduction of the external form is an important aspect to preserve facial esthetics (Figure 1.1). The paucity of overlying soft tissue as camouflage contributes to the exacting nature of oral and maxillofacial reconstruction and these requirements impose upon tissue engineering methods the ability

to compose and maintain accurate morphology. The advent of new three-dimensional imaging techniques with the capacity to produce stereolithographic skeletal models (Figure 1.2) that mirror both the normal anatomy and defect is a valuable adjunctive tool. These models assist in the fabrication of scaffolds to support the reconstruction of missing tissue.

1.1.2. Craniofacial Trauma and Resection

Common pathological entities include both benign and malignant cystic and neoplastic processes affecting the upper (maxilla) and lower (mandible) jaws as well as degenerative conditions involving the mandibular articulation (temporomandibular joints). These diseases, or the subsequent removal of pathologically involved tissue, can produce continuity defects of the jaws requiring the replacement of bone, cartilage and lining epithelium (Figure 1.3 and Figure 1.4). Since many of these conditions are frequently silent and the dimensions of the structures involved relatively small, their initial presentation is usually associated with significant tissue involvement. In addition to disease, non-physiological loading of bone can also produce loss of skeletal tissue affecting the jaws and joints. Edentulous bone loss as in Figure 1.5 involves the resorption of the alveolar processes of the jaws (i.e. that portion of the jaw bone surrounding the tooth roots) following tooth removal. This phenomenon is believed to be the result of direct loading of bone during mastication and the loss of physiological maintenance forces transmitted by the teeth. Over time, the loss of bone produces severely atrophied alveolar ridges, posing significant challenges to prosthetic reconstruction of the dentition and a predisposition to pathological fracture of the mandible [4].

Maxillofacial trauma constitutes another group of conditions providing opportunities for tissue engineering reconstruction. Whereas most forms of blunt trauma result in fractures where tissue loss is minimal, penetrating injuries produced by high velocity missiles and projectiles often create significant loss of bone and overlying soft tissue (Figure 1.6). Finally, consideration should be given to the various forms of congenital facial clefts that commonly affect the oral and maxillofacial region. In a limited form, failure of the maxillary processes to fuse unilaterally or bilaterally produces alveolar clefts (Figure 1.7 and Figure 1.8). When the upper lip, maxilla and palate are involved, a constellation of deformities associated with unilateral or bilateral cleft lip and palate patients is present.

In the reconstruction of anatomical defects, the causative events must be taken into account to ensure long-term success. Defects produced by traumatic, developmental and pathological conditions are associated with a defined end-point. Assuming that pathology has been completely eradicated or further traumatic insults do not occur, defects produced by these mechanisms can be fully characterized with respect to size and missing tissue types. In contrast, tissue loss as a result of parafunctional habits, non-physiological loading patterns and immunologically mediated degeneration often continue following reconstruction. This set of circumstances will adversely affect any biological constructs produced by tissue engineering techniques and impose an important limitation on the clinical application of their usage. Before biological, rather than alloplastic materials can be employed, correction of the underlying etiology is of paramount importance.

1.1.3. Current Treatment Modalities

There are several methods used for oral and maxillofacial reconstruction and the selection of a particular modality takes into account a number of important issues. Major factors that guide this process include the presence (or absence) of associated soft tissue, the vascularity and vascular pattern present, a multi-dimensional characterization of the defect size, the types of missing tissue, availability of tissue for transfer, and both patient and surgeon preference. Most reconstructive techniques can be categorized into four categories:

- Soft tissue pedicled flaps
- Non-vascularized soft and hard tissue grafts (the graft establishes in a delayed fashion, a vascular network following implantation, relying upon tissue diffusion to preserve the viability of the transplant)
- Soft and hard tissue vascularized grafts (the graft is immediately perfused through an existing arterial-venous system)
- Alloplastic reconstructions with prosthetic appliances

On occasion, composite techniques can be used, such as the staged reconstruction of a defect where soft tissue is first added to a defect site followed by bone at a later time.

1.2. Mandibular Defects

Reconstruction of the lower jaw is indicated following removal of tissue during surgical excision of a pathological lesion or following loss of tissue from a traumatic

injury. When malignant disease is present, not only is more radical removal of tissue required, but post-operative radiation therapy produces lasting compromise to both the cellularity and vascularity of the remaining tissue. Blast effects from missile injuries can also produce significant composite injuries with loss of bone soft tissue, and diminished vascularity of the tissue bed. Two techniques are commonly employed for the reconstruction of mandibular defects. Vascularized grafts are indicated when the vascularity of the tissue bed is compromised by radiation or excessive scarring. They are also valuable when there is a requirement to replace both hard and soft tissue at the same time [5]. Hard and soft tissue defects can also be reconstructed using non-vascularized grafts, but their success relies upon an adequately vascularized tissue bed, which can be compromised in irradiated or traumatically injured tissue, to support the survival of transplanted cells before a new supply is established[6].

As composite structures, vascularized grafts contain either soft tissue alone (muscle, subcutaneous tissue with or without epithelium) or include hard and soft tissue components (bone and soft tissue). Since the vascular supply to bone is contained within a peri-osseous cuff of muscle and fibrous tissue, it is not possible to transplant only bone. The additional tissue transferred into the site of a bony defect often produces a bulky graft. While this can be easily excised once a new vascular network is established, a second procedure performed several months after the initial transplantation is required. Another potential limitation to the use of vascularized bone grafts for the reconstruction of mandibular defects is the amount of bone available, since the dimensions of the graft are determined by the morphology of the donor site and not the size of the defect. Special techniques such as osteotomizing the graft and folding it upon itself have been described,

but this can compromise the blood supply to the graft. Vascularized grafts are harvested from a limited number of anatomical sites characterized by a dominant arterial supply – venous drainage system. In addition, the en bloc harvesting of the graft must not compromise either the function of the donor site or the vascular and neural supply of structures distal to the harvest. Commonly used donor sites that meet these requirements include the fibula, ilium, scapula and distal radius. Vascularized grafts transplanted to mandibular defects are anastomosed to patent vessels adjacent to the mandible, such as the facial, lingual or superior thyroid arteries and veins. This reconstructive approach is highly technique-sensitive and while experienced microvascular surgeons achieve successful outcomes in over 90% of cases, less experienced surgeons or patients with underlying vascular disease (e.g. diabetes) enjoy less success.

Mandibular defects can also be reconstructed using non-vascularized transplantations of autologous bone from various sites. Successful bone grafts rely upon adequate cellularity and a sufficiently cellular and vascular recipient bed. When the soft tissue bed is deficient or lacks a decent blood supply, addition of well-vascularized soft tissue is achieved by the rotation of a muscle flap (with or without skin) into the mandibular defect. The pectoralis major, latissimus dorsi and deltopectoral flaps have all been described for this purpose. The bony reconstruction is delayed for a period of three to six months until the soft tissue flap has healed. In patients whose soft tissue is adequate, but avascular as a result of radiation therapy, hyperbaric oxygen therapy can improve the quality of the vascular supply in a course of treatments lasting between four to six weeks where repeated exposures to pressurized room air promote tissue angiogenesis. This process adds both time and considerable expense to the reconstructive

process, but has been shown to be effective in improving the quality of the recipient bed. Once the soft tissue in a mandibular defect has been optimized with respect to quantity, cellularity and vascularity, autologous bone is transferred from a donor site and molded to fit the dimensions of the defect. The bone graft can be retained with screws fixed to a rigid bone plate, or held in position with the aid of cribs fashioned either from processed allogeneic bone or alloplastic materials. Depending upon the size of the defect, bone can be harvested from the anterior ilium (suitable for defects up to 4 cm in length), the posterior ilium (defects up to 8 cm in length), and the tibia or mandibular symphysis and rami (defects of less than 2 cm in length). Non-vascularized grafts, especially those combined with allogeneic bone are susceptible to infectionespecially following exposure to the intra-oral environment, with a frequency of 43% in one case series [7]. When a non-vascularized graft is colonized by organisms, infection often ensues and the graft fails to survive or integrate with the host bone. Aside from the potential for infection, non-vascularized grafts are less technique sensitive, allow “complete” reconstruction of a defect by customizing the volume of bone harvested, and are associated with less donor site morbidity [8].

1.3. Maxillary Defects

Defects of the upper jaw pose difficult reconstructive challenges from several perspectives, but must be undertaken to preserve speech, prevent the escape of food and fluids during eating, and maintain esthetics. Unlike the mandible which is related to the oral cavity alone, the maxilla is bounded both inferiorly by the mouth and superiorly by the nasal cavity and maxillary sinuses. Even when present, the thin lining epithelium does

not provide a sufficiently cellular or vascular bed to support the transplantation of sufficient quantities of non-vascularized bone and the potential for exposure of the graft to oral and nasal environments is high. Post-operative or post-traumatic scarring reduces the tissue envelope even more, further complicating reconstructive efforts. Staged reconstructions have been described involving the initial transfer of vascularized soft tissue with a pedicled flap, such as the temporalis muscle or temporo-parietal flap, followed by the addition of bone several months later [8]. As an alternative, vascularized flaps have been used because of their ability to transfer both hard and soft tissue at the same time [9]. However, the accompanying soft tissue and vascular pedicle may not be accommodated by the smaller dimensions of a maxillary defect and this has limited their use to hemi- or total maxillary reconstructions. The simultaneous transfer of a large bulk of overlying soft tissue also results in a post-operative recovery period of several months where the flap can prevent mouth closure and compromise eating.

As a result of these challenges, prosthetic appliances have become the most commonly used method to reconstruct maxillary defects. These devices incorporate teeth and a fitted base to separate the mouth from the superior defect [10]. Excellent restoration of both esthetics and function can be achieved, but the fact that they are not permanently fixed in place and in fact, require daily removal and cleaning, reduces their acceptability by patients. In addition, adjustments are required periodically to account for remodeling of the underlying tissue bed.

The reconstruction of maxillary alveolar clefts is one exception to the use of prosthetic appliances as a primary reconstruction technique, even though they can be used very effectively to restore missing teeth in the cleft site or obturate an oral-nasal

communication. When teeth are present in a cleft site, provision of bone is essential for eruption and support [11]. Alveolar grafting is therefore timed according to the presence and stage of development of adjacent teeth and is usually performed between the ages of eight and eleven years. The procedure involves the development of soft tissue flaps to isolate the mouth from the nasal cavity and placing autogenous bone between the cleft segments to restore maxillary continuity. Loss of the graft from infection, insufficient vascularity or lack of functional stimulus is not an infrequent occurrence and opportunities for tissue engineering alternatives exist. This would be especially true if new interventions minimized the extent of surgery, since post-surgical scarring has been associated with restricted growth and development of the maxilla.

1.4. Advances in Tissue Engineering and Regenerative Medicine in Craniofacial Reconstruction

Driven by the limited supply and inherent shortcomings of various autogenous, allogeneic, and prosthetic materials currently used for the reconstruction of oral and maxillofacial tissues, the potential for tissue engineered biomaterials as alternatives is under serious investigation with the hope that significantly improved therapies will result.

While a diverse number of strategies are presently under development, the fundamental tenets of tissue engineering (TE) remain the same. These include consideration of the biological and mechanical properties of the scaffold material and its interactions with relevant bioactive molecules and cell populations.

Although multiple tissue types exist in the oral and maxillofacial region, TE research in this field has focused primarily on the regeneration of single tissues: the bony craniofacial skeleton, lining epithelium, the cartilages of the temporomandibular joint, auricle, and nose, and the teeth and surrounding periodontal tissue.

1.4.1. Bone Applications

An ideal biodegradable TE bone construct should combine the biocompatibility and osteoinductive potential of autologous bone, with the availability and structural characteristics of allogeneic bone. Additional scaffold design considerations include porosity, pore interconnectivity, surface chemistry, and the ability to reproduce complex three-dimensional defects.

Scaffolds are responsible for a construct's initial mechanical integrity and provide surface area for cell attachment. Several biocompatible scaffold materials are currently used in oral and maxillofacial surgery, including naturally derived materials like collagen, gelatin, or hyaluronic acid, synthetic polymers like poly(lactic acid) and poly(glycolic acid) and ceramics like calcium phosphate granules, blocks and cements[12]. In addition to those materials clinically used, several materials have been tested using *in vivo* models for craniofacial bone, including alginate, chitosan, poly(propylene fumarate), oligo(poly(ethylene glycol)-co-fumarate), poly(caprolactone), and polyurethanes[12]. These materials are typically processed as porous structures or hydrogels that guide the morphology of regenerated tissue, allow for tissue in-growth, and control the release of bioactive molecules such as growth factors or nucleic acids.

Other approaches to tissue engineering use novel biomaterials capable of implantation through minimally invasive surgery. This can be achieved via *in situ* crosslinking or polymerization via chemical reactions initiated by mixing chemicals immediately before injection, transcutaneous photopolymerization or thermogelation[13-16]. Delivery of osteogenic factors or cells has been demonstrated with these techniques; however, parameters such as cell viability must be weighed against gel stiffness with such materials.

Growth factors act as mediators of cellular growth and differentiation during tissue regeneration and play an important role in extracellular matrix synthesis. Utilized as recombinant proteins in TE strategies, growth factors require a local population of target cells capable of effecting the desired response [17]. This constituency of cells may be naturally present at the wound site or added to the scaffold at the time of fabrication [18] prior to implantation.

Factors that have been used for the regeneration of *in vivo* TE craniofacial bone include the bone morphogenetic proteins (BMPs) [18, 19], transforming growth factor-beta (TGF-β) [20], fibroblast growth factors (FGFs) [21], insulin-like growth factors (IGFs) [22], and platelet-derived growth factor (PDGF) [23]. The bulk of experience concerning the use of growth factors for bone repair has involved BMPs [24] and this popularity has been extended into clinical investigations using recombinant human BMP-2 (rhBMP-2) for alveolar ridge augmentation [25], maxillary sinus floor augmentation [26], mandibular reconstruction following tumor resection [27], and distraction-assisted alveolar cleft repair [28]. A review by Herford et al., covers several cases of BMPs used in mandibular reconstruction secondary to tumor excision, trauma and infection,

highlighting the versatility of growth factor mediated bone regeneration [29]. However, the review notes a relatively small number, 37, of documented clinical cases in the literature with a significant failure rate of 13.5%. This highlights the need for further investigation of these growth factor based technologies in the craniofacial complex.

BMP-2 has found some definitive success in other aspects of oral and maxillofacial surgery, such as dental implants and sinus floor augmentation Jung et al [25]. examined the effect of combining recombinant human BMP-2 with a xenogeneic bone substitute in order to improve membrane-guided bone regeneration therapy of osseous defects in areas of dental implant placement. Although there was not a statistically significant difference in percentage of newly formed bone at the rhBMP-2 treated site versus the control site at 6 months, a larger fraction of mature lamellar bone (76% vs. 56%) was present in the experimental sites, as well as increased graft to bone contact (57% vs. 29.5%). In addition, Boyne et al. [26] completed a phase II randomized controlled study investigating the safety and efficacy of rhBMP-2 combined with an absorbable collagen sponge (ACS) versus bone graft for staged maxillary sinus floor augmentation. It was concluded that rhBMP-2 had a similar safety profile to bone graft with the added benefit of lacking donor site morbidity. In addition, the rhBMP-2/ACS treatment induced similar amounts of bone to the bone graft group, allowing for the placement and long-term functional loading of dental implants in approximately 75-80% of the patients treated.

The clinical use of rhBMP-2 to regenerate much larger bone defects has also been reported in the literature. Carstens et al. [28] described the use of "distraction-assisted in situ osteogenesis" (DISO) to treat a severe facial cleft, in which rhBMP-2/ACS

implantation was combined with distraction osteogenesis to create the patient's ramus and condyle as part of the surgical reconstruction. A similarly spectacular application of rhBMP-7 has been described by Warnke et al. [30] for the reconstruction of a 7 cm mandibular continuity defect in a patient who had received ablative tumor surgery and subsequent radiation treatment. A bone-muscle-flap prefabrication technique was utilized, in which computed tomography and computer aided design techniques were used to fabricate a custom titanium mesh cage replicating the contours of the missing mandible. Within this cage, a combination of xenogeneic bone mineral blocks coated with rhBMP-7 and autologous bone marrow were placed, prior to implantation of the entire construct within the latissimus dorsi muscle of the patient. Following seven weeks of implantation within this "*in vivo* bioreactor", the viable mandibular replacement was harvested from the patient along with part of the muscle containing a major artery and vein which were subsequently anastomosed with vessels at the recipient site using microsurgical techniques. Four weeks after this transplantation surgery, the patient was able to undertake a small amount of mastication and enjoy more solid foods. In a similar case of prevascularization, Mesimaki et al. implanted a titanium mesh containing β-TCP granules seeded with ASCs cultured in rhBMP-2 into the rectus abdominus muscle of a patient who had undergone hemimaxillectomy[31]. The mesh was harvested with a vascular pedicle 8 months later and anastomosed to vasculature in the face replacing the resected bone. This patient went on to receive dental implants for complete dental rehabilitation.

A significant drawback to growth factor strategies in tissue engineering is the shortage of naturally derived factors isolated from biological tissue. This deficiency has

been addressed with the development of techniques to produce biologically active proteins using recombinant engineering techniques. However, the use of recombinant proteins is not without concern [24]. Compared to animal models, bone regeneration in humans does not appear to be as robust. In order to overcome this species recalcitrance, administration of factors in excess of naturally occurring concentrations appears to be necessary. The augmented administration of exogenous factors may potentially stimulate harmful biological effects such as malignant transformation of cells and also prove to be too expensive when compared to alternative techniques for tissue regeneration. In an effort to mitigate cost, potential for harmful stimulation or disease transmission, autologous supplies of growth factors have been investigated, primarily through the use of platelet rich plasma (PRP). As a natural source of growth factors, PRP has been applied to craniofacial bone tissue engineering scaffolds, but with limited success, illustrating the inherent difference in the effect of therapies across species[32, 33].

Attempts to address the shortcomings of recombinant protein-based strategies have spurred investigation into the use of gene delivery for tissue engineering. By delivering the gene for the expression of a protein with specific effects on a target cell population, successfully transfected cells will elaborate the protein constitutively. This results in higher and more constant levels of protein production [34]. However, while both viral [35, 36] and non-viral [37] gene delivery vectors have been utilized for bone regeneration in cranial defect animal models, compromises must be made with each. Adenoviral constructs have commonly been used as viral vectors to transfect craniofacial tissues and have the advantage of efficiently transfecting both replicating and quiescent cells [38]. In addition, adenoviruses are easily manipulated, can be produced in high

titers, and large amounts of genetic information can be inserted into them. However, concerns related to viral vectors include *in vivo* homologous recombination and the possibility of an immune response from the expression of viral antigens on the surfaces of transfected cells. These concerns have led to the development of non-viral vector agents [34].

While numerous non-viral gene delivery systems exist, a common problem is their low *in vivo* transfer efficiency [38]. Nonetheless, such systems are able to deliver much larger genes with minimal immunogenicity. One promising modality of non-viral gene delivery for craniofacial applications is the use of cationic liposomes which have been used to regenerate cranial bone defects in rabbits by delivering BMP-2 plasmid cDNA [39]. The low transfection efficiency of uncondensed, naked plasmid DNA has also been addressed by the use of the cationic macromer poly(ethylene imine), which has been used to condense BMP-4 plasmid DNA and deliver it in a sustained and localized manner from poly(lactic-co-glycolic acid) scaffolds within critical size cranial defects [37].

Gene transfection can take place directly within the defect site by releasing the delivery vector *in vivo* from the TE scaffold [35, 36]. Indirect delivery methods have also been described utilizing a target cell population harvested from the patient, performing *in vitro* transfection of the cells, and then re-implanting the transfected cells into the defect along with the TE scaffold material [40]. While the direct technique may be simpler, it has a lower transfection efficiency and targets cells in a non-specific manner [24]. The indirect *ex vivo* approach on the other hand, requires additional harvesting and culturing procedures, but avoids the risks associated with placing viral vectors directly into the

patient and disturbing the host genome. *Ex vivo* transfected cells are not immunologically privileged and may still express viral antigens on their surface which can lead to a host response following implantation.

As a corollary to gold standard approaches where bone grafts and flaps include the donor site cells, some TE approaches to craniofacial reconstruction employ cell-seeded scaffolds as implants. These have potential benefits for regenerating tissues in large defects or those with compromised healing capacity, such as those affected by radiation therapy [6]. The majority of cell-seeded scaffolds have investigated mesenchymal stem cells (MSCs) or adipose derived stem cells (ASCs). Reviews have covered some of the work in these areas looking at various stem cell sources, delivery and other parameters such as *in vitro* expansion and differentiation[6, 41]. To highlight a few studies, MSCs were applied to ceramic and polymer scaffolds with and without PRP in both cranial and alveolar defects of rats and minipigs, respectively[32, 33]. In both studies, the addition of MSCs enhanced bone regeneration over all other groups irrespective of PRP presence. In another study, autologous, culture expanded MSCs were utilized in combination with alginate hydrogels for the treatment of large cranial bone defects in sheep [42]. Finally, pre-differentiated ASCs were applied to rabbit cranial defects on gelatin scaffolds showing enhanced bone regeneration within the defect[43]. However, in another rabbit cranial defect study, rhBMP-2 on collagen regenerated greater amounts of bone compared to ASCs or pre-differentiated ASCs, indicating that although cell delivery for bone regeneration in the craniofacial complex shows promise, issues of cell sourcing, purification and processing need to be investigated further[44].

Aside from the biological components of tissue engineering constructs, scaffold properties are also extremely important to the overall success of any particular strategy. A common misconception is that bone TE scaffolds for craniofacial applications do not require substantial strength since the craniofacial skeleton is not subjected to heavy loading. However, *in vivo* studies demonstrate that many craniofacial bones undergo levels of strain similar to that experienced by the appendicular skeleton [45], substantiating the need for mechanical strength of potential bone TE scaffolds. Ideal scaffold design must therefore reconcile the need for high porosity and interconnectivity which promotes tissue in-growth and scaffold degradability, with a requirement for mechanical strength. Computational methods for designing and fabricating scaffold architectures to optimize both pore interconnectivity and load bearing characteristics have been performed [46], and a proof of concept study has illustrated the effectiveness of scaffold design in fabricating a mandibular condyle for a minipig[47].

The surface characteristics of bone tissue engineering scaffolds also determine their ability to regenerate tissue in the wound healing environment. Surface chemistry has a significant effect on the interactions between the cell populations present in the defect and the biomaterial. Hydrophilic synthetic polymers such as oligo(poly(ethylene glycol) fumarate) (OPF) have been shown to impede bone healing in extraction sockets as compared to the hydrophobic polymer poly(propylene fumarate), based on the OPF macromer's prevention of protein adsorption and hence cell adhesion [48]. Interestingly, the resistance of OPF hydrogels to generalized cell adhesion has been used to advantage in the fabrication of biomimetic scaffolds, which are able to selectively encourage the migration of osteoblasts *in vitro* through the addition of specific binding peptides to their

surfaces such as osteopontin-derived peptide [49]. In addition to surface chemistry, surface topography can impact healing. In a series of studies, porous materials in the mandibles of New Zealand White rabbits were shown to enhance the healing of the overlying mucosal surface in a composite tissue defect model [50-52]. However, contrary to traditional tissue engineering materials with high porosity led to an increased inflammatory response not seen with lower porosity materials [50]. Two of these studies, investigated porous poly(methyl methacrylate) (PMMA), a material currently part of many Food and Drug Administration (FDA) cleared products. By creating porous PMMA and enhancing soft tissue interaction with the implant, these materials show promise for rapid translation to clinical use in a staged approach, whereby the implants serves to temporarily maintain the bone space during soft tissue regeneration and is removed for the definitive therapy.

1.4.2. Oral Mucosa Applications

Oral mucosa regeneration has followed many of the strategies of skin tissue engineering, in that cultured epithelial sheets showed inadequate results due to fragility, contractility and failure due to lack of underlying supporting tissue. Thus many approaches have considered the use of thick cultured grafts containing single or multiple cell types. An extensive review by Moharamzadeh et al. covers scaffold materials, cell sources and culture medium [53]. Many of the same materials have been investigated for oral mucosal engineering as in bone and cartilage such as collagen, fibrin, gelatin, PLGA, and PCL. Additionally, various cell sources have been used, primarily keratinocytes and fibroblasts either from oral or skin origins. Finally, growth factors like epidermal growth factor have been employed to promote proliferation. In one study, fibroblasts and

keratinocytes were cultured on a collagen composite scaffold [54]. The culture led not only to cell specific markers for a full thickness mucosa but structural components including a basement membrane and extracellular matrix. A similar study used gingival fibroblasts and keratinocytes harvested from patients on a clinically available collagen matrix, resulting in cell markers and tissue structures similar to mucosal tissue [55]. *In vivo*, mucosal grafts of collagen precultured with gingival fibroblasts and keratinocttes have maintained their phenotype as mucosal tissue after 60 days of implantation[56]. Finally, one group has shown translation of tissue engineered mucosal graft. Creating a mucosal graft *in vitro* using canine cells cultured on AlloDerm, the group translated this technique by first using human cells *in vitro* [57, 58]. Subsequently, in a 30 patient study comparing AlloDerm alone to AlloDerm precultured with autologous cells, the precultured grafts show enhanced wound healing with earlier vascularization and maturation of the submucosal layer at 28 days after grafting [59].

In addition to oral mucosa, composite grafts for muco-cutaneous junctions such as the lips. Peramo et al. presents a novel approach to creating these junctions, where oral mucosal cells and skin cells are cultured on AlloDerm *in vitro* with a separation barrier [60]. This barrier is lifted and the cells are allowed to migrate into the junction space and interact. The cell construct was then lifted to air-liquid interface for maturation of the construct and characterized for morphology and immunohistochemical staining for keratin content. Biochemical markers were consistent with spatial distribution in mucocutaneous tissues, illustrating the possibility of this strategy to be employed for tissue engineering lips.

1.4.3. Composite Tissue Applications

Success with the regeneration of single tissue types such as bone and cartilage has encouraged investigators to attempt the reconstruction of structures composed of multiple tissue types. Such anatomic structures may exist as composites of hard and soft tissues, which differ in their cellular composition and mechanical properties, yet perform as a single functional unit [61].

The temporomandibular joint condyle serves as an example of a maxillofacial composite structure consisting of articular cartilage and subchondral bone and provides an excellent opportunity for composite osteochondral tissue engineering. A study performed by Alhadlaq et al. [62], used adult bone marrow MSCs, expanded in culture and induced to differentiate into separate osteogenic and chondrogenic lineages *in vitro*. The resultant cells were then encapsulated in poly(ethylene glycol) based hydrogels and the cell-polymer solutions crosslinked in a mold which provided the correct stratified organization of the osteogenic and chondrogenic layers. Finally, the osteochondral constructs were implanted into the dorsum of immunodeficient mice for up to 8 weeks. Histological and immunohistological analysis revealed both structural and immunohistochemical differences between the osteogenic and chondrogenic layers, which served as a primitive proof of concept of the potential for composite tissue engineered constructs in the craniofacial region. In a similar study trying to regenerate tissue within an osteochondral defect, a gradient scaffold releasing BMP-2 on the osteogenic side of the scaffold and TGF-β1 on the chondrogenic side was fabricated[63]. This construct showed increased osteo- and chondrogenesis on the respective sides.

1.5. Tables and Figures

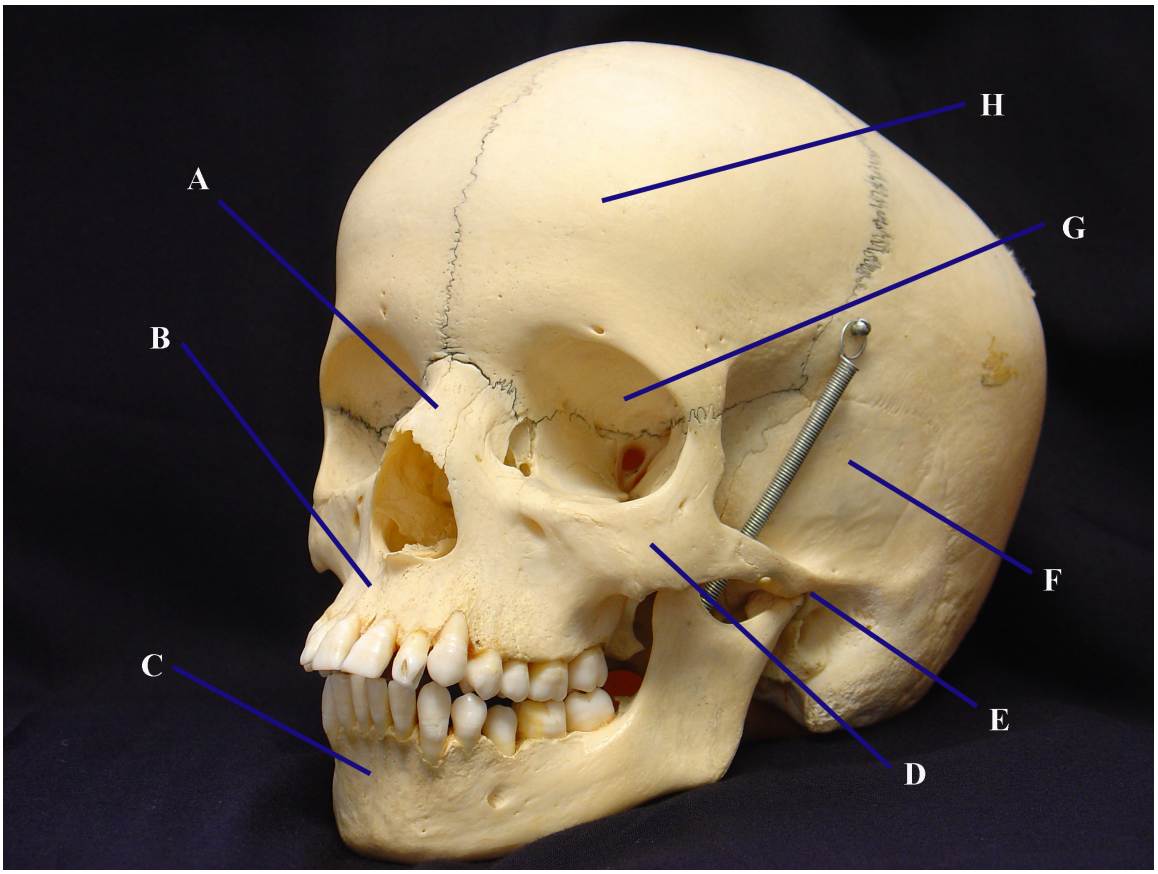

Figure 1.1. The human skull is a complex region composed of many bones. Several key structures include the: (A) nasal bone; (B) maxilla; (C) mandible; (D) zygomatic bone; (E) temporomandibular joint; (F) temporal bone; (G) orbital cavity; and (H) frontal bone.

Figure 1.2. Stereolithographic model of a patient demonstrating the extent of a maxillary hard tissue defect.

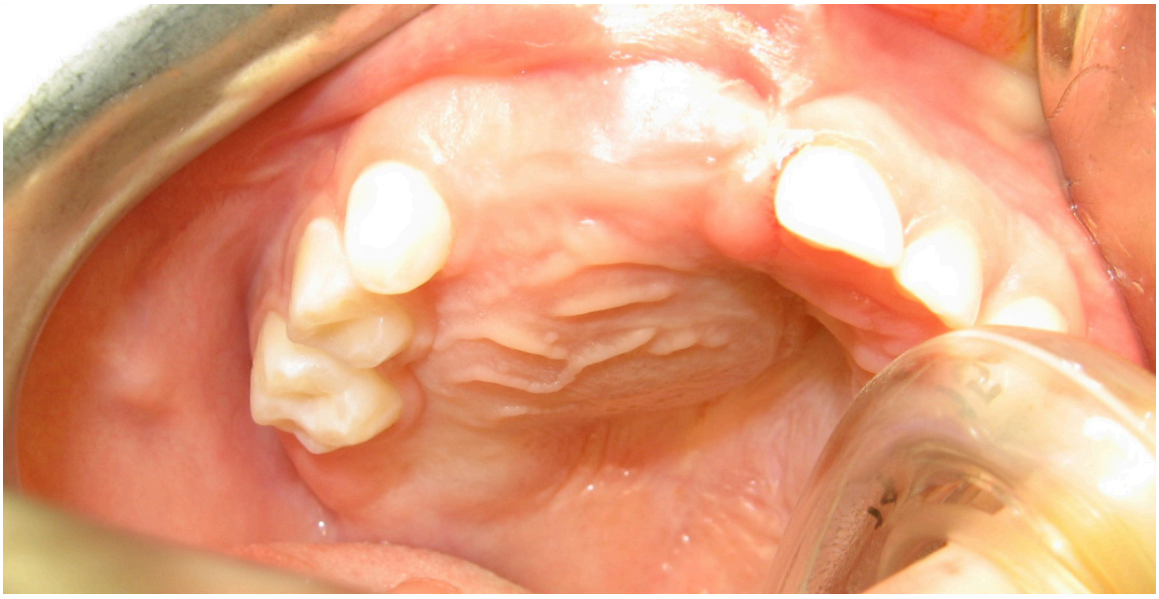

Figure 1.3. Intra-oral photo of a patient with a giant cell tumor of the maxilla, which presents as a swelling of the palate and erosion of the supporting bone resulting in the loss of adjacent teeth.

Figure 1.4. Coronal CT scan of the same patient in Figure 1.3 with a giant cell lesion of the right maxilla which has produced marked bone destruction and displacement of developing teeth. Sinusitis of the left maxillary sinus is an incidental finding.

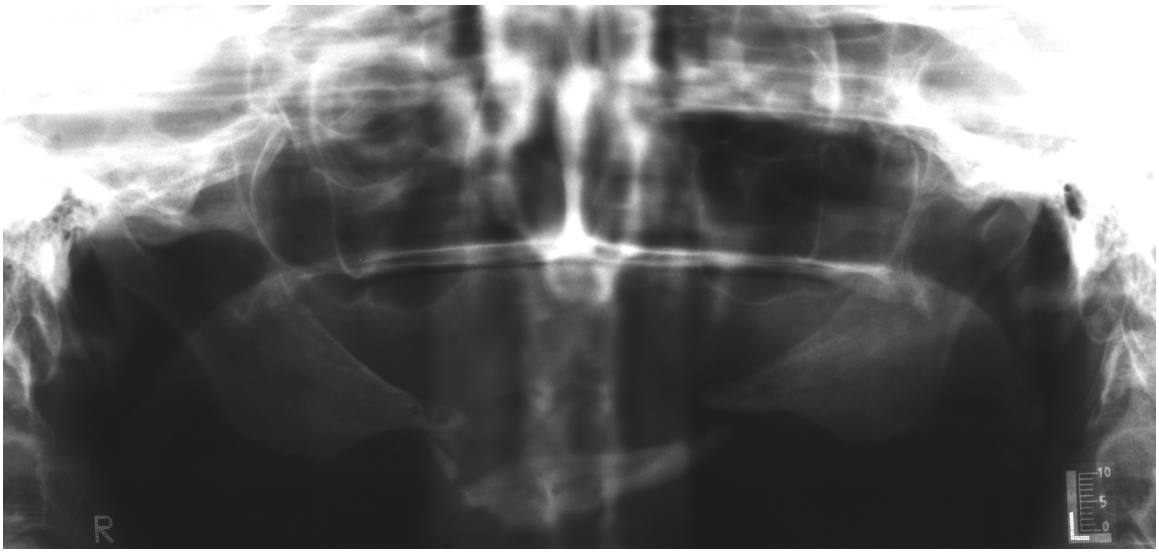

Figure 1.5. Panoramic radiograph of a patient with a fractured atrophic mandible (courtesy of Kamal Busaidy, D.D.S.).

Figure 1.6. 3-D reconstructed radiograph of a patient with a self-inflicted gunshot wound demonstrating the significant disruption and loss of maxillofacial skeletal structures.

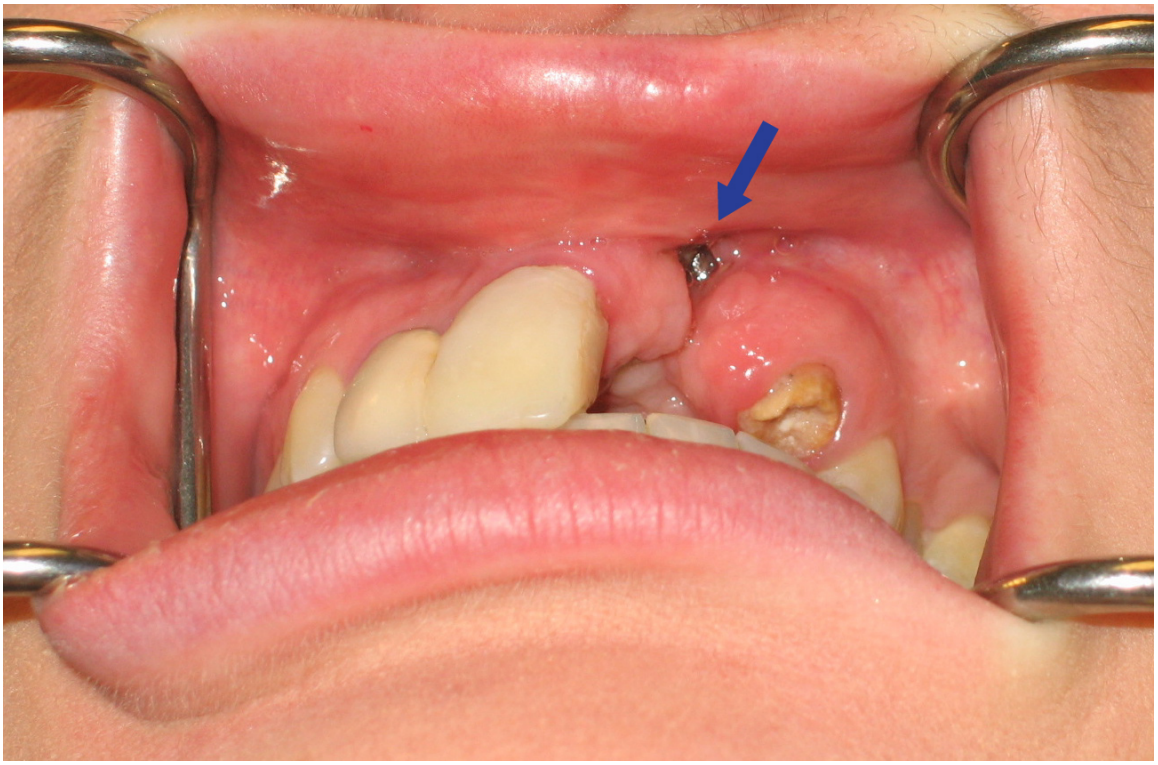

Figure 1.7. Intraoral view of a left maxillary alveolar cleft. An oro-nasal fistula is present at the superior-most aspect of the cleft (see arrow).

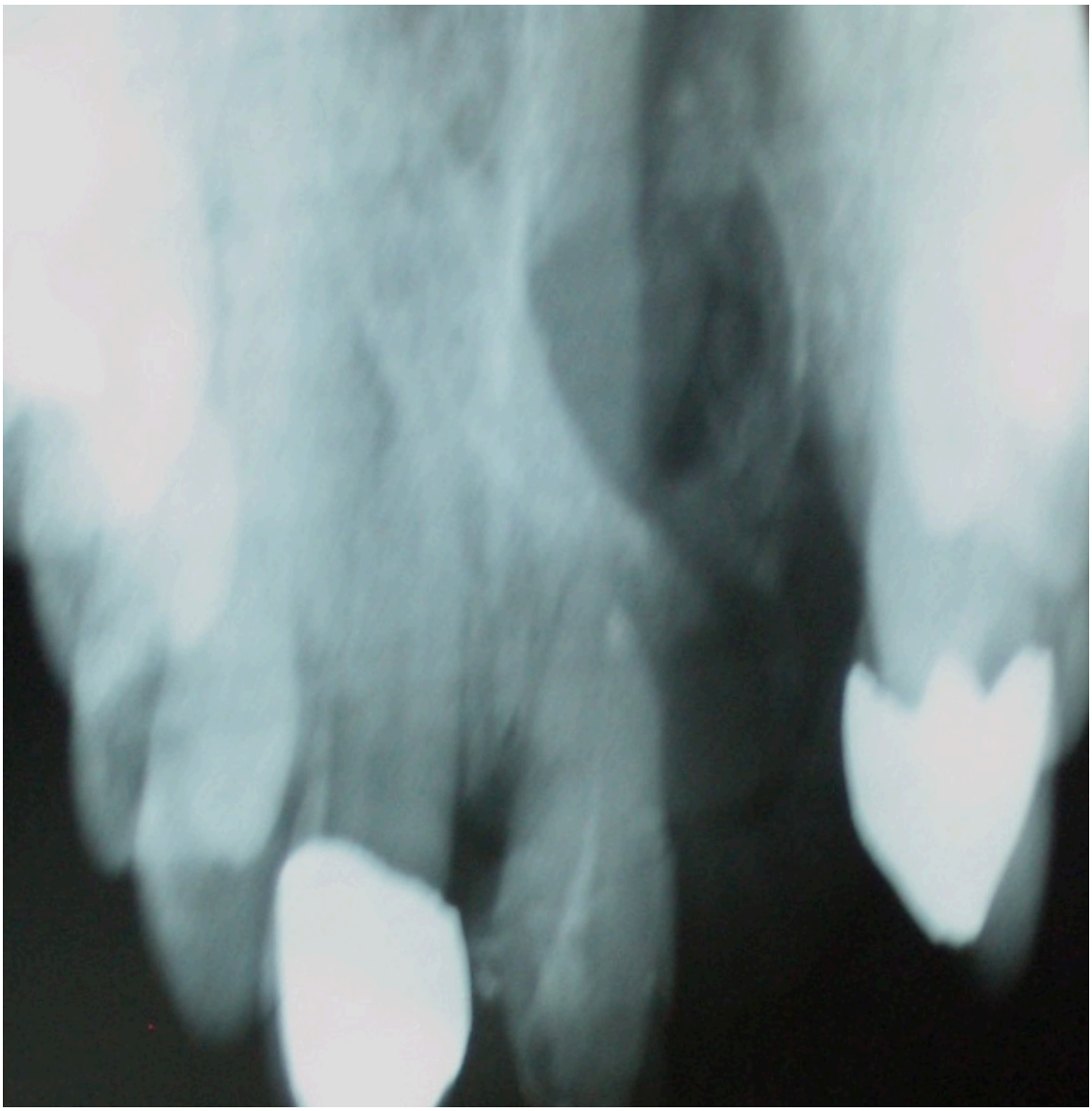

Figure 1.8. Radiograph of a cleft of the maxillary alveolar bone.

Chapter 2

Objectives

Tissue engineering in the craniofacial complex holds great promise for regenerating all tissue types present in the craniofacial complex. These strategies typically employ complex approaches utilizing multiple arms of the tissue engineering paradigm: cells, bioactive factors, and scaffolds. Considering the regulatory landscape and the time to clearance or approval of such strategies concomitantly with the pressing clinical needs of today, alternative strategies employing concepts from tissue engineering, conventional reconstruction and regulatory experience should be considered. The work presented in this dissertation follows these principles by attempting to enhance the use of materials currently part of products approved or cleared by the United States Food and Drug Administration (FDA). This strategy should accelerate the regulatory process and more rapidly impact clinical practice.

The overarching strategy investigated in this thesis is the two-stage repair of craniofacial defects with an antibiotic-releasing porous polymethylmethacrylate (PMMA)

space maintainer and a stabilizing bone regenerating implant in the same patient. To evaluate this strategy several aspects were investigated individually.

2.1. Specific Aim 1: Porous Space Maintenance

2.1.1. Study 1: Evaluation of Soft Tissue Coverage over Porous Polymethylmethacrylate Space Maintainers Within Nonhealing Alveolar Bone Defects

Prefabricated porous PMMA scaffolds fabricated with carboxymethylcellulose gel (CMC) as the porogen were evaluated for soft tissue coverage and tissue response in a composite tissue defect model of the rabbit mandible.

2.1.2. Study 2: *In situ* Formation of Porous Space Maintainers in a Composite Tissue Defect

Porous PMMA scaffolds fabricated with CMC as the porogen were formed *in situ* and evaluated for soft tissue coverage and tissue response in a composite tissue defect model of the rabbit mandible to assess the effect of polymerization and curing on the tissue response.

2.2. Specific Aim 2: Antibiotic-releasing Porous Space Maintainers

2.2.1. Study 1: Antibiotic--releasing Porous Polymethylmethacrylate/Gelatin/Antibiotic Constructs for Craniofacial Tissue Engineering

Colistin-releasing porous PMMA scaffolds fabricated with gelatin microparticles as the porogen were evaluated for physical properties and release kinetics.

2.2.2. Study 2: Evaluation of Antibiotic--releasing Porous Polymethylmethacrylate/Gelatin Scaffolds

Colistin-releasing porous PMMA scaffolds fabricated with a clinical grade gelatin matrix as the porogen were evaluated for physical properties and release kinetics.

2.2.3. Study 3: Evaluation of Antibiotic-releasing Porous Polymethylmethacrylate Space Maintainers in an Infected Composite Tissue Defect Model

Colistin-releasing porous PMMA scaffolds fabricated with a clinical grade gelatin matrix as the porogen were evaluated for kidney function, soft tissue coverage, tissue response and infection clearance in a composite tissue defect model in a rabbit mandible that was inoculated with *Acinetobacter baumannii*.

2.3. Specific Aim 3: Bone Regeneration

2.3.1. Study 1: Biodegradable Composite Scaffold Incorporating an Intramedullary Rod and Delivering Bone Morphogenetic Protein-2 for Stabilization and Bone Regeneration in Segmental Long Bone Defects

Porous poly(propylene fumarate) (PPF) scaffolds with bone morphogenetic protein-2 (BMP-2) delivering poly(lactic-*co*-glycolic acid) (PLGA) microparticles with a solid PPF intramedullary rod were evaluated for bone regeneration, tissue response and mechanical stabilization in a rat femoral segmental defect model.

Chapter 3

Evaluation of Soft Tissue Coverage over Porous Polymethylmethacrylate Space Maintainers Within Nonhealing Alveolar Bone Defects[‡,*]

The incidence of traumatic facial injuries relative to injuries at other anatomic locations has risen sharply during combat operations in Iraq and Afghanistan compared to previous military conflicts [64]. The predominant cause of these wounds is improvised explosive devices, which often cause extensive damage to bone and soft tissues [65].

[‡] This chapter was published as Kretlow JD, Shi M, Young S, Spicer PP, Demian N, Jansen JA, Wong ME, Kasper FK, Mikos AG. "Evaluation of Soft Tissue Coverage over Porous Polymethylmethacrylate Space Maintainers Within Nonhealing Alveolar Bone Defects." *Tissue Eng Pt C Methods.* **16**, 1427-1438 (2010).

[*] The doctoral candidate performed portions of the presented work including animal tissue harvest, processing and analysis.

Similarly, combat related ballistic injuries often involve high velocity projectiles that cause significant and widespread damage to multiple types of tissue [66].

Even in the civilian population, traumatic craniofacial bone injury is often accompanied by injury or loss of surrounding soft tissues [67]. One of the major difficulties reconstructive surgeons face when treating injuries involving significant bone loss is contracture and scarring of the overlying soft tissue envelope, which compromises facial projection and makes staged repair of bony structures difficult [68, 69]. Previously, definitive bone reconstruction was delayed until soft tissue coverage and a sterile wound environment were achieved [70, 71]. More recently, despite reports of local complications and wound infection rates as high as 100% in civilians suffering gunshot wounds to the face [72, 73], early definitive repair of facial gunshot wounds via free tissue transfer has become common as the well vascularized tissues that are transferred survive well in hostile wound environments [71, 74].

The field of regenerative medicine and the technologies borne from tissue engineering offer great hope towards providing an alternative and possibly better approach to regenerating injured or destroyed tissues. Most proposed tissue engineering strategies, however, currently require planning in the form of material fabrication, autologous cell harvest and expansion, and/or *ex vivo* tissue generation. Additionally, little to no evaluation of tissue engineering approaches is currently performed in wound environments involving infection, significant vascular injury, and large-scale tissue devitalization such as that encountered in a battlefield wound. Therefore, the successful use of a tissue engineering approach to provide immediate, definitive regeneration of

tissues injured during craniofacial trauma such as those encountered during military service is unlikely using current approaches.

In the absence of immediate reconstruction, clinical management of facial bone loss can involve the placement of an alloplastic space maintainer to provide a template for future definitive reconstruction and prevent wound contracture into the space normally occupied by bone [75]. Polymethylmethacrylate (PMMA), is commonly used in such space maintenance applications [75, 76] and others within the craniofacial complex [77]. Although PMMA has many desirable characteristics for such applications (moldable, FDA-regulated, familiar to surgeons), a number of problems exist with respect to wound healing around PMMA implants and other alloplastic craniofacial implants [78-80].

For the purposes of facilitating a long-term tissue engineering approach to treating composite craniofacial defects, a temporary implant or space maintainer would allow time for a regenerative medicine approach to be used to definitively regenerate the injured or absent tissue. In addition to providing space maintenance, such a temporary implant could be used to "prime" the defect site, enabling better long-term success of the definitive regenerated tissue construct. Previous work has shown that recipient site characteristics such as vascularity are important for the regeneration of new bone tissue and support of grafted tissue [81-83]. For mandibular reconstruction, the defect site and surgical approach along with recipient site complications such as infection, intraoral exposure, and prolonged antibiotic use have been significantly linked to graft failure [84, 85]. An ideal temporary space maintainer will therefore not only maintain the osseous

void and prevent soft tissue collapse or contracture into the space but also will allow or promote soft tissue coverage and healing without serving as a nidus for local infections.

Despite the aforementioned shortcomings associated with solid PMMA implants, we hypothesized that an implant made of modified PMMA could fulfill many of these criteria. Previously, a number of groups have explored different methods for making porous PMMA [86-91]. Based on this work, we hypothesized that porous PMMA implants with reproducibly tunable pore structure could be fabricated using a carboxymethylcellulose (CMC) hydrogel as an aqueous porogen. When tested in a clean/contaminated rabbit mandibular defect, we hypothesized these implants would be able to maintain the defect space while promoting soft tissue coverage of the implant.

3.1. Material and Methods

3.1.1. Experimental design

For the first part of this study, porous PMMA implants were synthesized and characterized using a CMC hydrogel as an aqueous phase to impart porosity on the implants. The percent of CMC in the aqueous phase and the ratio of aqueous phase:polymer phase were varied in order to control the bulk and surface characteristics. Following characterization of the porous implants, two formulations, one with high bulk porosity and pore interconnectivity and one with lower porosity and less pore interconnectivity, were compared over 12 weeks *in vivo* to a solid PMMA implant within a modified rabbit mandibular defect.

3.1.2. Implant fabrication and characterization

Solid and porous PMMA implants were fabricated using a clinical grade PMMA bone cement (SmartSet High Viscosity, DePuy Orthopaedics, Warsaw, IN) consisting of a powder of methylmethacrylate / methyl acrylate copolymer, benzoyl peroxide, and zirconium dioxide and a liquid phase with methylmethacrylate (MMA), N,N-dimethyl-*p*-toluidine, and hydroquinone. For the solid implants, the solid and powder phases were mixed according the manufacturer's specifications for approximately 90 seconds and, once they reached a dough-like consistency, packed into custom-fabricated 10 mm diameter × 6 mm height cylindrical Teflon® (DuPont, Wilmington, DE) molds. The solid implants were then allowed to harden at room temperature for 30 minutes before being removed from the molds and vacuum-dried overnight.

For porous implants, 7 wt% and 9 wt% CMC hydrogels were prepared by dissolving the appropriate amount of United States Pharmacopeia grade low viscosity CMC (Spectrum Chemical Manufacturing Corp., Gardena, CA) in distilled water. The powder component of the PMMA cement was then mixed with the CMC hydrogel such that the powder was uniformly suspended within the aqueous phase. The liquid component of the PMMA cement was then added to the mixture of aqueous/powder phases. Aqueous phase weight percentages of 30, 40, and 50 wt% were used to fabricate the implants, resulting in 6 experimental groups. The aqueous and polymer phases were then stirred by hand for approximately 90 seconds and packed into Teflon® molds of the same size as the solid PMMA implants. The porous implants within molds were then allowed to harden for 30 minutes before being removed from the molds, placed within individual cassettes, and the aqueous phase was then leached from the implants in

deionized, distilled water as previously described [92]. The porous PMMA implants were then vacuum dried overnight in a laboratory freeze dryer (Lyph-Lock 4.5, Labconco Corp., Kansas City, MO).

Implant porosity and pore interconnectivity were analyzed using microcomputed tomography (microCT) as previously described [93]. Briefly, implants (n=3) from all experimental groups were scanned using a SkyScan 1172 microCT imaging system (SkyScan, Aartselaar, Belgium). High resolution 1280 × 1024 pixel images were created by scanning at an 8 μm/pixel resolution with no filter at voltage and current settings of 40 kV and 250 μA, respectively. Serial tomograms were reconstructed, resliced, and analyzed using NRecon and CTAn software packages provided by SkyScan. For porosity and pore interconnectivity analyses, the scanned object volumes were binarized using a global threshold of 60-255. Porosity and interconnectivity were determined using a 9 mm diameter × 5 mm height cylindrical volume of interest to eliminate edge effects. Pore interconnectivity was determined by repeatedly applying a shrink wrap algorithm with minimum interconnection sizes ranging from 40-320 μm. Interconnectivity is reported as the percentage of pore volume accessible from outside the volume of interest with pores considered accessible only if the interconnection to that pore allowed a sphere with diameter of the user defined minimum interconnection size to pass through.

Scanning electron microscopy (SEM) was also used to examine the external surface of the implants. Implant surfaces were sputter-coated with gold for 40 s at 100 mA using a CrC-150 sputtering system (Torr International, New Windsor, NY) and

observed at an accelerating voltage of 10 kV using a FEI Quanta 400 field emission scanning electron microscope (FEI company, Hillsboro, OR).

3.1.3. *In vivo* implant evaluation

Solid PMMA implants and porous implants (9 wt% CMC within the aqueous phase and both 30 and 40 wt% total aqueous phase in the implant) were evaluated *in vivo* using a modification of a nonhealing rabbit mandibular defect model [94]. All surgical procedures followed protocols approved by the Institutional Animal Care and Use Committees at both Rice University and the University of Texas Health Science Center at Houston. Eighteen healthy male adult New Zealand White rabbits (n = 6 per group), at least 6 months old and weighing 3.5-4 kg were purchased from Myrtle's Rabbitry (Thompson Station, TN). Prior to implantation, all implants were sterilized using ethylene oxide.

Briefly, each animal was given preoperative intramuscular doses of buprenorphine hydrochloride (0.1 mg/kg body weight) for postoperative analgesia and 0.5 mL Durapen® (150,000 U/mL penicillin G benzathine and 150,000 U/mL penicillin G procaine) for perioperative antibiotic coverage. Prior to induction, ketamine hydrochloride (40 mg/kg body weight) and xylazine hydrochloride (7.5 mg/kg body weight) were given, after which rabbits were placed in a supine position, intubated and placed under general anesthesia using an isoflurane/O_2 mixture (2.5-3% isoflurance for induction, 2% for maintenance) with constant cardiac and respiratory monitoring. The animals were then surgically prepped and draped, after which a 7 cm midline incision through the skin and superficial fascia was made beginning 0.5 cm posterior to the

mentum. Using blunt dissection and electrocauterization, the left masseter was exposed and the soft tissue along the inferior border of the body of the left hemimandible was mobilized such that the periosteum covering the body of the mandible could be incised and elevated, exposing a 4 cm × 1.5 cm area on the lateral surface of the mandible. A 10 mm titanium trephine (Ace Surgical Supply, Inc., Brockton, MA) attached to a Stryker TPS® surgical handpiece (Stryker, Kalamazoo, MI) operating at 15,000 rpm with copious normal saline irrigation was used to create a bicortical defect through the exposed body of the left mandible. A 701 bur in combination with the surgical drilling unit was used to cut a 2-3 mm window through the alveolar ridge in the middle of the defect to provide access for removal of the crowns of the associated teeth and provide intraoral exposure of the defect. The defect site was thoroughly washed with normal saline, after which an implant was placed within the defect. The order of implant placement was randomized; and none of the surgical personnel, who were the same throughout the study, were aware of which implant was being used. Prior to closure, a titanium supporting plate (1.5 mm 6-hole heavy gauge titanium; Synthes, West Chester, PA) was secured in place to prevent iatrogenic fracture during the course of the study. The incision was then closed in 3 layers (muscle, fascia, and skin) using degradable sutures (Vicryl polyglactin sutures, Ethicon, Somerville, NJ). Following wound closure, anesthesia was reversed, and the animals were extubated.

Postoperatively, the animals were given access to food and water *ad libitum*. Food was limited to a soft recovery diet (Critical Care for Herbivores, Oxbow Pet Products, Murdock, NE) and shredded or mashed fruits and vegetables to reduce stress on

the mandible. All animals survived the 12-week post-operative period without complications.

3.1.4. Gross characterization

After 12 postoperative weeks, each rabbit was euthanized via intravenous injection of 1 mL Beuthanasia-D® (390 mg/mL pentobarbital sodium and 50 mg/mL phenytoin sodium). The left hemimandibles were then carefully dissected from the cranium with care taken to preserve the soft tissue surrounding the implant and within the oral cavity. The oral mucosa and dentition covering the alveolus of each specimen was examined to detect any areas of implant or bone exposure. Specimens were individually placed in 10% neutral buffered formalin and stored on a shaker table at 4 ˚C for 72h.

3.1.5. Histology

After fixation, samples were dehydrated and stored in 70% of ethanol and then embedded in MMA. Following polymerization of the MMA, 3 coronally oriented 10 μM thick sections through the center of each implant were cut using a modified diamond saw technique [95] and subsequently stained using methylene blue/basic fuchsin.

Each of the stained sections was analyzed using light microscopy (Zeiss Axio Imager Z1 and AxioCam MRc 5, Carl Zeiss AG, Oberkochen, Germany) by two blinded observers (SY and FKK). A quantitative scoring system (Table 3.1) was used to score the tissue response at the implant interface and within the pores of the porous implants.

3.1.6. Statistical analyses

Implant porosity data were analyzed using single factor analyses of variance (ANOVA) with post hoc pairwise comparisons made using Tukey's HSD. Oral mucosal wound healing, as observed grossly and confirmed by microscopy, was analyzed using a Fisher-Freeman-Halton test. Histological scoring was analyzed using nonparametric statistics. The tissue response at the implant interface was analyzed using a Kruskal–Wallis one-way analysis of variance with subsequent pairwise analyses made using the Dwass-Steel-Critchlow-Fligner test. A Mann-Whitney U test was used to analyze the tissue response within the pores of the two porous implant types. The a priori level of significance for all analyses was chosen as $\alpha = 0.05$. All analyses were performed using R version 2.10.0 (R Foundation for Statistical Computing, Vienna, Austria).

3.2. Results

3.2.1. Implant fabrication and characterization

Porous PMMA/CMC implants were reproducibly fabricated as described in the Materials and Methods section. MicroCT analyses showed that porosity increased as expected with increasing incorporation of the aqueous phase (Figure 3.1). Significant differences in implant porosity were observed between all groups as the aqueous phase incorporation increased. Varying the amount of CMC within the aqueous phase did not significantly alter the implant porosity.

Pore interconnectivity also increased with increasing aqueous phase incorporation (Figure 3.2). Interconnectivity appeared to be affected by the percentage of CMC in the

aqueous phase; the more negative slope observed for implants with 9% CMC within the aqueous phase indicates that more of the interconnections in these implants were smaller than for those implants fabricated with 7% CMC in the aqueous phase.

SEM images and microCT reconstructions also showed differences in the porosity and surfaces of the fabricated implants (Figure 3.3). The porosity increases with increasing aqueous phase incorporation quantitatively detected with microCT are seen in cross sections and surface images of the implants. Furthermore, the pore size appears more consistent within implants fabricated using 9% CMC in the aqueous phase, likely resulting in the relative abundance of smaller pore interconnections within these implants when compared to those fabricated using 7% CMC.

3.2.2. *In vivo* implant evaluation

Based on the implant characterization, solid PMMA implants, 9% CMC 30 wt% (16.9 ± 4.1% porosity, 39.7 ± 9.4% interconnectivity at a 40 μm minimum connection size) and 9% CMC 40 wt% (44.6 ± 2.1% porosity, 81.2 ± 1.0% interconnectivity at a 40 μm minimum connection size) implants were chosen for implantation in the *in vivo* phase of the study. All animals survived the surgery and post-operative period without complications. No changes in eating habits or activity were noted by the investigators, husbandry staff, or veterinary staff.

3.2.3. Gross characterization

At the time of animal euthanasia and implant/hemimandible harvest, no signs of mobility or infection were noted in any of the animals or visible tissues following

harvest. Wound healing (closure) of the oral mucosa over the alveolar ridge at the site of the intraoral communication was assessed grossly (Figure 3.4) and correlated to histological results (Figure 3.6) to confirm the gross observations. Wound healing was considered incomplete when any exposed bone or implant could be grossly observed and histology also indicated a failure of soft tissue coverage over the implant or within the defect. The increase in oral mucosal wound healing observed in defects filled with both low and high porosity implants (83% of defects healed in each group) versus non-porous PMMA implants (50% healed) was not statistically significant ($p > 0.08$).

3.2.4. Histology

Histology and histological scoring were performed to assess the ability of the implants to maintain space within the surgically created osseous void and to view and quantify the soft tissue response around and within the implants. At low magnifications allowing coronal views of the entire implant and defect in cross section, all implants successfully maintained the defect space within the hemimandible. This space maintenance was confirmed by the lack of tissue collapse or contracture into the space occupied by the implants with the exception of tissue invading the pores of the porous implants (Figure 3.6).

At higher magnification, the tissue response at the implant-tissue interface and within the implant pores could be observed (Figure 3.7). At the implant-tissue interface, both the low porosity and solid implants were in many cases surrounded by a thin, well-organized fibrous capsule. The low porosity implants were also in direct contact in many areas with any newly formed bone observed at the implant interface. The high porosity

implants were primarily surrounded by an abundance of inflammatory plasma cells at the implant interface, and a similar inflammatory cell population was observed within the pores of the highly porous implants. When a quantitative scoring system was applied, the interfacial tissue response for the highly porous implants was statistically significantly different from the response observed around both the solid and low porosity implants (Figure 3.8, $p < 0.05$). Similarly, the difference in tissue response within the pores of the low and high porosity implants was statistically significant (Figure 3.8, $p < 0.05$).

3.3. Discussion

Temporary space maintainers have historically been used clinically to prevent soft tissue collapse into bony defects and provide a template for delayed bone healing or grafting [75, 96]. Recently, however, space maintenance has been used infrequently, particularly in the staged repair of traumatic injuries, as immediate free tissue transfer has eliminated the need for space maintenance and staged repair. Additionally, problems with existing biomaterials such as problems with healing of surrounding tissues, implant extrusion, or bacterial colonization have further limited the use of space maintainers, particularly in applications where soft tissue healing or infection may be a concern [97, 98]. Unfortunately, due to limitations in current tissue engineering technology, injuries involving lacking or devitalized soft tissues or the possibility of infection are precisely the type a staged repair using temporary space maintenance might allow a regenerative medicine approach to be undertaken.

The present study aimed to evaluate methods to reproducibly fabricate and characterize porous PMMA implants using a CMC porogen and to then develop an

animal model to test selected formulations in a non-healing bone defect that approximated a more toxic wound environment than most traditional animal models. In the first part of the study, porous PMMA implants were fabricated in a one step process by incorporating a CMC hydrogel that could be leached away rapidly *in vitro* or *in vivo*. Varying both the amount of CMC within the aqueous phase and the relative amount of aqueous phase to polymer phase allowed for well-controlled porosity and pore interconnectivity. As expected, higher percentages of porogen resulted in greater implant porosity, while increasing the viscosity of the aqueous phase porogen by incorporating of greater amounts of CMC within the hydrogel led to a more consistent pore size and higher pore interconnectivity when the minimum interconnection size was decreased.

In the second part of the study, two formulations of porous PMMA implants and solid PMMA implants were implanted into non-healing rabbit mandibular defects that had been contaminated through an open communication with the oral cavity. Porous PMMA formulations were selected such that both a highly porous, highly interconnected implant (9% CMC 40 wt%) and an implant of lower porosity and lower interconnectivity could be compared (9% CMC 30 wt%). Healing of the communication into the oral cavity was assessed as well as the tissue response both around and within the implants. All formulations successfully maintained space within the defect. Soft tissue was only observed within the defect when it was penetrating the pore network in the two formulations of porous implant. The oral mucosal defects created to allow communication into the bone defect healed in more cases (5/6 healed for both low and high porosity implants) when the bony defects were filled with porous implants than

when filled with solid implants (3/6 healed), although the differences between groups was not statistically significant.

Although the gross mucosal defect closure over the high and low porosity implants was equivalent, microscopically, the tissue response around and within the pores of the low porosity implants was more favorable. At the implant – tissue interface, a small, well formed capsule or direct tissue – implant contact was typically observed around the low porosity implants. Immature fibrous tissue with few inflammatory elements was generally seen within the filled pores of the low porosity implants. Contrastingly, the tissue surrounding and within the pores of the highly porous implants was almost exclusively inflammatory, consisting mostly of plasma cells. Thus the low porosity and solid implants elicited a more favorable soft tissue response than the highly porous implants, while the porous implants may have provided a template for improved wound healing in comparison to the solid implants.

The current study has a number of strengths. First, although porous PMMA has been well studied [87, 89, 99-102], including porous PMMA fabricated using an aqueous phase consisting of a CMC hydrogel as a porogen [88, 103], the present study is one of the first systematic studies of fabrication methods to quantitatively examine the effect of both the ratio of aqueous phase to polymer phase but also the effect of the aqueous phase viscosity as done by varying the amount of CMC within the aqueous phase. Increasing the viscosity of the aqueous phase by using a 9 wt% CMC hydrogel, as opposed to a 7 wt% CMC gel as has been previously used [104], resulted in a more consistent pore architecture with smaller, more consistently sized pore interconnections. Because of this, both porous implant formulations chosen for the *in vivo* study were fabricated with 9 wt%

CMC hydrogels. An additional benefit of the chosen materials is that both PMMA and CMC are FDA regulated for craniofacial applications, and the fabrication of the implants can be done in a standard operating room with only minor alterations in the manufacturer recommended preparation of PMMA.

A strength of the *in vivo* portion of the study was the development of a more clinically relevant animal model that may better simulate the type of clinical situation in which the technology investigated may be used. The animal model was based on a previously developed rabbit mandibular defect [94] that was modified to allow contamination of the wound through an opening into the oral cavity. This conferred several advantages. First, mucosal wound healing within the rabbit oral cavity is a well-established method for evaluating wound healing [105-109], particularly when evaluating biomaterial-guided wound healing [110-115]. Second, in the clinical setting, the presence of intraoral communication is significantly correlated to decreased bone graft survival time [85], and thus an implant evaluation strategy that focuses on the closure of these communications is relevant for a situation where definitive repair will be performed using a standard or tissue engineered bone graft. With relation to the presence of these intraoral communications, infection is a major concern when dealing with any implantable biomaterial [116], particularly PMMA [117, 118], and thus evaluating the tissue response to the implant in an environment where it will most likely be exposed to bacteria strengthens any conclusions drawn with respect to optimal material formulations. Finally, although the observed differences in oral mucosal wound healing does not allow one to draw any definitive conclusions about how the presence of porosity affected the oral mucosal wound healing, this study establishes the statistical parameters necessary to

determine the statistical power needed to achieve significance in future studies using this model. While a difference in healing clearly existed between both the high and low porosity implants and the solid PMMA implants, the difference was not significant. Somewhat surprisingly, the difference in tissue response to the porous implants based on histological scoring was significantly different and may be an important parameter not only for initial wound healing but also for subsequent bone regeneration [119-121].

This study is not, however, without weaknesses. First, an ideal tissue engineering solution to the problem of complicated craniofacial bone defects would not involve multiple interventions and delayed reconstruction. An ideal solution would use a degradable material [122] that could address the issues of soft tissue coverage, infection, and bone regeneration concurrently, thus eliminating the need for and risks associated with repeated operations. At present, such a solution does not exist nor does there appear to be any such solution developed for use in the near future. While the animal model developed is viewed by the authors as one of the strengths of this method of material evaluation, the complexity of the model may also be viewed as a weakness. Not only is the tooth bearing segment of the mandible more complicated in structure than many craniofacial bones, it also is exposed to very different mechanical stresses than other bones [123]. Furthermore, the method of wound contamination was poorly controlled. Oral flora of the rabbits and the amount of flora that passed through the communication was likely variable between animals.

Limited research is available investigating PMMA strictly for use as a space maintainer; however, PMMA has a long track record of use in craniofacial applications. In an early study using PMMA to repair canine mandibular defects, Worley reported that

repair failed in 7 of 11 dogs due to wound dehiscence over solid PMMA implants [124]. Kangur et al. reported similar problems with mucosal dehiscence over solid PMMA used to fix canine mandibular fractures and attributed the presence of an acute inflammatory tissue response to the PMMA to this oral communication [125]. Despite these findings, a number of studies exist that report no complications with solid PMMA use in craniofacial applications [75, 98, 126, 127].

Porous PMMA, as previously mentioned has also been investigated in animal studies and limited clinical use. In a long term study in guinea pigs comparing porous and solid PMMA implanted in the hypodermis, van Mullem et al. reported implant extrusion occurred in 4/36 solid implants and none of the porous implants [90]. Similar to the present study, the same study noted that foci of inflammatory cells were found more frequently around and within the porous PMMA implants (1:1 aqueous phase:polymer phase) than the solid implants. Clinically, the porous PMMA seems to have been used successfully with little note of complications [128], and, while reports of long-term results are rarely found, it should be noted that the current study differs from those previously published as the intent is for the porous implants to only be used as temporary implants.

Using the presented methods for fabrication and evaluation, the porous PMMA implants appeared to promote or allow wound healing of the oral mucosa better than the solid implants, although not significantly so. Significant differences in the tissue response to the two formulations of porous implants were also observed. A number of

possible explanations exist for these two findings. The trend of improved wound healing with use of the porous implants may best be explained by increased tissue integration within the pores of the implants. This may have limited implant micromovement and improved the rate at which new tissue formed across the implant to close the communication. Similar improvements in wound healing and implant retention have been found when using porous polyethylene for the fixation of bone-anchored hearing aids [129, 130].

The inflammatory tissue response around and within the highly porous implants was likely caused by increased bacterial seeding of these implants. The increased porosity and interconnectivity of these implants compared to those of the low porosity and lower interconnectivity group likely led to bacterial accumulation deeper within the implant in areas where the bacteria could not effectively be cleared. Kiechel et al. compared infection control within porous and nonporous PMMA seeded with *Staphylococcus aureus* and implanted in the paravertebral fascia of rabbits and found increased infections occurred in animals implanted with porous PMMA implants [131]. Sclafani et al. found that increased porosity increased the resistance to infection in implants inoculated 14 days after implantation but not if the implants were inoculated at the time of implantation [132]. Thus in applications and models where contamination or infection exists at the time of implant placement, an appropriate balance with respect to porosity is needed to allow tissue ingrowth and implant integration but not bacterial seeding deep within the implant. If contamination is not present at the time of implantation, fibrovascular ingrowth has been shown to occur rapidly and thus a more porous implant may be acceptable [133]. Additionally, studies of induced membranes or

capsules around PMMA implants suggest that the formation of well-formed capsule around the implants, as seen more frequently around the low porosity implants in this study, may facilitate greater success of later efforts aimed at definitive bone regeneration, provided the capsule is not destroyed during implant removal and any necessary debridement [119-121]. Finally, it is important to note that the method of fabrication of the porous PMMA implants may lead to particulate PMMA release [134], which could account for the inflammatory response elicited by the highly porous implants [135].

Based on the results of the present study, the low porosity space maintainers appear to be a promising alternative to solid PMMA for temporary implantation as part of a regenerative medicine approach to treating traumatic craniofacial injuries. Future work in this area should focus on tissue regeneration within the maintained space as well as release of any bioactive factors from the space maintainer such as antibiotics or growth factors that may better ensure success of later stage tissue engineering efforts. The characterized implants may provide a critical step in allowing the use of regenerative medicine approaches as an alternative to traditional approaches in treating contaminated or open traumatic defects. The methods described for the fabrication of these implants may be applicable to a wide variety of different materials, and the animal model described may provide a more useful analogue to clinical situations where tissue engineering strategies may need to be used in possibly contaminated environments.

3.4. Conclusions

Methods were developed allowing porous PMMA space maintainers to be reproducibly fabricated using a CMC hydrogel as an aqueous phase porogen. Porosity

and pore interconnectivity can be controlled by varying the ratio of the aqueous phase to polymer phase and the concentration of CMC within the hydrogel, respectively. *In vivo*, porous space maintainers potentially improve oral mucosal healing over a clean/contaminated bone defect created in the rabbit mandible. The tissue response to a porous implant of low porosity and pore interconnectivity was more favorable than the response to a more porous and interconnected implant. This low porosity implant may be ideal for temporary space maintenance within craniofacial defects. The described methods may be applicable in a variety of tissue engineering applications and may allow broader application of current tissue engineering approaches that may not be suitable for use in more harsh wound environments.

3.5. Tables and Figures

Table 3.1. Histologic scoring system for implants at the implant-tissue interface as wel as in the pores of porous implants.

Hard tissue response at the implant-bone interface	Score
Direct bone-to-implant contact without soft interlayer	4
Remodeling lacuna with osteoblasts and/or osteoclasts at surface	3
Majority of implant is surrounded by fibrous tissue capsule	2
Unorganized fibrous tissue (majority of tissue is not arranged as capsule)	1
Inflammation marked by an abundance of inflammatory cells and poorly organized tissue	0
Hard tissue response within the pores of the scaffold	
Tissue in pores is mostly bone	4
Tissue in pores consists of some bone within mature, dense fibrous tissue and/or a few inflammatory response elements	3
Tissue in pores is mostly immature fibrous tissue (with or without bone) with blood vessels and young fibroblasts invading the space with few macrophages present	2
Tissue in pores consists mostly of inflammatory cells and connective tissue components in between (with or without bone) or the majority of the pores are empty or filled with fluid	1
Tissue in pores is dense and exclusively of inflammatory type (no bone present)	0

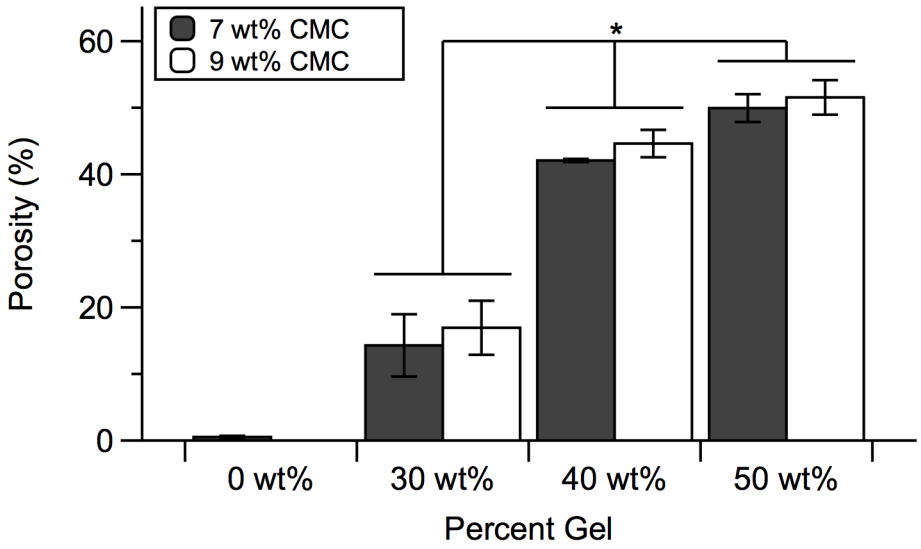

Figure 3.1. Porosity values as calculated by microcomputed tomography (microCT). Samples were scanned and the resultant scans were reconstructed, reoriented, and binarized. Implant porosity was determined using a cylindrical (9 mm diameter × 5 mm height) volume of interest slightly smaller than the impalnt dimensions to eliminate edge effects. Data are reported as means ± standard deviation (n = 3). The asterisk indicates a significant difference ($p < 0.05$) as detected using analysis of variance and Tukey's post hoc tests between the groups marked with the same wt % of carboxymethylcellulose (CMC) (7 or 9 wt%). No significant differences were found as a result of changing the % CMC from 7 to 9 wt%.

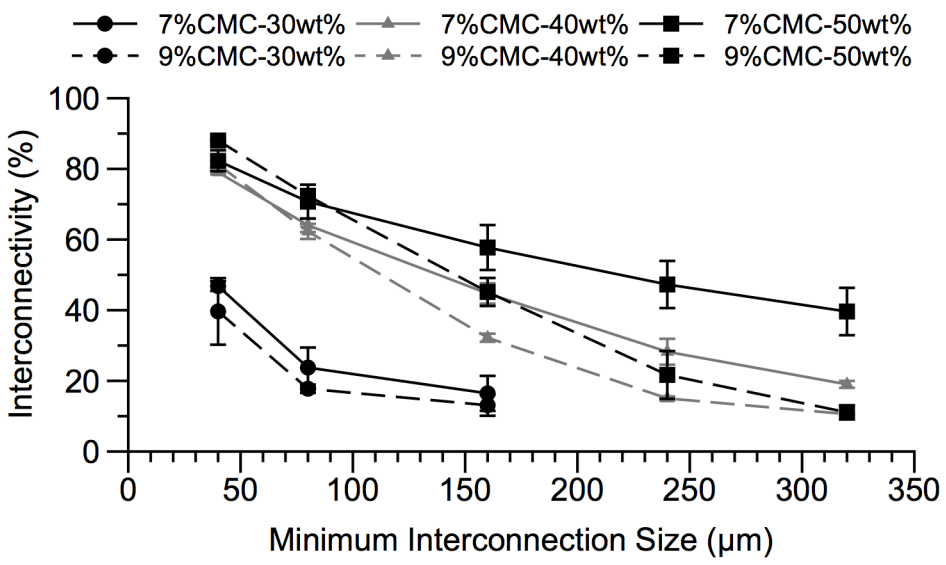

Figure 3.2. Implant interconnectivity percntages as a function of the minimum interconnection size. Samples were scanned and processed as reported in the Materials and Methods section, and a built in software package was used to determine the percentage of the implant porosity that was accessible from outside the volument of interest. Data are reported as means ± standard deviation (n = 3).

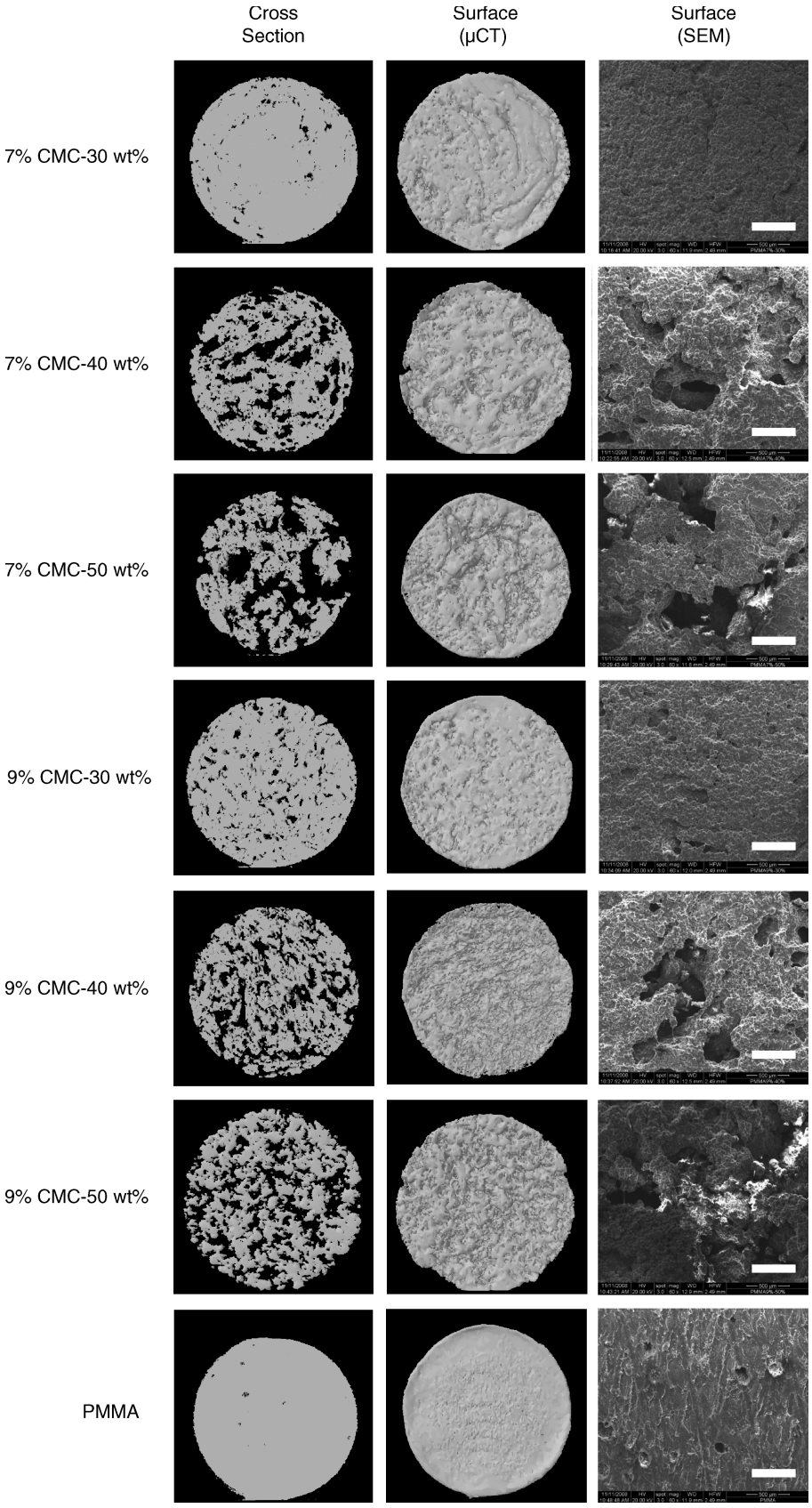
Cross Section
Surface (μCT)
Surface (SEM)
7% CMC-30 wt%
7% CMC-40 wt%
7% CMC-50 wt%
9% CMC-30 wt%
9% CMC-40 wt%
9% CMC-50 wt%
PMMA

Figure 3.3. Representative images of implant cross sections and surfaces. Cylindrical implants (10 mm diameter × 6 mm height) from each experimental group were scanned by microCT or scanning electron microscopy (SEM). Virtual microCT cross sections of the implants were made by slicing through the center of the axially oriented implant. For electron micrographs, the scale bars represent 500 µm.

Figure 3.4. Representative gross views of harvested tissue covering the alveolus and the implant. (A) Failure of wound healing over a solid polymethylmethacrylate (PMMA) implant is shown. The exposed implant is denoted by white arrows. (B,C) Well-healed soft tissue covering the intraoral exposure is seen where dentition is missing over low-porosity (B) and high-porosity (C) implants.

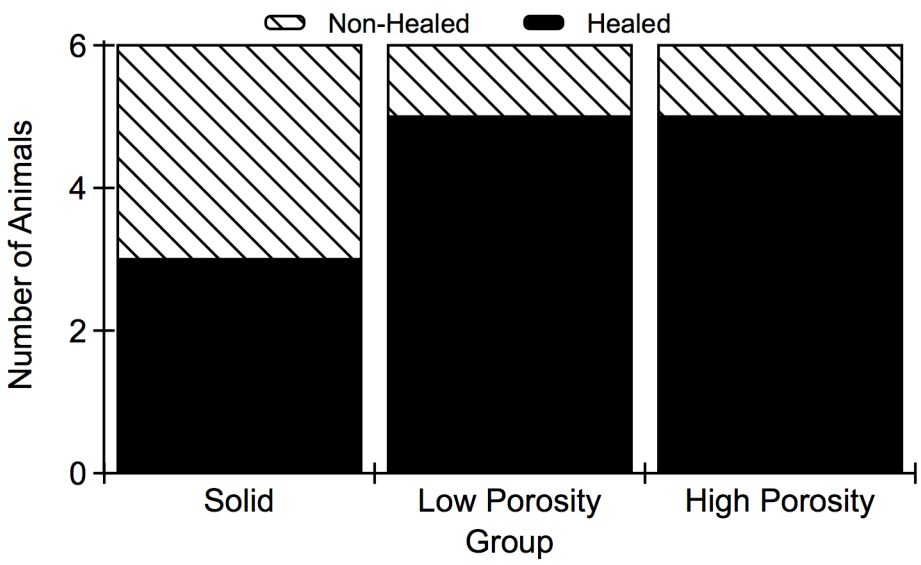

Figure 3.5. Oral mucosal coverage over implant by type.

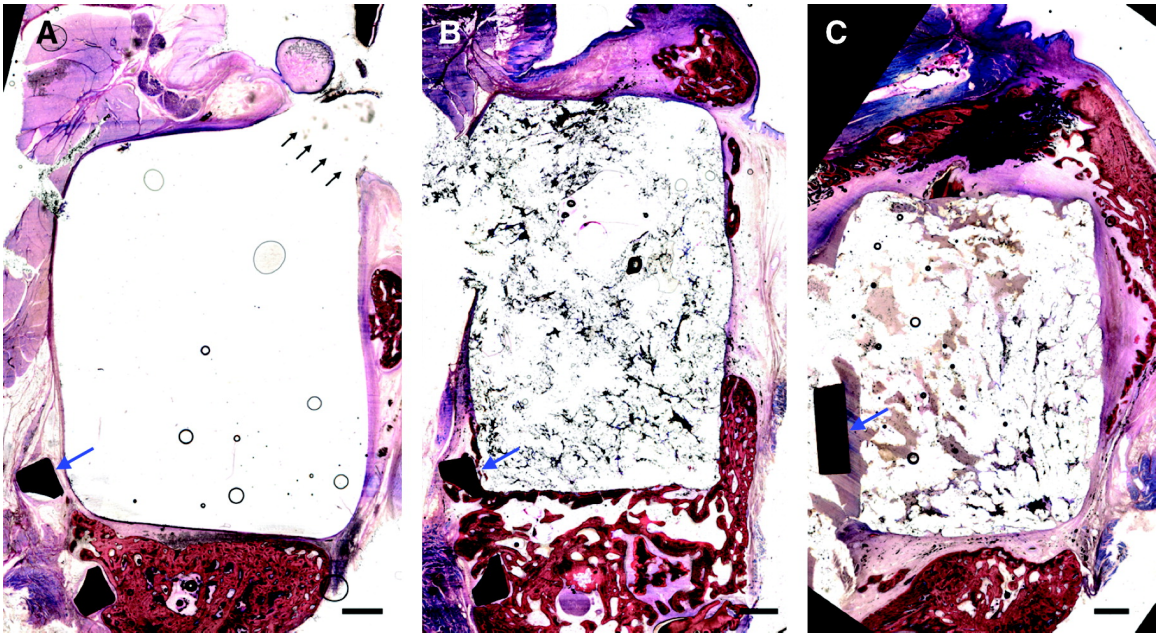

Figure 3.6. Representative light micrographs (25X magnification) of coronally sectioned tissue samples throught the center of the (A) solid PMMA, (B) low-porosity, and (C) high-porosity space maintainers. The intraoral exposure of the solid implant (A) is shown with black arrows. Blue arrows denote the titanium plate used to stabilize the mandible. Tissue ingrowth is seen within both porous implants; for all implants, the original defect space appears well maintained with minimal tissue collapse or contracture. In (B) and (C), soft tissue discontinuities at the left (buccal) side of the implant capsule are due to embedding and processing artifacts. Scale bars represent 1 mm.

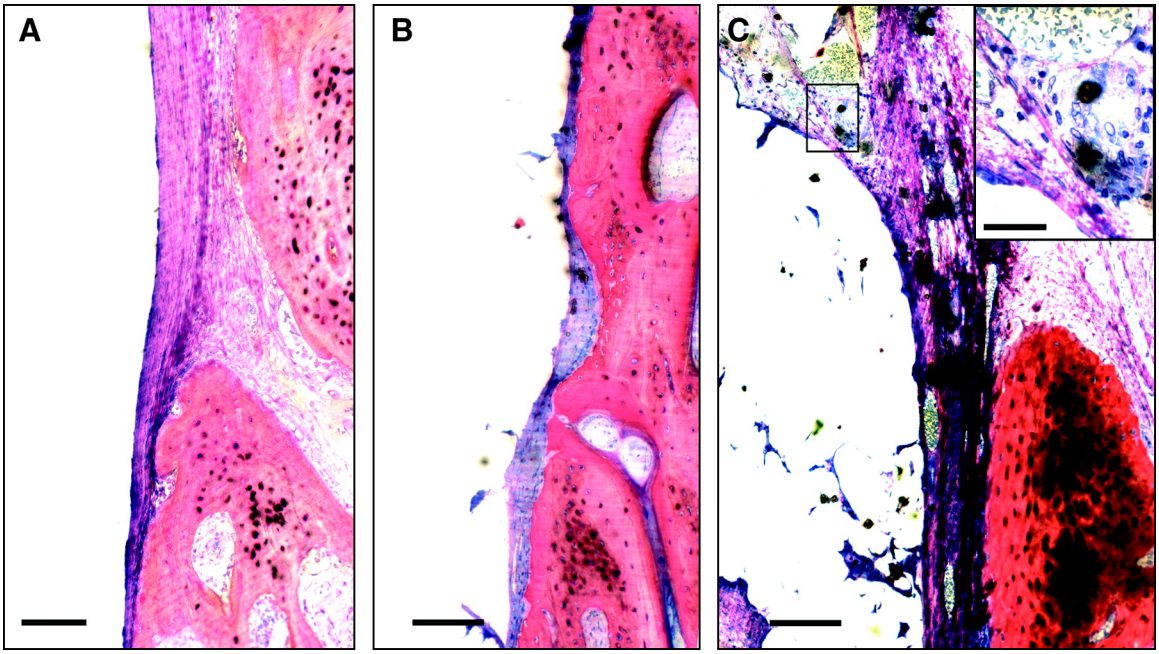

Figure 3.7. Representative light micrographs (200× magnification) of the lingual surface of coronally sectioned tissue samples through the center of the implanted (A) solid PMMA, (B) low-porosity, and (C) high-porosity space maintainers. Regenerated bone is seen near the surface of all implants. A well-formed capsule is seen in (A), while only a thin layer of loosely organized fibrous tissue is seen at the surface of the low-porosity space maintainer (B). An abundance of plasma cells is seen at the surface and penetrating the surface porosity (inset) of the highly porous space maintainer (C). Scale bars represent 100 µm for the larger images; the inset scale bar represents 25 µm.

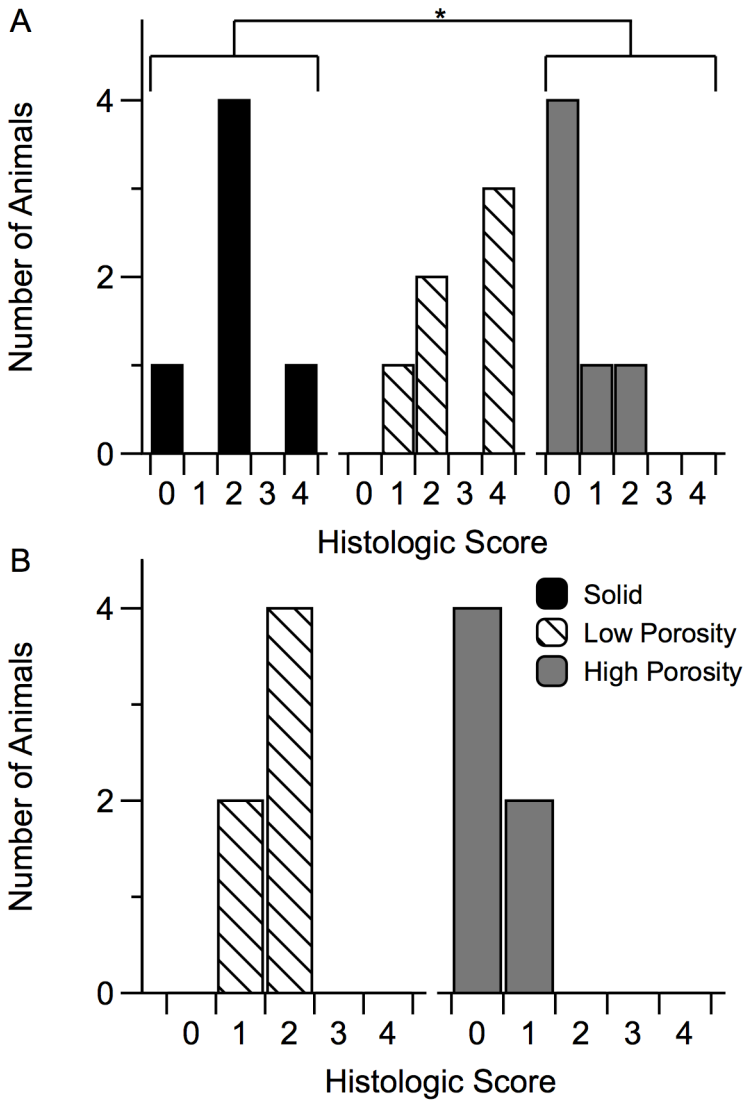

Figure 3.8. Score distributions for the graded (A) implant interface for all formulations tested *in vivo* and (B) tissue response within the pores for the two porous implant formualtions. Scoring criteriea are defined in Table 3.1. Significant differences ($p < 0.05$) between groups, denoted by asterisk, were determined using pairwise Dwass-Steel-Critchlow-Fligner tests for implant interface scoring (A) and a Mann-Whitney U-test for the tissue response within pores (B).

Chapter 4

In situ Formation of Porous Space Maintainers in a Composite Tissue Defect[‡]

Craniofacial defects present a complex set of injuries to repair due to the diversity of tissue form, function and type. Consequently, craniofacial trauma and tumor resections frequently result in composite defects, with greater than 90% of significant mandibular reconstructions involving an additional soft tissue defect [136]. Several studies have shown that the immediate reconstruction of craniofacial defects results in improved outcomes measured both aesthetically and functionally [71, 137-140]. However, the complication rates are greater for immediate reconstructions than for

[‡] This chapter was published as Spicer PP, Kretlow JD, Henslee AM, Shi M, Young S, Demian N, Jansen JA, Wong ME, Mikos AG, Kasper FK. "*In situ* Formation of Porous Space Maintainers in a Composite Tissue Defect." *J Biomed Mater Res A.* **100**, 827-833 (2012).

secondary reconstructions [141]. These complications typically involve the failure of a bone graft or the lack of viable soft tissue to support bone regeneration [141, 142].

Space maintenance alleviates many of these complications by allowing an alloplastic material to conserve the bony space, thereby preventing wound contracture and delaying bone regeneration within the defect until a suitable wound bed has been created. However, the implantation of bone grafts or synthetic graft materials commonly results in failure due to infection or wound dehiscence [126, 142-144]. Previous research has shown that porous materials for space maintenance or contouring lead to greater soft tissue integration and therefore decreased wound dehiscence relative to non-porous materials [50, 51, 132]. For example, in a study by Sclafani et al., the use of porous polyethylene implants led to decreased extrusion in a rat subcutaneous model [132]. Additionally, the skin healed more frequently after intentional exposure in the porous implants compared to solid silicone either by secondary intention or skin grafting [132]. Kretlow et al. investigated the tissue response to the implantation of porous PMMA space maintainers in a rabbit composite craniofacial tissue defect [50]. In this study, porous PMMA implants were fabricated by mixing PMMA bone cement with carboxymethylcellulose (CMC) gels, which created a porous structure through phase separation, as PMMA and CMC are hydrophobic and hydrophilic, respectively. Implantation of the porous PMMA constructs resulted in soft tissue healing with a reduced inflammatory response in the case of low porosity ($16.9 \pm 4.1\%$) implants as compared to those of high porosity ($44.6 \pm 2.1\%$). Additionally, in a study by Shi et al., PMMA/CMC constructs were evaluated mechanically compressively and found to have adequate properties to maintain the bony space with compressive moduli and 2.0% offset

strength of 262-586 MPa and 8-20 MPa, respectively.[15] However, while formulating a relationship between soft tissue healing and inflammatory response and the porosity of a space maintainer, the study by Kretlow et al. utilized prefabricated implants created in the laboratory with shape-specific molds. While prefabrication provides a controlled manner by which to evaluate eventual material parameters for scientific study, *in situ* polymerizable implants are important for clinical use as craniofacial defects non-uniform in shape and size. However for *in situ* polymerization any generated heat or unreacted monomer, as well as any variability due to intraoperative mixing, molding, and polymerization, can adversely affect the implant performance.

The present study investigates the biocompatibility of low porosity PMMA implants formed *in situ* as space maintainers in a rabbit composite craniofacial tissue defect. We hypothesize that low porosity space maintainers formed *in situ* will enhance soft tissue healing as compared to solid space maintainers formed *in situ*. We also hypothesize that low porosity space maintainers will not increase the inflammatory response of the hard and soft tissue surrounding the implants over solid space maintainers.

4.1. Materials and methods

4.1.1. Materials

Clinical grade bone cement (SmartSet High Viscosity Bone Cement, Depuy Orthopaedics, Warsaw, IN) was used as received. U.S. Pharmacopeia grade CMC

(Spectrum Chemical Manufacturing Group, Gardena, CA) was sterilized by exposure to UV light for 30 min.

4.1.2. Materials Preparation

Solid and porous PMMA implants were made as previously described [50, 145]. Briefly, CMC gels were made by dissolving sterilized CMC powder into sterile distilled water at 9 wt%. PMMA implants were prepared using the ratio (40 g of the powder phase to 18.88 g of the monomer phase of bone cement) set forth in the manufacturer's instructions and for the porous implants the CMC gel accounted for 30 wt% of the total implant. The porous implants had a porosity of 16.9 ± 4.1% and an interconnectivity of 39.7 ± 9.4%, 17.8 ± 1.2% and 13.1 ± 3.0% with a 40, 80 and 160 μm minimum interconnection size, respectively, as reported previously [50].

4.1.3. Surgical Procedure

22 adult male New Zealand White rabbits (Myrtle's Rabbitry, Thompsons Station, TN) aged greater than 6 months for skeletal maturity were used in this study. All manipulations followed protocols approved by the Institutional Animal Care and Use Committees of Rice University and the University of Texas Health Science Center at Houston and NIH guidelines for the care and use of laboratory animals (NIH Publication #85-23 Rev. 1985) have been observed. The surgical procedure was completed as described previously [50].

Briefly, anesthesia was induced with injection of a mixture of ketamine hydrochloride (40 mg/kg body weight) and xylazine hydrochloride (7.5 mg/kg body

weight). The rabbits were then intubated and maintained on 2% isoflurane in oxygen. Each animal was given a preoperative dose of buprenorphine hydrochloride (0.1 mg/kg body weight) for perioperative pain control and 0.5 mL Durapen® (150,000U/mL of penicillin G benzathine and penicillin G procaine each) for perioperative antimicrobial coverage. The animals were sterilely prepped and a midline incision, 1 cm posterior to the mentum, was used to expose the inferior border of the mandible. The masseter was lifted from the buccal surface of the body of the mandible. Using a 10 mm trephine (ACE Surgical, Brockton, MA) and a surgical drill (Stryker, Kalamazoo, MI), a 10 mm bicortical defect was created. Additionally, using a 701 cutting bur, a 2-3 mm notch was created in the superior border of the defect and the overlying crown removed to create intraoral communication and a mucosal defect as shown in Figure 4.1.

Solid implants (n=10) were prepared by mixing the liquid phase of the bone cement into the powder phase. Porous implants (n=10) were made by first mixing the powder phase (containing polymeric microparticles, benzoyl peroxide and barium sulfate) of the bone cement into the CMC gel, then mixing in the liquid phase (containing methyl methacrylate monomer and N,N-dimethyl-p-toluidine). All implants were mixed by hand until doughy and then shaped by hand to approximately fit the bone defect. The implants were placed into the bone defect approximately 5 min after initiation of polymerization (addition of liquid phase) and molded to fit once inside the defect as shown in Figure 4.1.

A 6-hole 1.5 mm titanium plate (Synthes, West Chester, PA) was attached with two screws on each side of the defect to prevent iatrogenic fracture of the mandible. Finally, the wound, except the mucosal defect, which was left open to allow for

continued oral communication, was closed in layers. Animals were given a postoperative intramuscular dose of ketoprofen for inflammation control. Each rabbit was extubated and closely monitored postoperatively. The animals were fed ad libitum with a diet of soft chow (Critical Care for Herbivores; Oxbow Pet Products, Murdock, NE) to reduce stress on the mandible.

4.1.4. Gross Observation

After 12 weeks, animals were euthanized with 1 mL of Beuthanasia-D® (390 mg/mL pentobarbital sodium and 50 mg/mL phenytoin sodium) and the hemimandible was extracted. The oral mucosa was observed grossly for complete coverage of the implant and bone. Each sample was assigned a healed or non-healed status based on this coverage, where exposure of bone or the implant was deemed non-healed and complete coverage was considered healed.

4.1.5. Histology

Each hemimandible was placed in 10% neutral buffered formalin for 72 hours. After fixation, each specimen was dehydrated using an ethanol gradient (70%-100%). The dehydrated samples were embedded in methylmethacrylate and three 10 μm sections were taken coronally through the center of the implant to include the mucosal defect using a microtome with an inner circular diamond blade (Leica Microsystems, Nussloch, Germany). The sections were stained with methylene blue and basic fuchsin to assess the soft tissue and hard tissue responses to the implant. The stained sections were scored by three reviewers (P.P.S., A.M.H. and F.K.K.) using a quantitative tissue-

implant scoring system for the tissue-implant interface and within the pores for porous samples as shown in Table 4.1 and as previously described [92]. Each sample received one score from a consensus of the reviewers based on the average of the three sections from the sample.

4.1.6. Statistical Analysis

Healing status based on gross observations was analyzed with Fisher's Exact Test, while histology scores, a nonparametric data set, were analyzed with the Mann Whitney-U Test. An a priori level of significance was set at $\alpha = 0.05$.

4.2. Results

4.2.1. Surgical Procedure

All rabbits underwent surgical manipulation and recovery well. Two rabbits were replaced within the study due to complications, resulting in 22 total rabbits, with 10 rabbits included in each group for analysis. Both complications were unrelated to the surgical manipulation or implantation and involved a foot problem and an abdominal infection.

4.2.2. Gross Observation

Representative gross images of healed and non-healed specimens from each group are shown in Figure 4.2. As shown in Figure 4.3, 6 out of the 10 rabbits that received solid implants and 3 out of the 10 that received porous implants were considered non-

healed based on the criteria described above. These results do not show significantly greater healing in the porous group ($p = 0.185$).

4.2.3. Histology

Representative histologic images from each group showing similar tissue responses for both solid and porous implants are shown in Figure 4.4. Histologic scoring, shown in Figure 4.5, revealed no significant difference between the solid and porous groups for the tissue-implant interface, although, as can be seen in Figure 4.4, the porous group did have several instances of direct interaction with the bone surface, a feature not seen in any solid implants. Additionally, the scores for the tissue inside the pores for the porous group are presented in Figure 4.5, reflecting the presence of primarily fibrous tissue.

4.3. Discussion

Early intervention has been shown to be advantageous in the reconstruction of craniofacial defects; however, the ultimate success of a bone regeneration technique applied early after bone excision or wound debridement may be limited, given the complexity of the tissue environment, need for critical care stabilization or availability of reconstructive surgeons at that time. Consequently, temporary placement of a material to support soft tissue healing around the defect can prime the wound bed to support the success of a subsequent definitive repair. Yet, current materials fail to properly integrate with the surrounding tissue to sustain healthy soft tissue healing during implantation in such space maintenance approaches.

In a previous study, our group found that, when fabricated *ex vivo,* porous PMMA constructs enhanced wound healing and elicited a favorable soft tissue response compared to solid constucts [50]. This approach, while a useful proof of principle, does not accurately reflect the intraoperative construct fabrication and implantation technique that would ideally be utilized to address complex craniofacial wounds. This study hypothesized that porous implants created in the operating room and formed *in situ* would enhance soft tissue healing over a bone defect in a composite tissue model compared to non-porous implants. Additionally, porous implants were hypothesized not to increase the inflammatory response of the surrounding tissue compared to non-porous implants, as evaluated by histology.

Porous implants showed a trend towards increased soft tissue healing of the composite defect, although differences were not statistically significant with the given sample size. This trend is consistent with previous studies using the same materials in prefabricated implants [50]. This result validates the use of porous PMMA space maintainers as an alternative to solid PMMA.

Histologically, the porous implants performed similarly to the solid implants with scores that were not significantly different. This finding indicates that the *in situ* formation of porous space maintainers does not increase the inflammatory response of the surrounding tissue as could be postulated based on the potential for inflammatory stimuli, such as thermal energy release during polymerization or exposure to unpolymerized monomer.

The composite tissue defect used in this study separates the healing of a soft tissue defect over an implant from the inflammatory response of the tissue to the implant, which allows for study of the gross soft tissue healing over such implants. Additionally, this study perpetuates the enhancement of soft tissue healing over porous space maintainers in a clinically relevant scenario using clinically available materials, validating the process and procedure for fabricating porous space maintainers *in situ*. However, while separating the effects of solid and porous implants formed *in situ*, the presence of materials is less controlled. In the study by Kretlow et al., the CMC gel porogen was leached from the prefabricated implants prior to implantation, whereas this phase was included in the implants in the present study [50]. While the effect on soft tissue to the implant could be altered by the presence of CMC, previous in vitro studies have shown that the dissolution of CMC out of the implant occurs very rapidly, thus minimizing the duration of immediate tissue contact. Moreover, while this model includes a composite defect more similar to that of craniofacial trauma or resection, the possibility of dehiscence is limited to the mucosal surfaces, as the implant is surrounded by bone on all other sides. Skin dehiscence is an important complication of craniofacial reconstruction, and further studies would be necessary to elucidate any differences between the soft tissue healing in a composite defect with a skin defect.

Previous studies have investigated the *in situ* polymerization of PMMA in contact with bone. Many of the studies have focused on the temperature rise and the residual monomer release from the implants, both of which have been shown to contribute to increased inflammatory responses in the tissue immediately adjacent to the PMMA implanted [146-150]. Several studies have shown decreased setting temperature of

porous PMMA versus solid PMMA, as there is reduced monomer per unit volume as well as a non-reacting phase acting as a heat sink [104, 145]. Similar to this study, where the solid and porous groups performed similarly histologically, a 14 week study by Nathanson et al. and a 12 week study by Kretlow et al. showed no difference in histological assessment of solid or porous implants at the end time point [50, 100]. Contrary to these studies, van Mullem et al. observed porous implants with 50 wt% of CMC gel as the porogen were surrounded by well-vascularized fibrous tissue, while solid implants had a thick fibrous capsule in a long term study of 8 and 24 months, indicating the possibility for further remodeling of the surrounding tissue in the porous implant group, which could differentiate the histological scores [90].

The hypothesis that porous implants enhance tissue remodeling around the implant is supported by studies investigating the role of surface structure on tissue interfaces. These studies have shown a response dependent on surface roughness, where increased surface roughness leads to greater remodeling of the surrounding tissue [151, 152]. In addition, these studies indicate the possibility for greater bone remodeling for rough surfaces over smooth surfaces, as increased bone deposition is seen when cultured with osteoblast like cells and increased osteoclastic activity when cultured with macrophages.

In addition to surface characteristics, PMMA particulates play an important role in the inflammatory response, as they have been shown to increase macrophage activation and release of tumor necrosis factor-alpha, a cytokine that enhances bone resorption when produced chronically [153-156]. In a study by Beck and Boger, PMMA particulate release was observed to be greater for porous PMMA than for

solid PMMA [134]. While these particulates may play a role in the remodeling process of the tissue surrounding the porous implants, the histological results from the present study indicate no difference, suggesting the effect of surface characteristics balances that of particulates.

In addition to effects described above regarding the advantages of porous structures for soft and hard tissue integration, interconnected porous structures increase the surface area available for drug delivery. In space maintenance, drug delivery can be used to prime the wound bed by treating any infection present [145, 157]. Alternatively, growth factors could be used to enhance the regeneration of soft tissue or vascularity around the implant.

While this study validates the effectiveness of porous space maintainers in a more clinically relevant model and formation process, further studies could be warranted to elucidate the effects observed. Firstly, an increase in animal numbers could be utilized to determine the significance of the mucosal healing or histological differences. As stated above, moving from prefabricated implants to those formed intraoperatively, several parameters are changed: *in situ* polymerization, exposure to unpolymerized monomer, and presence of the porogen, CMC. To adequately understand the effect of each of the parameters, further study would be necessary, such as investigation of a prefabricated implant from which the porogen had not been leached prior to implantation. Additionally, wound dehiscence, while more common on the mucosal surface of mandibular implants, can occur on the skin surface. The intact inferior border of the mandible does not allow for testing of this possibility, while a continuity defect of the mandible would provide such an analysis. Nevertheless, the

present study supports the use of porous space maintainers for the treatment of composite tissue defects in the craniofacial region.

4.3.1. Conclusion

This study analyzed the effects of porous PMMA space maintainers formed *in situ* on the mucosal healing and long term tissue response in a rabbit composite mandibular defect model against similarly formed solid implants. The porous implants showed a trend of enhanced soft tissue healing and coverage of the implant over solid groups. Additionally, the increased surface area and presence of porogen did not elicit an extended inflammatory response over the solid implants.

4.4. Tables and Figures

Table 4.1. Histologic scoring system for implants at the implant-tissue interface as well as in the pores of the porous implants.

Hard tissue response at the implant-bone interface	Score
Direct bone-to-implant contact without soft interlayer	4
Remodeling lacuna with osteoblasts and/or osteoclasts at surface	3
Majority of implant is surrounded by fibrous tissue capsule	2
Unorganized fibrous tissue (majority of tissue is not arranged as capsule)	1
Inflammation marked by an abundance of inflammatory cells and poorly organized tissue	0
Hard tissue response within the pores of the scaffold	
Tissue in pores is mostly bone	4
Tissue in pores consists of some bone within mature, dense fibrous tissue and/or a few inflammatory response elements	3
Tissue in pores is mostly immature fibrous tissue (with or without bone) with blood vessels and young fibroblasts invading the space with few macrophages present	2
Tissue in pores consists mostly of inflammatory cells and connective tissue components in between (with or without bone) or the majority of the pores are empty or filled with fluid	1
Tissue in pores is dense and exclusively of inflammatory type (no bone present)	0

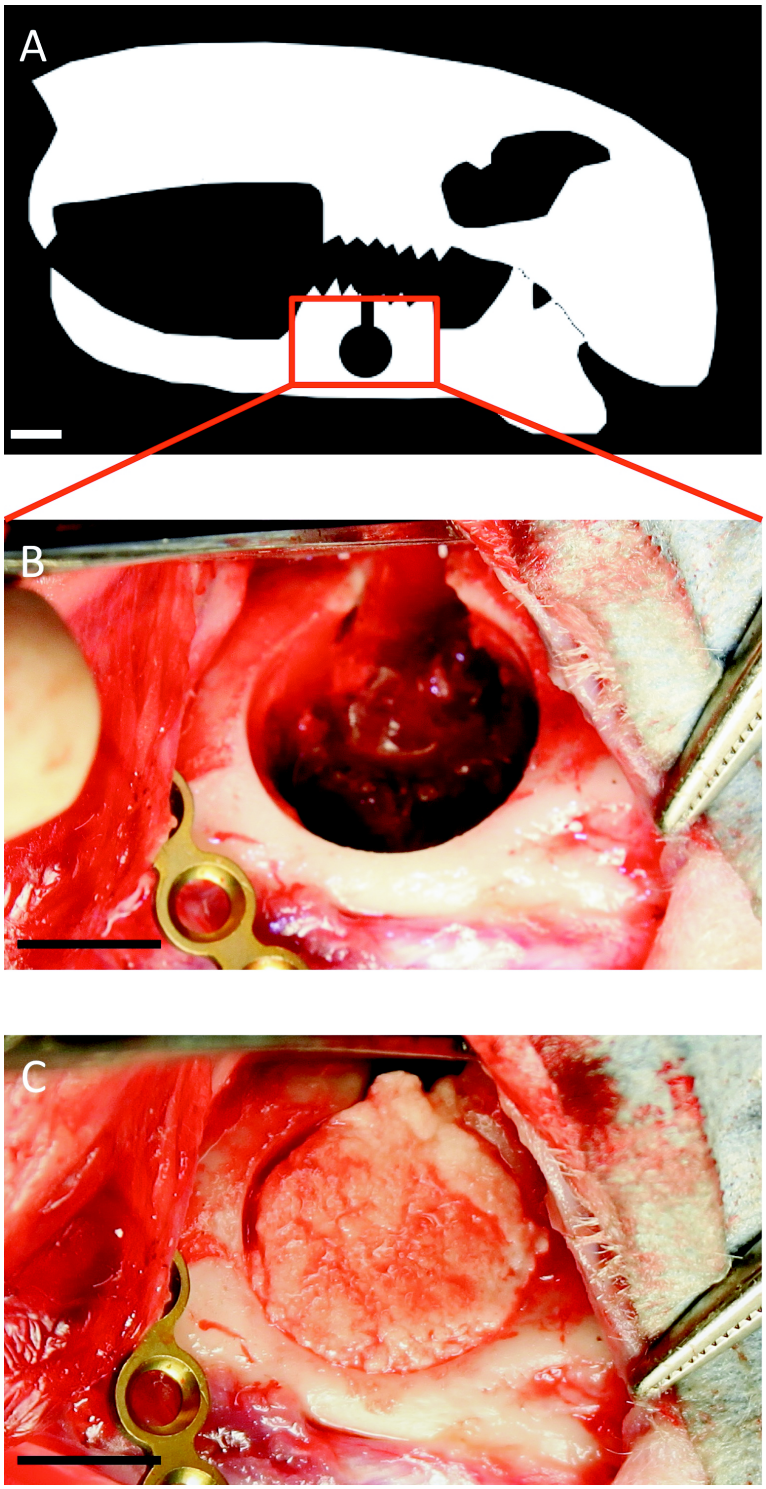

Figure 4.1. Schematic (A) and photograph (B) of defect in rabbit mandible (scale bars indicate 10 mm and 5 mm, respectively). Photograph (C) of rabbit mandibular defect filled with a porous implant (scale bar indicates 5 mm).

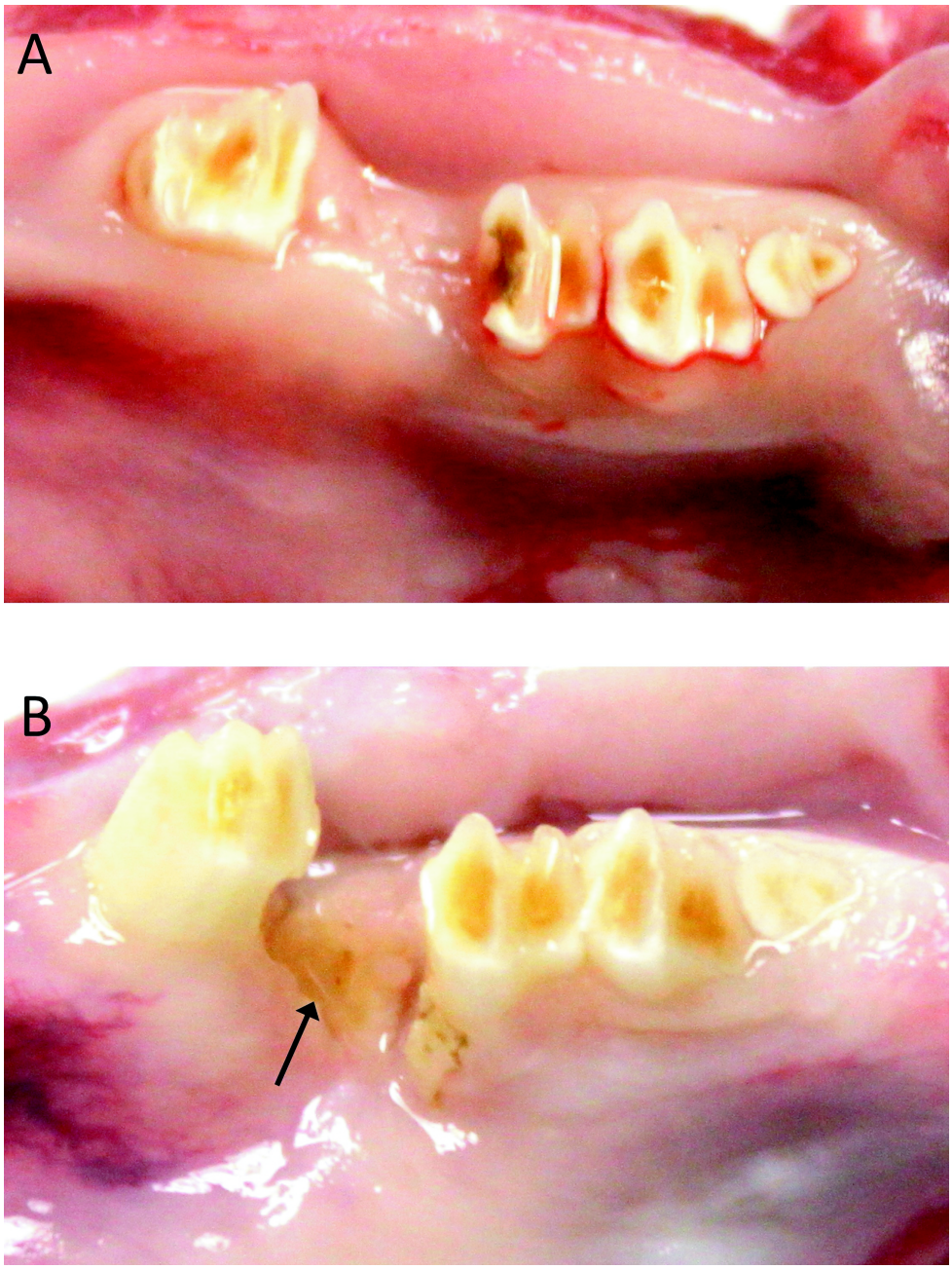

Figure 4.2. Photographs of the oral mucosa over the composite defect for (A) a well-healed porous implant and (B) a poorly healed, exposed solid implant after 12 weeks of implantation. The black arrow indicates implant exposure.

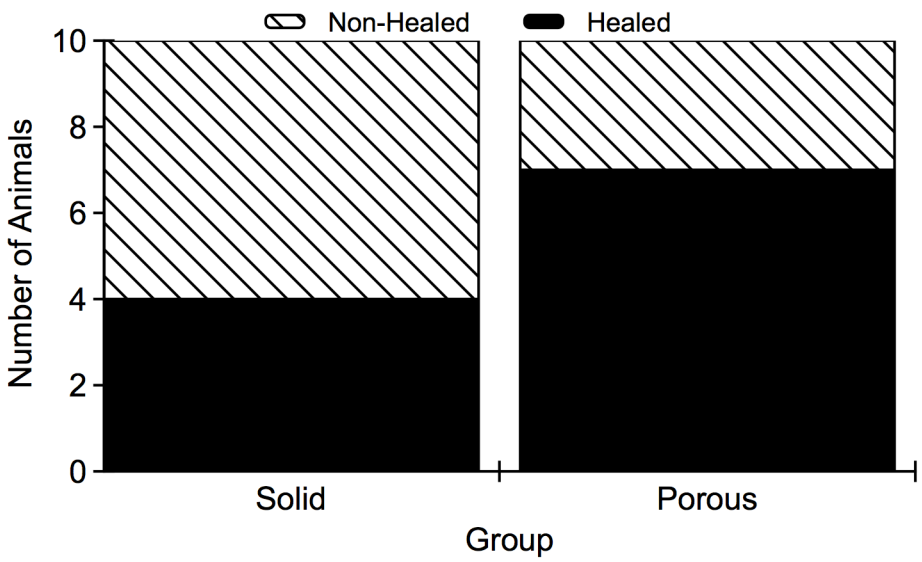

Figure 4.3. Number of implants with healed and non-healed oral mucosa for solid and porous implants after 12 weeks of implantation (n = 10 for each group).

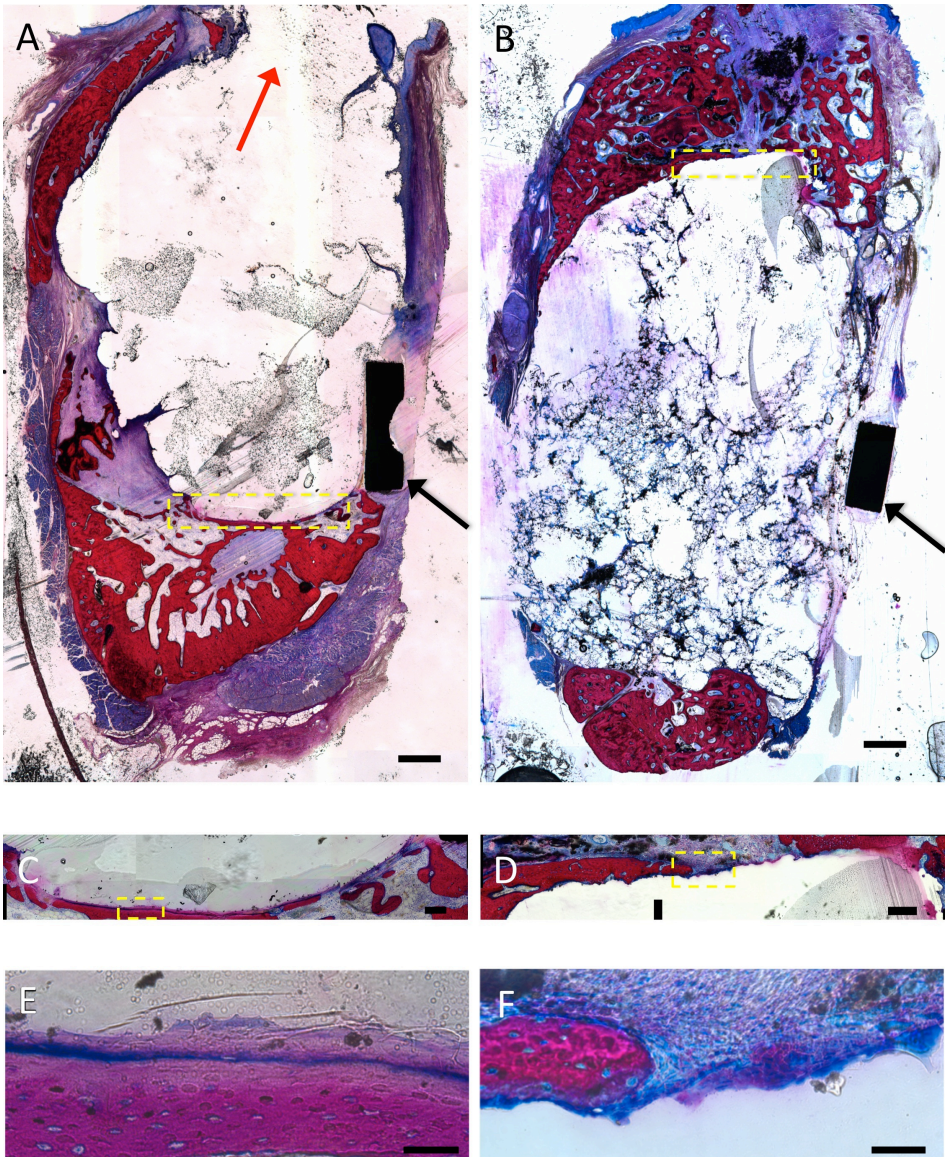

Figure 4.4. Representative images (1000 µm scale bar) from (A) the solid implant group and (B) the porous implant group with higher magnifications, highlighted in yellow, (200 µm scale bar) of each (C) and (D), respectively. Histologic scores were made using magnifications shown in images (A-D). Additional higher magnification images (C) and (D), highlighted in yellow, are shown in (E) and (F), respectively (50 µm scale bar). The solid implant shown was scored as a 1 according to Table 4.1, as an unorganized fibrous capsule was present around the majority of the implant (A and C). The porous implant shown was scored as a 2 due to the presence of an organized fibrous capsule, based on the magnifications shown in (B and D). Black arrows show the titanium plate. Red arrow indicates dehiscence.

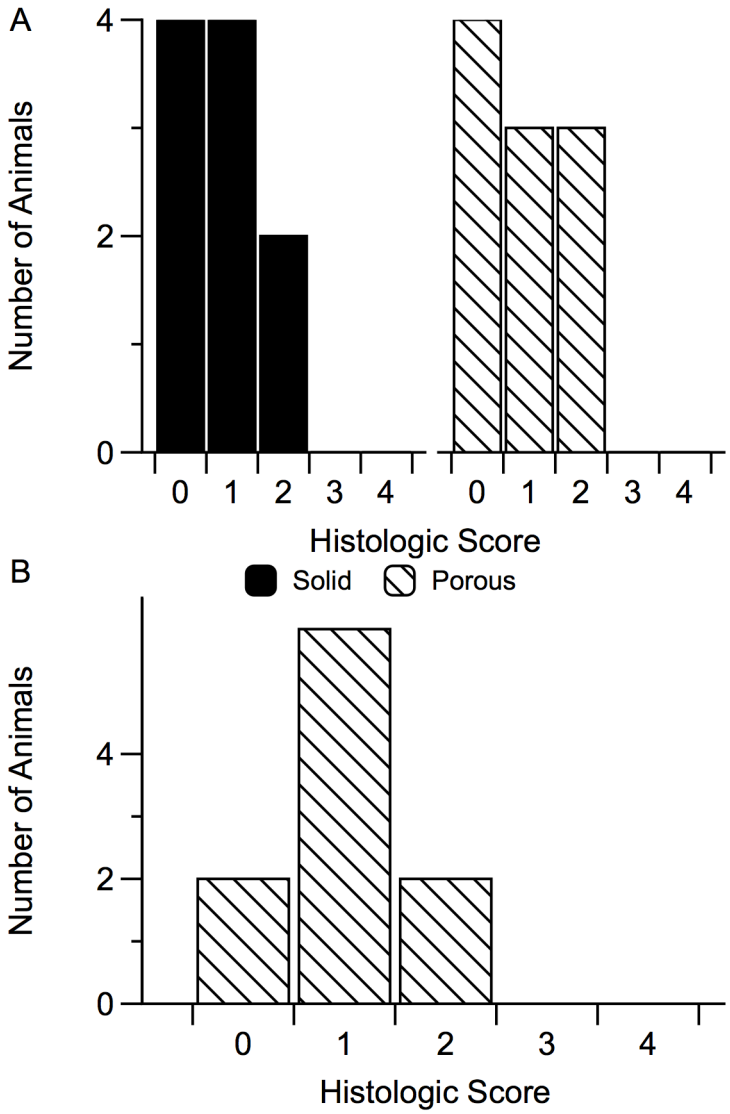

Figure 4.5. Histologic scores of the inflammatory response at the (A) tissue-implant interface of solid and porous implants and (B) the tissue in the pores of the porous implants. There was not a significant difference between the solid and porous groups as determined by the Mann-Whitney U test.

Chapter 5

Antibiotic-releasing Porous Polymethylmethacrylate/Gelatin/Antibiotic Constructs for Craniofacial Tissue Engineering[‡,*]

Traumatic injuries in the craniofacial area are one of the most debilitating forms of injury due to the important aesthetic and functional role of the craniofacial complex [12]. Using current technologies, traumatic craniofacial bone injuries accompanied by local infection, significant vascular injury, and large-scale tissue devitalization (e.g., those encountered on the battlefield) involve a staged repair [158]. Tissue engineering approaches to regenerating the devitalized tissues is usually delayed until soft tissue

---

[‡] This chapter was published as Shi M, Kretlow JD, Spicer PP, Tabata Y, Demian N, Wong ME, Kasper FK, Mikos AG. "Antibiotic-releasing Porous Polymethylmethacrylate/Gelatin/Antibiotic Constructs for Craniofacial Tissue Engineering." *J Control Release.* **152**, 196-205 (2010).

[*] The doctoral candidate performed portions of this work including fabrication of constructs and *in vitro* antibiotic release.

coverage and a sterile wound environment are achieved [72]. One of the major challenges faced by reconstructive surgeons is contracture and scarring of the overlying soft tissue envelope before definitive reconstruction, which compromises the restoration of functional characteristics of the affected region and makes the aesthetic restoration particularly challenging. Over the course of a staged reconstruction, the placement of a temporary space-maintaining implant may eliminate many of the aforementioned complications [50, 75, 159].

Towards the goal of treating traumatic craniofacial injuries with significant bone/tissue loss and active/latent infection, our laboratory is developing a two-stage regenerative medicine approach that initially uses an alloplastic implant (i.e., a space maintainer) to not only maintain the void space but also to prime the wound site (e.g., promote tissue healing/coverage and address local infections) for later, definitive reconstruction [50, 145]. The deliberate maintenance of the bony space prevents distortion of surgical landmarks, wound contracture into the space, and fibrosis of the tissue bed [50, 75]. Successful space maintenance creates a soft tissue envelope with preserved volume and well-healed surrounding tissues, ideal for the placement of a tissue engineered construct designed for bone regeneration during the subsequent reconstruction stage [75]. To fulfill these functions, a porous space maintainer is favorable because fibrovascular and other soft tissues can potentially grow into the surface pores to promote wound/tissue healing [50, 86, 103, 160-163]. Tissue ingrowth into the pores also creates a stable interface to anchor the implant to the host tissues, possibly preventing the wound dehiscence encountered when using a solid implant [50]. Additionally, a space maintainer capable of local antibiotic delivery can potentially eliminate infection-associated

complications during the space maintenance phase and later reconstruction. Infections following traumatic injuries (including combat wound infections and osteomyelitis, a bone infection usually associated with severe fractures exposed to environmental bacteria) are a common occurrence [72, 159, 164-166]. Active and latent posttraumatic and postsurgical infections may potentially hinder wound healing and tissue regeneration, underscoring the importance of effective, early eradication/prevention of infection through the use of antibiotics. Given that most supporting materials lack the capacity to release drugs in a precisely controlled manner, incorporating a drug delivery system into the space maintainer (which is capable of controlled antibiotic release during the space maintenance phase) becomes an important strategy [145].

Previously we have demonstrated that a porous polymethylmethacrylate (PMMA) construct with porosity imparted by incorporating a carboxymethylcellulose (CMC) hydrogel phase successfully maintained the bony space within a nonhealing rabbit mandibular defect model and provided a template for improved wound healing when compared to solid PMMA implants [50]. To modify this system enabling local drug delivery, drug-loaded poly(lactic-*co*-glycolic acid) (PLGA) microspheres were also incorporated into the PMMA/CMC constructs, creating porous constructs capable of extended antibiotic delivery [145].

Simplifying these porous PMMA constructs by incorporating a porogen and particulate drug carrier, we further developed a gelatin microparticle (GMP)-incorporating PMMA construct (i.e., a PMMA/gelatin/antibiotic construct) in which the GMPs serve as both drug carrier and porogen (Figure 5.1).

Gelatin is derived from collagen, a natural polymer that is the major constituent of skin, bone and connective tissue. Used in pharmaceuticals, wound dressings and adhesives, gelatin has a number of desirable biomaterial properties (e.g., biodegradability, biocompatibility and biosafety) [167-170]. As a protein, gelatin has a high content of amino acids such as glycine, proline, and hydroxyproline that potentially accelerate soft tissue healing, making gelatin particularly attractive as a major component of a space maintainer for promoting tissue healing and coverage. With respect to drug delivery, the highly hydrophilic gelatin absorbs drug solution upon contact to form a hydrogel. The loose gel matrix is able to immobilize drug molecules and subsequently control drug release by a diffusion or degradation-controlled mechanism [168].

In PMMA/gelatin/antibiotic constructs, the GMPs are loaded by absorbing the drug solution while swelling to form a particulate hydrogel. This hydrogel is then dispersed within the PMMA polymer phase, creating porosity during the curing of PMMA (Figure 5.1). In practice, the assembly of PMMA bone cement, GMPs, and antibiotic drug can be completed within minutes using a simple mixing procedure. Such an approach provides great flexibility with respect to the material composition during the course of fabrication: the type and amount of antibiotic can be decided at the time of fabrication based on a specific clinical need, and the physical properties of constructs (e.g., porosity and mechanical strength) can be tailored to meet the requirements of space maintenance and drug release kinetics. The system is a simple combination of materials with United States Food and Drug Administration (FDA) history. PMMA bone cement is FDA-approved for adhering prosthesis to bone, kyphoplasty and repairing cranial defects [171, 172]. Gelatin-based/containing products have been approved by FDA for

commercial use [173, 174]. Given the ease of practical handling and FDA-regulatory status of each component, the PMMA/gelatin/antibiotic construct engineered for clinical applications has the potential to transition readily from experimental research into clinical use.

The aim of the present *in vitro* study was to elucidate the influence of material composition on PMMA/gelatin/antibiotic construct physicochemical properties and provide predictive insight into the expected space maintenance and drug delivery capability of these space maintainers over time *in vivo*. Specifically, colistin, a polymyxin antibiotic, was chosen to address infections with *Acinetobacter* species [175, 176], the most common pathogen associated with combat-related traumatic injuries [165, 166, 177, 178]. It was hypothesized that the overall porosity (which impacts tissue ingrowth as well as drug release from the space maintainer) would be tailored by the percent of gelatin incorporated and the gelatin swelling, as controlled by varying the weight ratio of drug solution versus gelatin. To test these hypotheses, five formulations of PMMA/gelatin/antibiotic constructs with swelling ratio (3:1, 4:1, or 5:1 drug solution : gelatin by weight), gelatin incorporation (15 or 20 wt% in the polymer phase), or drug loading (15 or 20 wt% in GMPs) were investigated for drug release kinetics over 2 weeks. The construct morphology, porosity, compressive mechanical property, and degradation were also examined over a period of 12 weeks.

5.1. Materials and Methods

5.1.1. Materials

Gelatin (isoelectric point, IEP = 9) was obtained from Nitta Gelatin Corporation (Osaka, Japan). Colistin sulfate salt was purchased from Sigma-Aldrich (St. Louis, MO). Clinical PMMA bone cement (SmartSet®, High Viscosity) from DePuy Orthopaedics Inc. (Warsaw, IN) was used. The bone cement formulation is supplied as a two-component system, consisting of separate liquid and powder components. The liquid component consists mainly of MMA monomer with hydroquinone as a stabilizer. The powder component contains a PMMA based polymer with the initiator benzoyl peroxide and the radiopaque agent zirconium dioxide. All other reagents were purchased from Sigma-Aldrich (St. Louis, MO) and used as received.

5.1.2. Preparation of gelatin microparticles

Chemically crosslinked GMPs were fabricated via a water-in-oil-emulsion process followed by glutaraldehyde crosslinking in aqueous solution [179]. Briefly, gelatin (5 g) was dissolved in double-distilled water at a concentration of 10 w/v% and added dropwise to 250 ml olive oil (containing 0.5 v/v% Span 80 as stabilizer) to create a water-in-oil emulsion under stirring at 500 rpm. The solution was chilled by ice water and stirred for 30 min. The solution was then added to 100 ml chilled acetone and stirred for another 1 h. GMPs were then collected by washing with chilled acetone and vacuum filtration. The GMPs were allowed to air dry and then dispersed into 500 ml double distilled water containing 0.1 v/v% Tween 80 as stabilizer and 10 mM glutaraldehyde for

chemical crosslinking. The reaction was continued for 20 h and then terminated by the addition of glycine (25 mM) to block residual aldehyde groups. The microparticles were washed by chilled double-distilled water and then acetone and collected by filtration. The air-dried microparticles were then quickly frozen with liquid nitrogen and lyophilized for 24 h. The lyophilized GMPs were sieved through a mesh with 250 μm pores to remove undesired aggregations.

The morphology of dehydrated GMPs was characterized by scanning electron microscopy (SEM). The dry microparticles were sputter-coated with gold for 40 s at 100 mA using a CrC-150 sputtering system (Torr International, New Windsor, NY) and observed under a FEI Quanta 400 field emission scanning electron microscope (FEI Company, Hillsboro, OR) at an accelerating voltage of 10 kV.

To study the swelling behavior of GMPs in varying amount of phosphate buffered saline (PBS) solution, dry microparticles were swollen in PBS buffer (pH 7.4) at weight ratios of 3:1, 4:1, 5:1, 7:1 or excess (infinite). The swollen microparticles were observed under a light microscope (Nikon microscope, Eclipse E600, Japan) immediately. The diameter of the swollen microparicles in each image was measured using Image-Pro Plus 5.1 software (Media Cybernetics Inc., Bethesda, MD). Each measurement took the average diameter of over 100 particles. The mean diameter of swollen microparticles was expressed as mean ± standard deviation for n=3 separate swelling experiments.

5.1.3. Preparation of gelatin-incorporating PMMA constructs

Antibiotic-releasing porous PMMA/gelatin/antibiotic constructs were fabricated by the sequential assembly of GMPs, antibiotic drug, and a clinical grade PMMA bone cement (Figure 5.1). The incorporation of GMPs (15 wt% or 20 wt% of dry GMPs relative to the polymer phase of gelatin+PMMA+MMA), the swelling ratio of drug solution versus GMPs (3:1, 4:1, or 5:1 by weight), and the drug loading in the GMPs (15 wt% or 20 wt%) were varied to tailor the bulk porosity and drug content of the constructs. The weight of powder components (gelatin, drug and PMMA) and volume of liquid components (PBS solution, MMA) were predetermined based on the composition. The components were assembled according to the following procedure: the antibiotic drug was first dissolved in PBS solution. This solution was then added dropwise to the dry GMPs which absorbed the solution to form swollen microparticles. These drug-loaded GMPs were then immediately dispersed (or incubated at 37ºC for 1 h or 24 h before dispersing) in the PMMA powder by manually stirring the mixture. The monomer liquid was then added into the mixture and the two phases were mixed carefully to facilitate uniform distribution of the monomer while minimizing air entrapment. After reaching a dough-like consistency (approximately 90 s), the mixture was inserted into custom fabricated Teflon molds (sized as described below depending on the type of testing to be performed) and allowed to harden at ambient temperature (21°C) for 30 min. After removal from the molds, the cured constructs were used directly for *in vitro* drug release characterization or were lyophilized prior to drug release. The constructs were lyophilized prior to the characterization of porosity, compressive strength, and internal morphology by SEM.

The compressive mechanical properties of cylindrical constructs (6 mm in diameter, 12 mm in height, n=6-8) were measured in accordance with ISO5833 [180] using a mechanical testing machine (MTS, 858 Mini Bionix, Eden Prairie, MN) [145]. The offset compressive yield strength was determined as the stress at which the stress–strain curve intersected with a line drawn parallel to the slope defining the modulus, beginning at 2.0% strain (based on ISO5833).

Cylinders 10 mm in diameter and 6 mm in height, as designed for a previously developed rabbit mandibular defect model [50, 94], were used for the *in vitro* drug release and degradation study.

5.1.4. *In vitro* drug release

An *in vitro* drug release study was carried out in triplicate at 37°C in PBS buffer (pH 7.4) containing bacterial collagenase 1A — an enzyme that recognizes and digests part of the gelatin amino acid sequence [181]. A concentration of 400 ng/ml collagenase 1A was utilized in this study to model the tissue collagenase concentration in the synovial fluid mimicking that found following surgical trauma or in the presence of osteoarthritis [182-184]. Each construct was incubated in 5 ml PBS-collagenase buffer under mild shaking. At predetermined time intervals, the release medium from each sample was completely removed and replaced with fresh PBS-collagenase buffer. The release medium was filtered with a 0.2 μm filter. The colistin concentration in the release medium was determined using a high-performance liquid chromatography (HPLC) system consisting of a Waters 2695 separation module and a 2996 photodiode array

detector (Waters®, Milford, MA) [145]. The separation was performed using an XTerra® RP 18 column (250 cm × 4.6 μm, Waters®) at a column temperature of 45°C and flow rate of 0.5 ml/min in a mobile phase consisting of acetonitrile (HPLC grade with 0.1 vol% trifluoroacetic acid) and water (HPLC grade with 0.1 vol% trifluoroacetic acid). Peaks were eluted with a linear gradient of 5–65% acetonitrile in water over 20 min. Absorbance was monitored at λ = 214 nm. The two main components colistin A and colistin B were eluted at approximately 16.2 min and 16.9 min, respectively. Standard solutions with colistin in PBS buffer (pH 7.4) were tested in the range of 5–1000 μg/ml. Calibration curves were obtained using the combined peak area of colistin A and colistin B versus the colistin concentration.

The daily release of colistin was calculated from the absolute amount of colistin released between three or four consecutive days divided by the corresponding release time as well as the construct volume, and was expressed as μg colistin/ml construct/day [145]. The cumulative release (%) was expressed as the percent of total colistin released over time.

5.1.5. Degradation of PMMA/gelatin/antibiotic constructs

PMMA/gelatin/antibiotic constructs were degraded over a period of 12 weeks. Each construct was incubated in 5 ml PBS-collagenase buffer under mild shaking. At predetermined time intervals, the release medium from each sample was completely removed and replaced with fresh PBS-collagenase buffer. The degraded constructs were washed with double-distilled water and lyophilized for testing to determine the change of

porosity with degradation. The bulk porosity of each construct before and after degradation was determined using a microcomputed tomography imaging system.

5.1.6. Microcomputed tomography (microCT)

A SkyScan 1172 microCT imaging system (Aartselaar, Belgium) was used to perform nondestructive imaging and quantify the 3D microarchitectural morphology of original and degraded constructs [145]. The samples (n=3) were imaged with an X-ray tube voltage of 40 kV and current of 250 mA without a filter. Volumetric reconstruction and analysis were conducted using the software NRecon and CTAn provided by SkyScan [145].

5.1.7. Statistical analysis

To compare *in vitro* colistin release at a single time point, porosity, and compressive modulus, single-factor analyses of variance (ANOVA) with a 95% confidence interval ($p<0.05$) were performed. In the case of statistically significant differences, Tukey's post hoc test was conducted. Data are presented as means ± standard deviation.

5.2. Results

5.2.1. Gelatin microparticles

Dehydrated microparticles had a dense polymer structure after fabrication (Figure 5.2A), which, upon contact with PBS solution, swelled immediately forming hydrogel

microparticles (Figure 5.2B). The mean diameter of swollen microparticles (20.5±1.6-26.8±2.5 μm) is greater than that of dehydrated particles (15.2±0.4 μm) ($p<0.05$). The mean microparticle diameter increased with increasing weight ratios of PBS solution versus gelatin ($p<0.05$), suggesting an increase in the total volume of swollen GMPs with greater amounts of PBS solution present for swelling. When a swelling equilibrium was likely reached at 5:1 or higher weight ratio of PBS solution versus gelatin, the mean diameter of swollen gelatin particles remained relatively constant (Figure 5.3).

5.2.2. Microparticle-incorporating PMMA/gelatin/antibiotic constructs

The GMPs with swelling ratio of 3:1, 4:1 and 5:1, which covered a wide range of particle size, were used for incorporation into PMMA cement. Curing of the mixture occurred when the initiator in the powder phase started polymerization of the reactive MMA monomer, thus trapping the gelatin hydrogel microparticles within the polymerizing matrix and yielding various drug loadings and porosities depending on the material composition (Table 3.1 and Figure 5.4).

Cross sections of gelatin-incorporating PMMA constructs are shown in the SEM images (Figure 5.4A). All constructs were porous with the GMPs homogenously distributed within the PMMA polymer phase. MicroCT analysis yielded 2D cross sections (Figure 5.4B), which showed a uniform pore distribution. By visual inspection, the structure became looser and the pores were more extensively interconnected with increasing porosity. MicroCT was also used to nondestructively quantify the porosity (Figure 5.4B inset data) and interconnectivity (Table 5.1). The bulk porosity of constructs was tailored by the amount of gelatin incorporated and the amount of drug solution added

for gelatin swelling (Table 5.1and Figure 5.4). Greater drug solution addition (higher weight ratio of drug solution versus gelatin) led to significantly higher porosity (e.g., the porosity increased from 9.3±1.4% to 27.0±1.5% when the swelling ratio of drug solution versus gelatin increased from 3:1 to 5:1 by weight, $p<0.05$). Increasing gelatin incorporation (20 wt% versus 15 wt%) also resulted in significantly greater porosity when the weight ratio of drug solution versus gelatin was fixed ($p<0.05$). Varying drug loading in the microparticle phase did not alter the porosity ($p>0.05$). The pore interconnectivity (determined by microCT with a 40 μm minimum connection size) correlated closely with the porosity (Table 5.1). The constructs containing higher amounts of aqueous phase (G15D15S5:1 and G20D15S4:1) and thus significantly higher porosities than the other three formulations, featured extensively interconnected pore structures (49.0±6.7% and 51.4±1.8%, respectively), suggesting that approximately half pores in the each construct were connected to their outside environment through openings of at least 40 μm.

As shown in Table 5.1, the weight percent of drug in the construct was affected by both the gelatin incorporation in the construct and the drug loading in the GMPs. Generally, higher gelatin incorporation in the construct or higher drug loading in the microparticles resulted in a greater weight percent of drug incorporated in the construct. With the same weight percent of gelatin incorporation and microparticle drug loading, the construct drug content per unit volume depended on the porosity (which correlated to the density of constructs). Constructs with lower porosity had higher amounts of drug per unit volume (mg drug/ml construct). The five formulations investigated in this study featured a drug content 2.6-3.6 wt%, or 18.2-28.3 mg/ml construct (Table 5.1).

The compressive moduli and offset yield strengths (2.0% offset) were determined based on ISO5833 (Table 5.1). The compressive moduli of porous PMMA/gelatin/antibiotic constructs varied between 180±30 and 450±30 MPa depending on the bulk porosity of constructs, with the higher porosity constructs having lower compressive moduli. The compressive moduli of PMMA/gelatin/antibiotic constructs were 6-15 fold lower than that of solid PMMA (2670±220 MPa). The offset yield strengths of PMMA/gelatin/antibiotic constructs had similar porosity dependence and were lower than that of solid PMMA ($p<0.05$).

5.2.3. *In vitro* colistin release

Colistin release from the PMMA/gelatin/antibiotic constructs was studied *in vitro* immediately after fabrication. As shown in Figure 5.5 and Figure 5.6, where the colistin release was described as average drug release rate per day (μg colistin/ml construct/day) as well as % cumulative drug release, all five formulations of PMMA/gelatin/antibiotic construct achieved continuous colistin release over 10 or 14 days with the drug release rate higher than 10 μg/ml construct/day. The drug release duration and drug release rate were dependent on both the construct composition (Figure 5.5 and Figure 5.6) and the fabrication procedure (Figure 5.7 and Figure 5.8).

When the porosity was tailored by gelatin swelling ratio (with the drug loading in the GMPs fixed at 15 wt%), the constructs with lower porosity had reduced initial burst (both % and μg/ml/day) and relatively longer release durations (Figure 5.5). For example, the construct G15D15S3:1 (porosity 9.3±1.4%) released colistin over 14 days. The constructs G15D15S4:1 (porosity 15.6±1.8%) and G15D15S5:1 (porosity 27.0±1.5%),

which featured significantly higher porosities, achieved relatively shorter release durations of 10 days. Notably, the drug release rate of the construct G15D15S3:1 remained the highest after day 1 (Figure 5.5) ($p<0.05$), although its % cumulative release was significantly lower relative to the other two formulations after 14 days release ($p<0.05$).

When comparing the drug release from two constructs with different drug loadings but the same porosity (i.e., G15D15S4:1 and G15D20S4:1), a constantly greater rate of drug was released by the construct with the higher drug loading until day 3 ($p<0.05$). The release duration, however, was not altered by the drug loading (Figure 5.6). If both the porosity and the drug loading of one construct were significantly greater than those of another, the porosity played a more important role in modulating drug release (Figure 5.6). For example, the construct G20D15S4:1 featured greater porosity (29.4±0.9%) and higher drug loading (23.8 mg/ml) than G15D15S4:1 (porosity 15.6±1.8%, and drug loading 20.6 mg/ml). The drug release rate of G20D15S4:1 was significantly greater on the first day, but much lower after day 1 (i.e., the construct with higher porosity featured greater initial burst) (Figure 5.6) except on day 10 ($p<0.05$).

To elucidate whether incubating the drug-loaded GMPs at 37ºC for various periods prior to mixing with the PMMA cement will strengthen the association between the gelatin and drug, therefore impacting the release kinetics of constructs, the colistin release of G15D15S4:1 (which was fabricated by immediately mixing the drug-loaded gelatin with the PMMA cement) was compared with those of constructs fabricated from incubated (1 h or 24 h) drug-GMPs (Figure 5.7). Short term incubation (e.g., 1 h) of drug-

GMPs prior to construct fabrication did not significantly alter drug release kinetics. Both the drug release rate and the % cumulative release were similar ($p>0.05$). Incubating the drug-GMPs at 37ºC for 24h, however, reduced the first day initial burst (both % cumulative release and μg/ml/day) ($p<0.05$). In addition, the G15D15S4:1_24h incubation offered the highest drug release rate from day 7-10 (Figure 5.7) ($p<0.05$).

Interestingly, lyophilizing the gelatin-incorporating construct prior to the drug release study had an impact on the drug release kinetics (Figure 5.8). This was reflected by the reduced initial burst on the first day and enhanced drug release (i.e., greater drug release rate created from day 2 to day 14) of the lyophilized construct relative to the non-lyophilized construct ($p<0.05$). The release duration was extended from 10 days to 14 days by the lyophilization process (Figure 5.8).

The release kinetics of colistin from PMMA/gelatin/antibiotic constructs were analyzed using the Ritger-Peppas equation given by the following equation [163, 185, 186]:

Equation 5.1. Ritger-Peppas equation.

$$\frac{M_t}{M_\infty} = kt^n$$

where $\frac{M_t}{M_\infty}$ is the fraction of drug release at time t, k is the apparent release rate constant that incorporates the structural and geometric characteristics of the drug delivery system, and n is diffusional exponent which assumes the transport mechanism of the drug. Table 5.2 lists the n and k values of the tested formulations, which were obtained by

fitting the initial 60% of the release data in the logarithmic form of the equation. All the *n* values were close or equal to 0.45 with the coefficient of determination approaching to 1.

5.2.4. Degradation behavior of PMMA/gelatin/antibiotic constructs

To elucidate the porosity change of constructs due to gelatin degradation, constructs (cylinders 6 mm in height and 10 mm in diameter) designed for implantation within a recently developed rabbit mandibular defect model [50] were degraded *in vitro* over 12 weeks. The porosity was characterized by microCT and described as a function of time (Figure 5.9). The constructs G15D15S4:1, G15D15S3:1 and G15D20S4:1 which had relative low initial porosity (9.3±1.4-16.8±0.6%) did not undergo significant changes in porosity over 12 weeks ($p>0.05$); however, constructs with higher initial porosity (G15D15S5:1 with 27.0±1.5% porosity and G20D15S4:1 with 29.4±0.9%) exhibited an increased porosity over time. After 12 weeks, the porosity was significantly greater than the initial porosity before degradation ($p<0.05$).

5.3. Discussion

Space maintenance, as the initial stage of a two-stage regenerative medicine approach toward reconstructing large bony defects, preserves the bony volume and primes the wound site for the subsequent reconstructive or regenerative stage. While the porous structure of the space maintainer facilitates tissue healing and material retention by allowing tissue ingrowth into the pores, incorporating a drug delivery system into the space maintainer provides controlled antibiotic delivery to address local infections, potentially eliminating infection-associated complications during space maintenance. The

purpose of the current study is to design a porous PMMA-based construct with particulate gelatin incorporated for the dual purpose of space maintenance and drug release. The gelatin-incorporating PMMA construct, where the GMPs not only imparted porosity but also controlled the drug release of the construct, is a simple system that meets the aforementioned requirements. The fast assembly of drug and material makes the approach particularly practical in the operating room (Figure 5.1), offering a great deal of flexibility in the material composition of constructs. The current study focuses on the relationship between material composition and construct properties (porosity, drug release kinetics and degradation), providing direction in tailoring the material composition to meet specific clinical needs.

In these gelatin-incorporating constructs, chemically crosslinked gelatin was used in order to prolong the drug release duration. Our previous experiences demonstrated that PMMA constructs incorporating uncrosslinked gelatin, which undergoes rapid dissolution in PBS solution at 37ºC, rapidly released colistin (data not shown). In contrast, chemically crosslinked gelatin produces a smaller mesh size and degrades through polymer chain cleavage over a defined period (4-6 weeks for complete degradation in collagenase-containing PBS buffer, data not shown), providing a three–dimensional gel network for drug diffusion. From a practical standpoint, crosslinked GMPs were more stable during construct fabrication and remained as independent particles as they were dispersed in the curing PMMA phase, ensuring a uniform drug distribution within the polymeric matrix.

Crosslinked gelatin absorbed drug solution upon contact to form a hydrogel (Figure 5.2). Colistin was therefore loaded within the swollen GMPs at high weight

percentages (15 wt% or 20 wt%) by simple partitioning from a concentrated drug solution. The fast drug loading makes GMPs more practical than a majority of polymeric carriers where drugs have to be pre-loaded during carrier fabrication [145]. In such cases, the type and payload of drugs in the carrier are more difficult to modify for specific applications.

Due to the immiscibility between the gelatin hydrogel phase and PMMA polymer phase, a porous structure was successfully created in the curing material where the porosity (initial porosities of 9.3±1.4-29.4±0.9% and degraded porosities of 7.6±1.8-38.4±1.4%) was dependent on the amount of hydrogel phase incorporated (Figure 5.3 and Figure 5.4). The porosity characteristics of space maintainers potentially impact not only soft tissue penetrating the pore network [50, 162] but also the availability of open paths for drug release [145]. Previously we reported that both low-porosity PMMA/CMC constructs (16.9% porosity) and high-porosity constructs (44.6% porosity) were able to improve oral mucosal healing as compared to solid PMMA in a rabbit mandibular defect, while the low-porosity construct elicited a more favorable soft tissue response than the high-porosity construct [50]. In contrast, drug delivery may benefit from a more extensively connected pore network to achieve the complete release of entrapped drug [145]. Having the ability to control the porosity of gelatin-incorporating PMMA constructs over a wide range will allow a balance to be achieved between construct porosity and subsequent drug release to meet a specific need of space maintenance.

In the PMMA/gelatin/antibiotic construct, the incorporation of GMPs created a pore network consisting of interconnected pores among the PMMA polymer phase and a loose network of GMPs entrapped in the PMMA phase. The extensive availability of

open paths allows the drug loaded in GMPs to elute to the outer environment. This was reflected by the high cumulative release of colistin (77.8±0.6-96.5±0.7%) by PMMA/gelatin/antibiotic constructs over 10 or 14 days. The greater cumulative releases of colistin from the high-porosity constructs (G15D15S4:1, G15D15S5:1, G20D15S4:1 and G15D20S4:1) as compared to the low-porosity construct G15D15S3:1 (which featured the most limited porosity among the five formulations) also suggested that more open paths facilitated complete drug release from the construct. The % drug release of PMMA/gelatin/antibiotic constructs was significantly enhanced relative to those reported for existing antibiotic-releasing PMMA constructs in which antibiotic drugs are directly entrapped into the non-degradable cement, leading to an ineffective slow release [187-191]. With respect to the stability of released colistin, HPLC has been demonstrated to be a valid technique for evaluating the stability of colistin [192-194]. The high cumulative release determined by HPLC suggested that the majority of released colistin remained intact and stable.

In these gelatin-incorporating PMMA constructs, the material composition affected the colistin release kinetics. For example, the drug release duration could be extended by reducing the overall porosity of constructs (e.g., G15D15S3:1 with 9.3±1.4% porosity achieved 14 days release) (Figure 5.5); the drug release rate created by the released colistin was enhanced by loading greater amounts of drug in the GMPs (Figure 5.6). Mathematical analysis of the release data using the Ritger-Peppas equation helped to elucidate the drug transport mechanism from the PMMA/gelatin/antibiotic constructs [163, 185, 186]. According to this equation, all n values for the PMMA/gelatin/antibiotic constructs were close or equal to 0.45 (Table 5.2), indicating that the release of colistin is

governed by a Fickian diffusion mechanism [185]. For a defined polymer-drug device with a Fickian-controlled mechanism, the drug release can be manipulated by varying the initial concentration of drug within the matrix (which creates various penetrant concentration gradient of drug from the inside to the outside), and the geometry and composition of the pore network of the matrix. Our findings that the porosity and drug loading of PMMA/gelatin/antibiotic constructs affect the drug release kinetics thus agree with the Fickian diffusion mechanism.

Interestingly, incubating the colistin-loaded GMPs for 24 h prior to construct fabrication potentially allowed for stronger association between the gelatin and drug (probably via hydrogen bonding or electrostatic attractions [168, 169]). Therefore, the rate of colistin release was decreased as evidenced by the reduced initial burst and higher drug release rate at the later stage of drug release (Figure 5.7). Lyophilizing the construct before drug release could also result in reduced initial burst and extended the release duration (Figure 5.8), which could be attributed to the stronger association of polymer-drug or gelatin-PMMA achieved by the lyophilization process. These findings suggest alternative fabrication protocols could be explored to improve the drug release kinetics; however, utilizing such fabrication processes may result in increased drug loading or more preferable release at the expense of the ease of fabrication.

Local antibiotic delivery is ideal as a means of controlling local infection while eliminating systemic exposure to potentially toxic drug concentrations. Sufficient drug concentration created in the local environment promises higher efficacy relative to systemic administration. For example, local 5-day colistin release from PMMA beads significantly reduced the incidence of *Acinetobacter baumannii*–associated chronic

osteomyelitis caused in mice [178]. For these gelatin-incorporating PMMA constructs, the concentrations of daily released drug, which was calculated by dividing the amount of released drug by the construct volume, remained constantly higher than 10 μg/ml over the release duration. This suggests that an immediate drug level higher than 10 μg/ml may be created *in vivo* depending on the drug transport away from the construct. The drug level 10 μg/ml is well above the minimum inhibitory concentration (MIC) of colistin against *Acinetobacter baumannii* (0.5 μg/ml) [195], holding great potential for clearing local infections. Considering the cytotoxicity that the drug release may induce, the constructs are anticipated to be well tolerated *in vivo* since the drug loading per construct (8-13 mg) is far below the recommended one-time dosage of systemically administrated colistin (50-100 mg every 8 hours for a 60 kg adult) [175]. With the controlled release feature, the system will supply the drug over a prolonged period of time and create a favorable drug concentration. The systemic toxicity might be minimized further. Not only is the release rate favorable, but the 10 or 14-day release duration of PMMA/gelatin/antibiotic constructs meets the criteria of antibiotic coverage for treating an active infection (i.e., 5-10 day coverage required). In its current form, the system, however, is not suitable for long term antibiotic therapy.

As a space maintainer, the porosity change over time may consequently impact mechanical performance in an *in vivo* environment since mechanical strength is simply proportional to bulk porosity [145]. Providing that the degradation of gelatin microparticles is enzymatically accelerated with the presence of collagenase, the PMMA/gelatin/antibiotic construct was incubated in collagenase-containing PBS buffer to elucidate the impact of gelatin degradation on the construct porosity. A 12-week

degradation time was designated which was the designed postoperative evaluation period for a rabbit mandibular defect model [50] and similarly would most likely remain in place for human applications. As seen in Figure 5.9, the bulk porosity of G15D15S3:1, G15D15S4:1 and G15D20S3:1 remained unchanged with respect to bulk porosity over 12 weeks, suggesting limited gelatin degradation over time which was likely due to the relatively low porosity of the construct. Although the constructs with relatively higher porosities had slightly increased porosities after 12 weeks, the porosity was far below 50% and believed useful for application in the craniofacial complex. PMMA constructs with 50% porosity have been demonstrated to be mechanically sufficient in correcting craniofacial contour deformities and repairing defects in clinical applications and animal models [50, 86, 160].

The PMMA/gelatin/antibiotic approach has a number of strengths. First, it is a simple system involving few components with the capacity to easily modulate the physical properties of the fabricated constructs. Although various polymer systems entrapping gelatin have been described for the purpose of drug delivery [92], the present study is the first example using gelatin as both drug carrier and porogen. It is also the first systematic study of fabrication methods to quantitatively examine the effect of material composition on both release kinetics and porosity characteristics. Second, the practicality of this approach is applicable to a wide range of drug classes where drug loading can be completed via the fast assembly of drug, gelatin and PMMA. Drugs that may otherwise be damaged during the exothermic PMMA curing process may potentially be incorporated into such a system, as previous studies have shown the curing temperature of PMMA is reduced in the presence of an aqueous phase [145]. Besides the inclusion of

thermally sensitive drugs, alternative drug delivery mechanisms can be explored in this system. In addition to small molecules such as antibiotics delivered by a diffusion-controlled release mechanism, large proteins associate with gelatin by electrostatic attractions and release through gelatin degradation [92, 168, 169, 179, 196-198]. For example, vascular endothelial growth factor [179], which is able to promote wound healing and vascular ingrowth, could be incorporated and delivered in a controlled manner for the function of priming the wound site during space maintenance. Additionally, the particulate gelatin hydrogel plus the easy drug loading protocol may potentially allow the simultaneous loading and delivery of multiple types of bioactive molecules. Further studies should focus on broadening the versatility of this system and evaluating efficacy *in vivo*.

5.4. Conclusions

An antibiotic-releasing porous PMMA/gelatin/antibiotic construct was developed as a temporary implant for space maintenance/infection control during the initial step of a two-stage regenerative medicine approach to posttraumatic wound healing. The construct was fabricated through the sequential assembly of GMPs, antibiotic drugs, and PMMA bone cement where the GMPs served as both drug carrier and porogen. The porosity of constructs was tailored by both the amount of gelatin incorporated and the amount of drug solution added for gelatin swelling. The constructs achieved continuous release of colistin over 10 or 14 days, potentially creating a concentration of daily released drug well above the MICs of colistin against susceptible species. The porosity and *in vitro* colistin drug release kinetics of the PMMA/gelatin/antibiotic constructs were tuned by

varying the material composition, offering optimal opportunities to further refine the construct to match a specific clinical application in the two-stage regenerative medicine approach.

5.5. Tables and Figures

Table 5.1. Physical properties of PMMA/gelatin/antibiotic constructs.

Construct[1]	Gelatin wt%[1]	Drug wt%[1]	Swelling[1]	Drug content in dry construct		Porosity characteristics		Compressive mechanical properties	
				wt%	mg/ml construct	Bulk porosity[2]	Interconnectivity[2]	Compressive modulus (MPa)[3]	Offset yield strength (MPa)[3]
Solid PMMA	---	---	---	---	---	0.6±0.3%	---	2670±220	105±10
G15D15S3:1	15	15	3:1	2.6	23.2	9.3±1.4%	4.2±2.0%	450±30	20±1
G15D15S4:1	15	15	4:1	2.6	20.6	15.6±1.8%	8.8±9.4%	390±50	15±2
G15D15S5:1	15	15	5:1	2.6	18.2	27.0±1.5%	49.0±6.7%	200±10	8±1
G20D15S4:1	20	15	4:1	3.4	23.8	29.4±0.9%	51.4±1.8%	180±30	7±1
G15D20S4:1	15	20	4:1	3.6	28.3	16.8±0.6%	3.2±0.9%	360±50	15±1

[1]PMMA/gelatin/antibiotic constructs were named based on the weight percent of dry GMPs in the polymer phase, the weight percent of antibiotic drugs in the GMPs, and the swelling ratio of drug solution weight over gelatin weight.

[2]The bulk porosity was determined by microCT (n=3); the pore interconnectivity was determined by microCT with a connection size of 40 μm.

[3]The compressive mechanical property was determined using a mechanical testing machine in accordance with ISO5833 (n=6-8).

Table 5.2. Diffusion parameters of various PMMA/gelatin/antibiotic constructs determined based on Ritger-Peppas equation (n=3).

Construct	Cumulative release (%)	*n*	*k* ($1/h^n$)	Coefficient of determination (r^2)
G15D15S3:1	79.6±0.6%	0.44±0.01	0.18±0.01	0.9982-0.9984
G15D15S4:1	90.9±0.9%	0.45±0.01	0.25±0.00	0.9963-0.9973
G15D15S5:1	90.8±2.4%	0.45±0.02	0.30±0.00	0.9993-0.9999
G20D15S4:1	85.9±1.3%	0.45±0.01	0.27±0.01	0.9960-0.9971
G15D20S4:1	98.5±0.7%	0.45±0.00	0.25±0.00	0.9971-0.9973

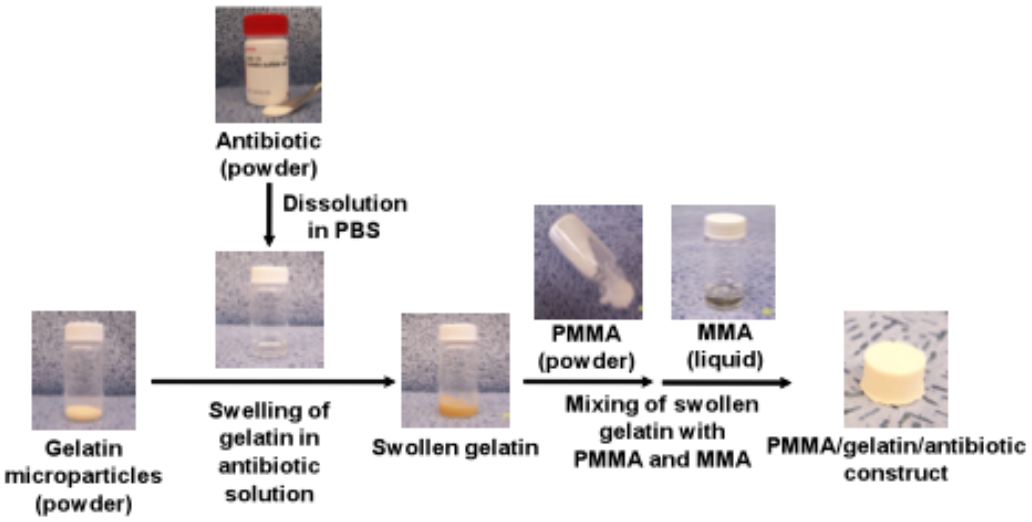

Figure 5.1. Fabrication of PMMA/gelatin/antibiotic constructs by the sequential assembly of GMPs, antibiotic drug, and PMMA bone cement: 1). antibiotic drug is dissolved in a predetermined volume of PBS buffer solution; 2). GMPs are swollen in the drug solution; 3). swollen GMPs are mixed with the two components of PMMA bone cement, first the PMMA powder and then the liquid MMA monomer. Fabrication can be completed within minutes.

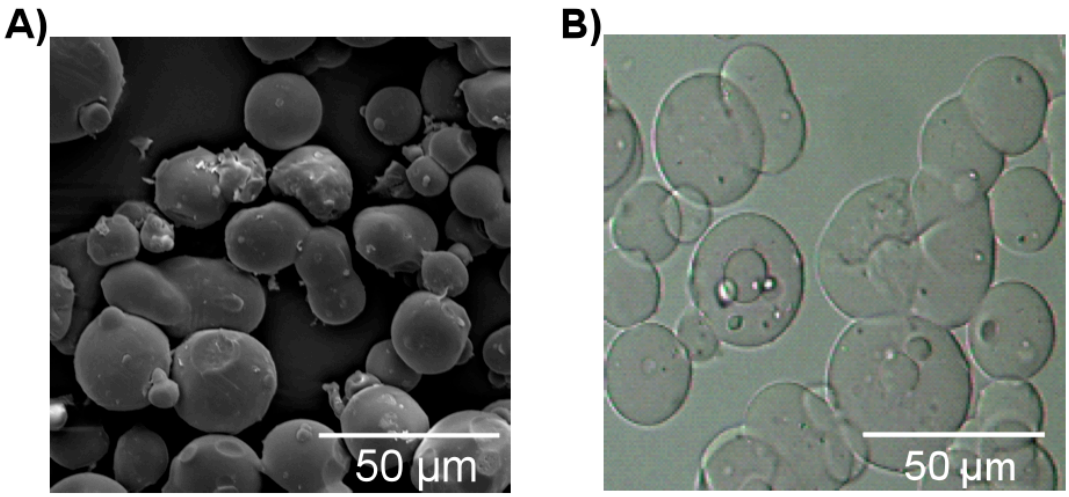

Figure 5.2. Morphology of GMPs: A) SEM image of dehydrated GMPs showing spherical shape and dense polymer structure; B) optical microscopy image of swollen microparticles in PBS solution showing spherical shape of hydrogel GMPs.

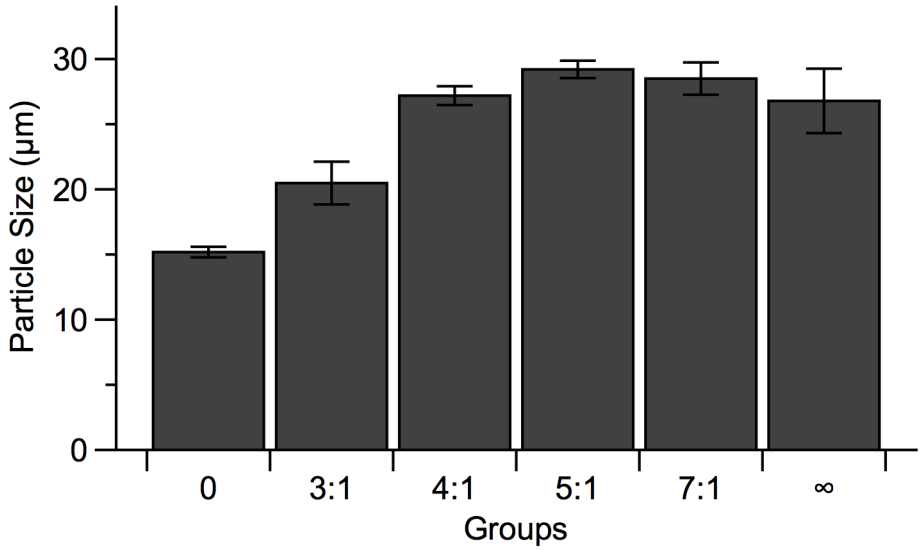

Figure 5.3. Swelling of GMPs in PBS solution by various swelling ratios (solution : gelatin by wt : wt): the mean diameter (mean ± SD based on n=3 separate swelling experiments) of swollen GMPs increased with greater amount of PBS solution added for swelling ($p<0.05$).

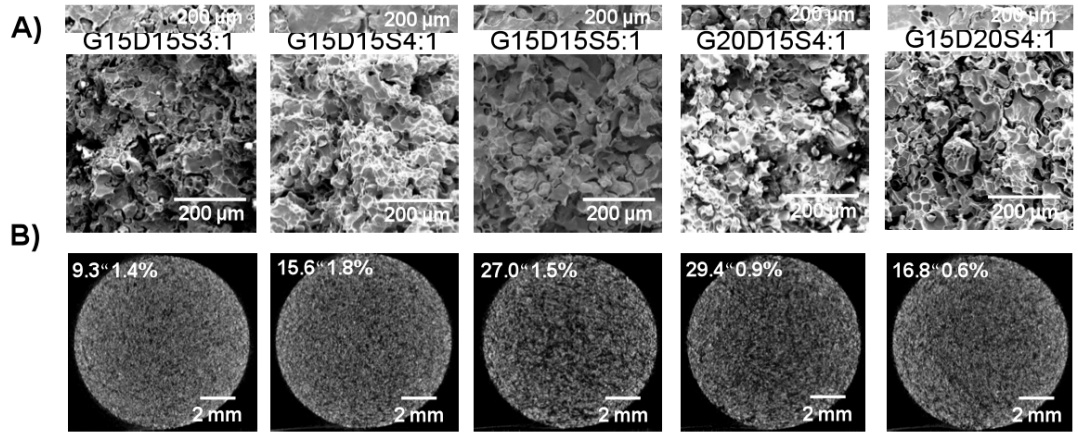

Figure 5.4. Morphology of PMMA/gelatin/antibiotic constructs characterized by A) SEM (scale bars represent 200 µm) and B) microCT (scale bars represent 2 mm, the porosity is indicated at upper left): a porous structure was created by the incorporation of gelatin microparticles; the bulk porosity is controlled by both the percent of gelatin incorporated and the weight ratio of drug solution versus gelatin for swelling.

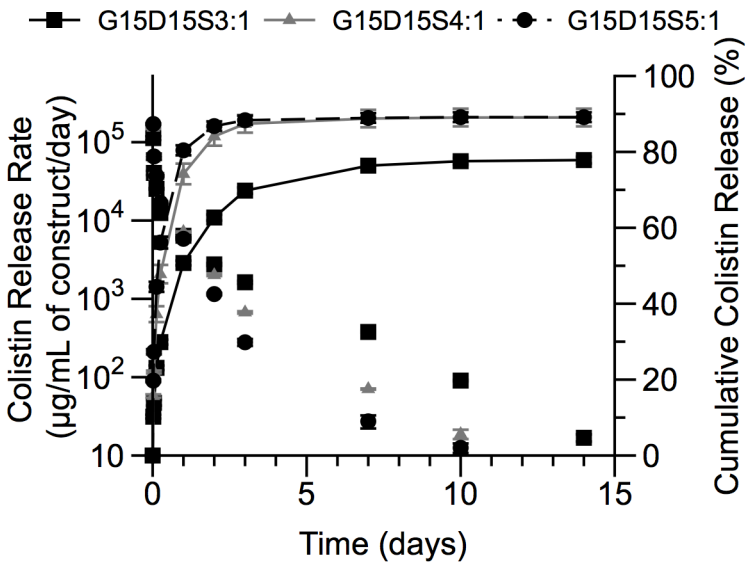

Figure 5.5. In vitro colistin release from the PMMA/gelatin/antibiotic constructs G15D15S3:1, G15D15S4:1and G15D15S5:1 where the higher weight ratio of drug solution versus gelatin resulted in greater porosity of constructs: the daily release rates indicated a continuous colistin release over 10 or 14 days with the drug release rate higher than 10 µg/ml; the longest release duration (14 days) was achieved by the construct featuring the lowest porosity (G15D15S3:1); the construct G15D15S3:1 created the lowest release rate on day 1 but the highest release rate on the following days of release ($p<0.05$); the cumulative release of colistin demonstrated that the lower porosity resulted in reduced % initial burst (on day 1) ($p<0.05$). Error bars represent standard deviation for n=3.

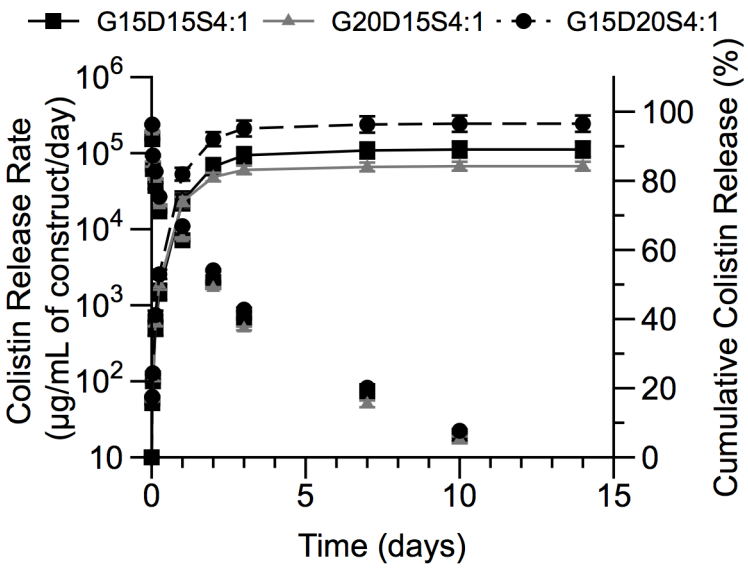

Figure 5.6. Comparison of colistin release from two constructs with the same porosities but different drug loadings (G15D15S4:1 and G15D20S4:1) and different porosities (G15D15S4:1 and G20D15S4:1). Comparing the different drug loading, the construct with higher drug loading had a higher drug release rate over the 10 day release duration ($p<0.05$); the cumulative drug release was similar. Comparison of colistin release from G15D15S4:1 and G20D15S4:1 where the higher weight percent of gelatin resulted in greater porosity and drug loading: the 20 wt% gelatin-incorporating construct created a higher release rate on day 1 but a lower release rate after day 1 ($p<0.05$); the cumulative drug release was similar. Error bars represent standard deviation for n=3.

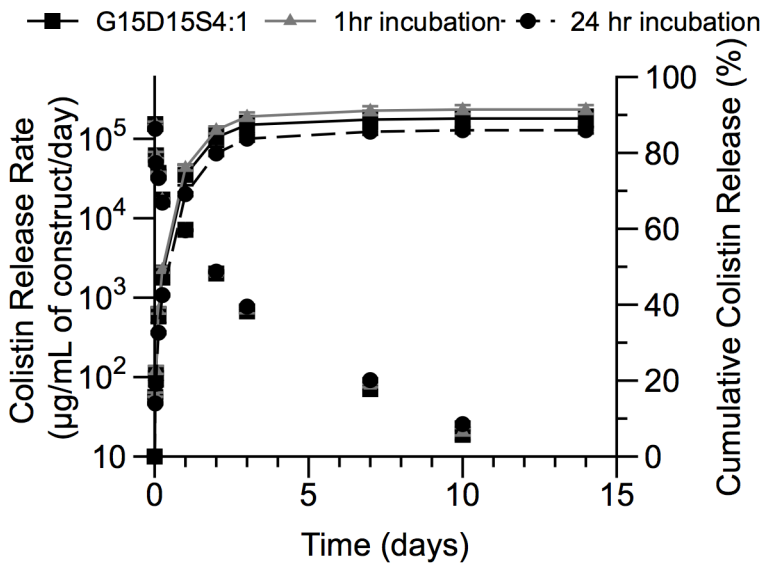

Figure 5.7. Comparison of colistin release from G15D15S4:1, G15D15S4:1_1h incubation, and G15D15S4:1_24h incubation where the drug-loaded GMPs were immediately mixed with the PMMA cement or incubated for 1 h or 24 h at 37ºC prior to mixing with the PMMA cement for the fabrication of constructs: incubating drug-GMPs prior to construct fabrication did not alter the release duration; incubating drug-GMPs for 24h prior to the construct fabrication reduced the initial burst on day 1 and increased the drug release rate from day 7-10 ($p<0.05$); the cumulative drug release was similar. Error bars represent standard deviation for n=3.

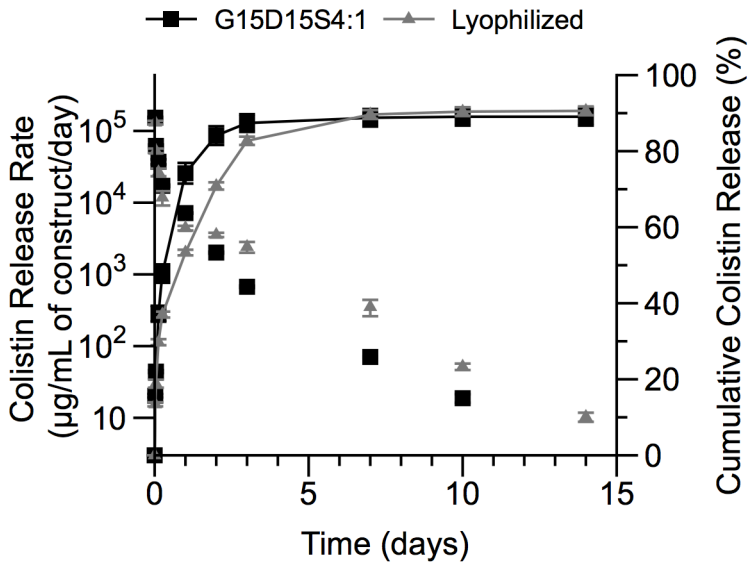

Figure 5.8. Comparison of colistin release from G15D15S4:1 and Lyophilized where the latter underwent 24 h lyophilization before the release study: the lyophilized constructs presented reduced initial burst, higher release amount after day 1 and longer release duration ($p<0.05$); the cumulative drug release was similar. Error bars represent standard deviation for n=3.

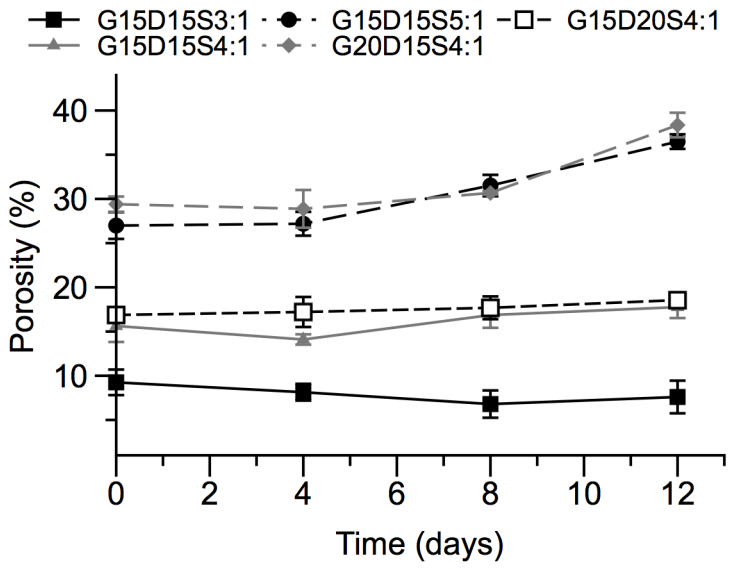

Figure 5.9. Bulk porosity changes of gelatin-incorporating PMMA constructs over a 12-week degradation period as determined by microCT: higher gelatin incorporation (20 wt%) or higher swelling ratio (5:1) resulted in greater porosity initially and throughout the degradation process ($p<0.05$); the porosity increased significantly after 12 week degradation ($p<0.05$); the three formulations that featured relatively lower porosity (G15D15S3:1, G15D15S4:1and G15D20S4:1) presented no change on the porosity over degradation ($p>0.05$). Error bars represent standard deviation for n=3.

Chapter 6

Evaluation of Antibiotic-releasing Porous Polymethylmethacrylate/Gelatin Constructs

Non-porous space maintainers have been previously shown to enhance craniofacial reconstruction by maintaining the bony structure and soft tissue envelope for later bone regeneration [199]. However, in many cases of bone loss, such as trauma or resection of a tumor that has invaded the mucosae, implantation of a foreign body could precipitate an infection. Some clinical products, such as polymethylmethacrylate (PMMA)-based bone cements, have incorporated antibiotics for local control of infection [190, 200-203]. In general, the release of these antibiotics is rapid and the majority of the loaded antibiotic remains in the cement, making them ineffective at long-term infection control [190].

Previous work from our laboratory has utilized particulate delivery systems, such as gelatin and poly(DL-lactic-*co*-glycolic acid) (PLGA) microparticles, to control the

release of antibiotics from porous PMMA-based constructs [145, 157]. A carboxymethylcellulose or gelatin gel was used as a porogen for these studies and increased weight percent of gel increased the porosity [50, 145]. Additionally, these studies illustrated that the antibiotic release, whether from PLGA or gelatin microparticles, could be controlled through fabrication parameters such as swelling, weight percent of gel or drug loading [145, 157]. In these studies, colistin, a polypeptide antibiotic, was incorporated into the gelatin or PLGA microparticles. Colistin was selected due to decreased resistance of *Acinetobacter baumannii* to the antibiotic [204]. *A. baumannii* is a common multi-drug resistant bacterial strain that has been observed to have increased incidence of infection in traumatic combat wounds [205-208]. Additionally, colistin is infrequently used systemically due to nephrotoxicity [209], which may be mitigated by local delivery because of decreased systemic concentrations.

This study investigated porous PMMA/PLGA/gelatin/colistin constructs for antibiotic release. It asked the following questions: 1) What are the effects of formulation parameters on the structure of the construct, including the setting temperature, porosity, and topography and 2) What are the effects of construct structure on the antibiotic release kinetics and activity?

6.1. Materials and Methods

6.1.1. Materials

Poly(DL-lactic-*co*-glycolic acid) (PLGA) was obtained from Lakeshore Biomaterials (Birmingham, AL) and had a copolymer ratio of 50:50, a weight average

molecular weight of 61.1 kDa, and a number average molecular weight of 37.3 kDa as measured by gel permeation chromatography [145]. Colistin sulfate salt was purchased from Sigma-Aldrich (St. Louis, MO). Poly(vinyl alcohol) (PVA) was 88% hydrolyzed with a nominal molecular weight of 22 kDA and was purchased from Acros Organics (Geel, Belgium). Surgiflo Hemostatic Matrix® was obtained from Ethicon (Somerville, NJ) and used as a source of gelatin. Bone cement was obtained from Depuy Orthopaedics (Smartset HV, Warsaw, IN).

6.1.2. Microparticle Fabrication

PLGA microparticles containing colistin were fabricated as previously described [145]. Briefly, a water-in-oil-in-water double emulsion solvent extraction technique was used. Colistin was dissolved in a solution of 0.4 wt% PVA at a concentration of 325 mg/mL as the internal phase. PLGA was dissolved in methylene chloride at a concentration of 50 mg/mL, added to the internal phase in a ratio of 20:1 oil:internal phase, and homogenized. This emulsion was added to a rapidly stirring outer phase of 0.4 wt% PVA with 0.5 M NaCl in a ratio of 10:1 outer phase:oil. After solvent extraction, the particles were washed, dried, and stored at -20°C. Blank microparticles were fabricated with an internal phase of 0.4 wt% of PVA alone. The entrapment efficiency of the microparticles was assumed to be 16.1 ± 2.5% based on previous determinations using the above fabrication method [145].

6.1.3. Space Maintainer Fabrication

Various groups of space maintainers were fabricated with the components shown in Table 1. For the setting temperature and porosity determinations, constructs with no

incorporated drug were used with weight percents of gelatin similar to previous studies which showed favorable results *in vivo* [50], namely 30 and 40 wt%. Similarly, two different gelatin matrix swelling ratios were chosen, low (LS, 1:1.9 water:gelatin weight ratio) and high (HS, 1:1.1 water:gelatin weight ratio) swelling, to determine the effect of matrix swelling ratio on the setting temperature and porosity. For the antibiotic-loaded constructs, antibiotic was loaded by swelling the gelatin matrix with an antibiotic solution with a concentration of 150 mg/mL or by incorporating antibiotic-loaded PLGA microparticles described above. Antibiotic-loaded gelatin swollen with the low swelling ratio (1:1.9) was added to constructs in 30 and 40 wt% to elucidate the effect of the amount of gelatin on the drug release kinetics. For these groups, the drug loading per amount of gelatin remained constant, altering the drug loading per scaffold; however, previous studies indicated that changing the drug loading per weight of gelatin did not affect cumulative release, but rather the amount of gelatin included affected the release kinetics [157]. Constructs with colistin-loaded gelatin in a high swelling ratio were not completed as previous experiments indicated high swelling ratios of gelatin resulted greater burst release compared to lower gelatin swelling ratios [157]. Finally, PLGA microparticles were used in the LS30, LS40, HS30 and HS40 groups with the same PLGA:PMMA ratio for all groups. Bone cement was used for all samples in a ratio of 2.11:1 of powder phase to monomer phase as supplied by the manufacturer.

To fabricate the various groups a simple mixing procedure was followed as previously described [145]. For Bone Cement control samples, the powder and monomer phases were mixed without the addition of a gel phase. The gelatin matrix was swollen in a 1:1.1, and 1:1.9 ratio of solution weight to gelatin weight for the high (HS), and low

(LS) swelling ratios, respectively. To fabricate the constructs, the powder phase of the bone cement was mixed into the gelatin hydrogel until completely incorporated. The monomer phase of the bone cement was added and mixed, and the mixture was pressed into poly(tetrafluoroethylene) (PTFE) molds (10 mm in diameter and 6 mm thick) and allowed to cure for 30 min. This procedure was followed for all methods except for thermal profiling where a larger mold according to ISO 5833 was used as described below in section 2.4 Setting Characterization.

For groups with colistin-loaded gelatin matrix, 300 mg of colistin were dissolved in the ddH_2O used to swell the gelatin matrix at a concentration of 150 mg/mL. The swollen gelatin matrix was used to fabricate porous constructs as described above in 30 and 40 wt% of the total construct mass. For groups with colistin-loaded PLGA microparticles, PLGA microparticles were added to the powder phase of the bone cement before fabrication. For the 30 and 40 wt% gelatin matrix constructs, 11 and 9.6 wt% PLGA microparticles were used. The drug content for each construct as shown in Table 1 was calculated based on the entrapment efficiency and PLGA wt% for the PLGA-loaded constructs and the swelling solution concentration and gelatin matrix wt% for the gelatin-loaded constructs.

6.1.4. Setting Characterization

The setting time and temperature were determined for the Bone Cement, LS30, LS40, HS30 and HS40 groups using ISO 5833. Briefly, the powder phase and powder phase/gelatin hydrogel mixture, for the non-porous and porous constructs respectively, were mixed with the monomer phase. This mixture was placed into a cylindrical PTFE

mold, 60 mm in diameter and 6 mm in height, with a thermocouple probe in the middle of the specimen disc penetrating the surface. The temperature was recorded over time (n = 1).

6.1.5. Porosity Characterization

Porous constructs from the LS30, LS40, HS30 and HS40 groups were characterized in terms of bulk porosity by microCT. A SkyScan 1172 microCT imaging system (Aartselaar, Belgium) was used to perform nondestructive imaging and quantify the 3D microarchitectural morphology of the constructs. The specimens (n=3) were imaged with an X- ray tube voltage of 40 kV and current of 250 μA without a filter. Volumetric reconstruction and analysis were conducted using the software NRecon and CTAn provided by SkyScan.

The surfaces of specimens were characterized by scanning electron microscopy (SEM). The surface was sputter-coated with gold for 40 s at 100 mA using a CrC-150 sputtering system (Torr International, New Windsor, NY) and visualized under a FEI Quanta 400 field emission scanning electron microscope (FEI company, Hillsboro, OR) at an accelerating voltage of 10 kV.

Finally, gelatin was leached from within the constructs by submersion into 5 mL of phosphate buffered saline (PBS, pH = 7.4) at 37°C with mild agitation. The PBS was exchanged at 1 and 3 days and at 1, 2, 4, 8, 9, 10, 11 and 12 weeks. MicroCT tomograms were taken according to the method described above at 1 and 3 days and at 1, 2, 4, 8, and 12 weeks.

6.1.6. Colistin Release

The release of each group containing colistin was determined by high performance liquid chromatography (HPLC) as previously reported [145, 157]. Each of three space maintainers for each group was placed in 5 mL PBS (pH = 7.4) at 37°C under mild agitation. For groups where the antibiotic was loaded into the gelatin matrix (names ending with Gel), the supernatant from each sample was completely removed and replaced with fresh PBS at 2 and 6 hrs and at 1, 2, 3, 7, 10 and 14 days. For groups where the antibiotic was loaded into PLGA microparticles (names ending in PLGA), the supernatant from each sample was completely removed and replaced with fresh PBS at 1, 2, 4, 7, 11, 14, 18, 21, 25, 28, 32, 35, 39, 42, 46, 49, 53, 56, 60, and 63 days. The timepoints were selected based on previous studies using similar particulate carriers with the addition of a greater number of timepoints for the PLGA-loaded constructs to ensure complete release of the drug [145, 157]. The supernatant was filtered with a 0.2 μm filter and the colistin concentration was determined using HPLC. The HPLC system comprised a Waters 2695 separation module and a 2996 photodiode array detector (Waters®, Milford, MA) with an XTerra® RP 18 column (250mm × 4.6mm, Waters®) at 45 °C. The elution was performed with a flow rate of 0.5 mL/min in a mobile phase consisting of acetonitrile (HPLC grade with 0.1 vol% trifluoroacetic acid) and water (HPLC grade with 0.1 vol% trifluoroacetic acid). Peaks were eluted with a linear gradient of 5–65% acetonitrile in water over 20 min. Absorbance was monitored at $\lambda = 214$ nm with the two components of colistin, colistin A and colistin B, eluted at approximately 16.2 min and 16.9 min, respectively. Standard solutions with colistin in PBS (pH 7.4) were tested in the range of 5–1000 μg/mL. Calibration curves were obtained using the

combined peak area of colistin A and colistin B versus the colistin concentration. The cumulative release (%) was expressed as the percent of total colistin released over time.

6.1.7. Bacterial Culture and Susceptibility

Acinetobacter baumannii (Isolate # 170) was obtained from Brook Army Medical Center as a cultured specimen from a deep wound of a soldier returning from Operation Iraqi Freedom. Antibiotics released from the LS30Gel and LS30PLGA groups on day 1 were tested by sterile filtering the supernatant and using the solution as a stock solution in the microdilution minimum inhibitory concentration (MIC) protocol according to ISO 20776. These solutions were selected as day 1 resulted in a sufficiently high stock solution concentration to complete the standard experiment for drug released from the gelatin matrix and from PLGA microparticles. This experiment compared the drug released from gelatin matrix and that released from PLGA microparticles with fresh colistin not loaded into a construct. Briefly, the stock solution was serially diluted with sterile Mueller Hinton broth to 50 µL aliquots with concentrations from 0 mg/L to 32 mg/L. *A. baumannii* cultured in Mueller Hinton broth was diluted to 1×10^6 CFU/mL and 50 µL of the inoculum was added to each well. The experiment was performed in triplicate and the concentration of colistin without growth at 18 hr of culture at 37°C was denoted the MIC.

6.1.8. Statistical Analysis

The porosity at each timepoint, the colistin released at each timepoint and the MICs were compared using ANOVA with post-hoc analysis by Tukey's honestly

significant difference. An *a priori* level of significance was set a α=0.05. All analyses were performed using MATLAB (Version R2011B, Natick, MA).

6.2. Results and Discussion

This study evaluated porous constructs fabricated from clinically available materials and the effect of their formulation on setting temperature, porosity, and topography of the construct. It also evaluated the effect of the structure on antibiotic release kinetics and activity.

6.2.1. Setting Characterization

The temperature profiles of the porous constructs are shown in Figure 1 compared to the profile of non-porous bone cement (Bone Cement). The exothermic reaction of MMA polymerization produced a rise in temperature in all groups, with the greatest increase in temperature with the Bone Cement group. The maximum temperatures reached were 40, 38, 43, 36, and 89°C for the LS30, LS40, HS30, HS40, and Bone Cement groups, respectively. During the curing of these constructs, the maximum temperature of porous constructs was diminished as compared to the Bone Cement group. The decreased maximum setting temperature of porous constructs compared to Bone Cement is consistent with previous studies where carboxymethylcellulose hydrogels were used as the porogen [145]. The setting temperature decrease in the porous constructs is due to the decreased amount of MMA per unit volume and the hydrogel acting as a heat sink during the exothermic polymerization.

6.2.2. Porosity

Figure 2 illustrates the increase in porosity over time for the porous constructs, which is consistent with previous studies showing the dissolution of the gelatin matrix from the pores of the construct [157]. HS40 had a significantly greater porosity than all other formulations for all timepoints, and LS40 had significantly less porosity than all other formulations after 1 week. Also, the LS40 and HS30 groups were significantly different at day 3. Representative microCT cross-sections are shown in Figure 3A-D illustrating the homogeneous distribution of pores. The increased porosity with an increase in aqueous porogen incorporation for the high swelling groups is consistent with a previous study also utilizing gelatin as the porogen [157]. The increase in porosity with increased porogen content seen in the high swelling group is expected; however, the decrease in porosity with greater porogen content in the low swelling group is unexpected. The change in concentration of gelatin in the porogen matrix may alter the interaction between the hydrophilic (gelatin hydrogel) and hydrophobic (PMMA) phases of the mixture, changing the stability of the pores before curing. Furthermore, Figures 3A-D show the homogeneity of the pore structure created with these materials.

Representative SEM images are shown in Figure 3E-H of the LS30, LS40, HS30, and HS40 groups. All four groups had roughness from pores exposed to the surface, an important feature for both tissue interaction and drug release.

6.2.3. Colistin Release

Colistin was released for up to 8 weeks from the constructs *in vitro*. Figures 4 and 5 show the release of colistin from the gelatin matrix and PLGA within the

PMMA-based constructs, respectively. Additionally, the release from the PLGA microparticles alone, not in a construct, is shown in Figure 5. Comparing the release from colistin-loaded gelatin matrix, the LS40Gel group released significantly more antibiotic than the LS30Gel group at 1 and 6 hours, but there was no difference in the cumulative release. The effect of porogen weight percent on release rate was shown previously in a study utilizing gelatin microparticles as the porogen [157], where increasing the amount of gelatin microparticles increased the release rate of colistin from the construct. However, in the previous study, increased weight percent of gelatin microparticles also increased porosity [157]. In this study, increased weight percent of gelatin matrix in the LS groups led to decreased porosity. Thus the weight percent of gelatin matrix may serve as an important factor for release of drug beyond the formation of porosity.

The swelling ratio significantly affected the release of colistin from the PLGA-loaded constructs (Figure 5), where increased matrix swelling in the PLGA-loaded constructs decreased the burst release of colistin. This was true for both 30 and 40 wt% constructs, which as shown in Figure 2, had differing effects on porosity. Thus, it is the matrix swelling ratio and not the porosity that affected the burst release of the PLGA-loaded constructs. In the previous study with gelatin microparticles, increased swelling of gelatin microparticles led to increased burst release; however, the porosity also increased with increased swelling [157]. Additionally, the colistin was loaded into the gelatin phase of the construct and not into PLGA microparticles.

6.2.4. Bacterial Susceptibility

The susceptibility of *A. baumannii* to colistin, colistin released from LS30Gel and colistin released from LS30PLGA was measured as the MIC according to ISO 20776 using the microdilution method. Colistin alone had an MIC of 5.33 ± 2.31 μg/mL, colistin released from the gelatin matrix (LS30Gel) had an MIC of 0.25 ± 0.00 μg/mL, and colistin released from PLGA microparticles (LS30PLGA) had an MIC of 0.17 ± 0.07 μg/mL. The MIC of colistin alone was statistically greater than the MIC of colistin released from either the gelatin matrix or PLGA. This result may be due to other molecules present in the supernatant of the released samples. The colistin control was dissolved in water per the standard, ISO 20776. However, the colistin released from samples was in the supernatant from the release study, which likely had degradation products and leachables from the constructs such as MMA, lactic and glycolic acid and the gelatin matrix. The supernatant could therefore have an effect on the antimicrobial efficacy of the test samples.

While this study evaluated several formulations with varying compositions, the consistency of each formulation's composition varies in more than one parameter as indicated in Table 1. This feature is evident in the drug content column, which shows various amounts of drug per mass of construct. These differences are caused by the other factors such as the loading of drug per mass of microparticle or the loading of drug per mass of dry gelatin matrix. These parameters were kept constant and thus when more gelatin matrix was incorporated into a construct a similar increase in drug content could be seen. While this allows for comparison between groups based on cumulative release,

similar studies where the drug content is maintained and the loading of drug per unit (PLGA or gelatin matrix) is altered could be similarly completed.

6.3. Conclusions

This study illustrated that the physicochemical properties of colistin-loaded porous space maintainers could be controlled through fabrication parameters. Specifically, the inclusion of the gelatin porogen decreased the setting temperature of the constructs and the weight percent of the gelatin included had variable effects on porosity for different swelling ratios. Also, the release of colistin from these constructs could be controlled through fabrication parameters, such as swelling and porogen weight percent as well as the delivery vehicle, such as the gelatin matrix or PLGA microparticles. The release kinetics in this study were shown to depend more on fabrication parameters than the physicochemical properties of the construct, which could have impact on future studies as physicochemical properties and release kinetics may be tuned separately. Antibiotic release constructs can be fabricated to release various amounts of drug over an extended period of time by varying the fabrication parameters.

6.4. Tables and Figures

Table 6.1. The composition of PMMA/PLGA/gelatin/colistin constructs examined.

	Gelatin matrix parameters		Construct composition				
Group	Swelling Ratio	Drug in gelatin (wt%)	Gelatin hydrogel incorporation (wt%)	Powder phase of bone cement (wt%)	Monomer phase of bone cement (wt%)	Colistin-loaded PLGA (wt%)	Drug content (wt%)
Bone Cement	0	0	0	67.8	32.2	0	0
LS30	1:1.9	0	30	47.5	22.5	0	0
LS40	1:1.9	0	40	40.8	19.2	0	0
HS30	1:1.1	0	30	47.5	22.5	0	0
HS40	1:1.1	0	40	40.8	19.2	0	0
LS30Gel	1:1.9	4.9	30	47.5	22.5	0	1.5
LS40Gel	1:1.9	4.9	40	40.8	19.2	0	2.0
LS30PLGA	1:1.9	0	26.7	42.3	20.0	11	1.8
LS40PLGA	1:1.9	0	36.2	36.9	17.4	9.6	1.5
HS30PLGA	1:1.1	0	26.7	42.3	20.0	11	1.8
HS40PLGA	1:1.1	0	36.2	36.9	17.4	9.6	1.5

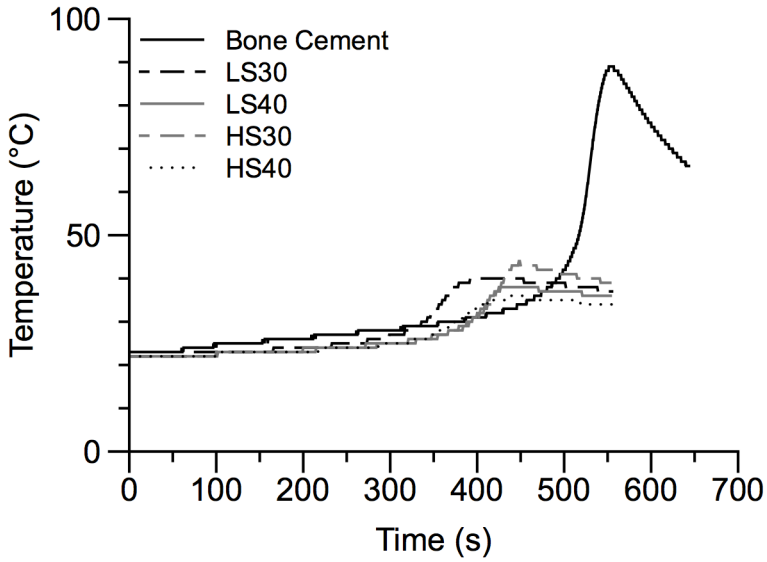

Figure 6.1. Temperature profiles of the LS30, LS40, HS30 and HS40 groups during curing compared to Bone Cement (n=1).

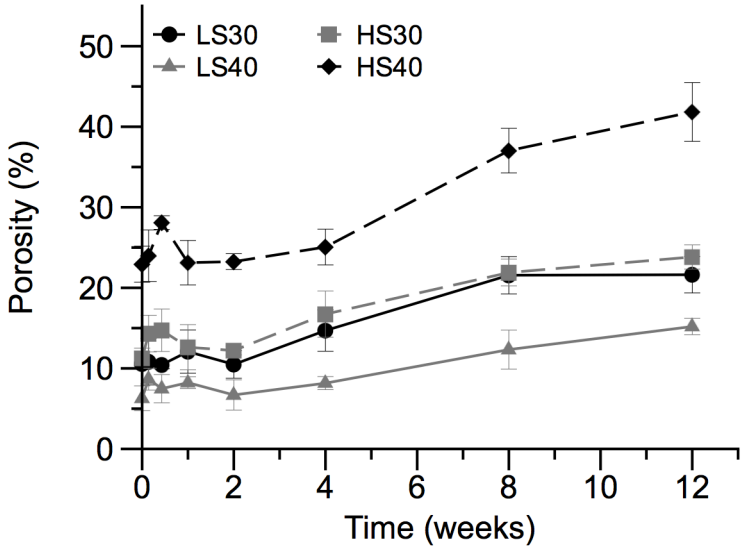

Figure 6.2. Change in porosity over time illustrating the dissolution of the gelatin matrix as measured with microcomputed tomography for the LS30, LS40, HS30 and HS40 groups (n = 3). HS40 is significantly different from all other groups for all timepoints, LS40 and HS30 were significantly different at day 3, and LS40 was significantly different from all other groups after 1 week ($p < 0.05$).

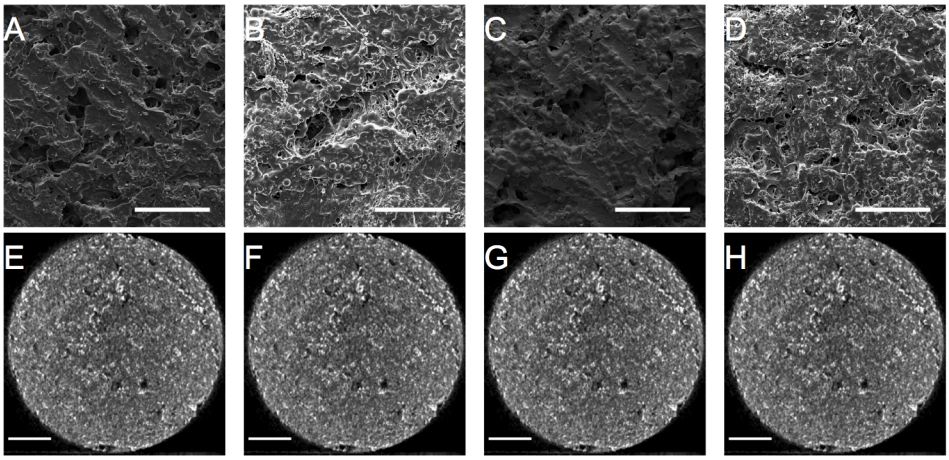

Figure 6.3. Scanning electron micrographs (A-D) and microcomputed tomography cross-sections (E-H) of the LS30 (A, E), LS40 (B, F), HS30 (C, G), and HS40 (D, H) groups. Scale bars indicate 500 µm and 2 mm for the SEM and microCT cross-sections, respectively.

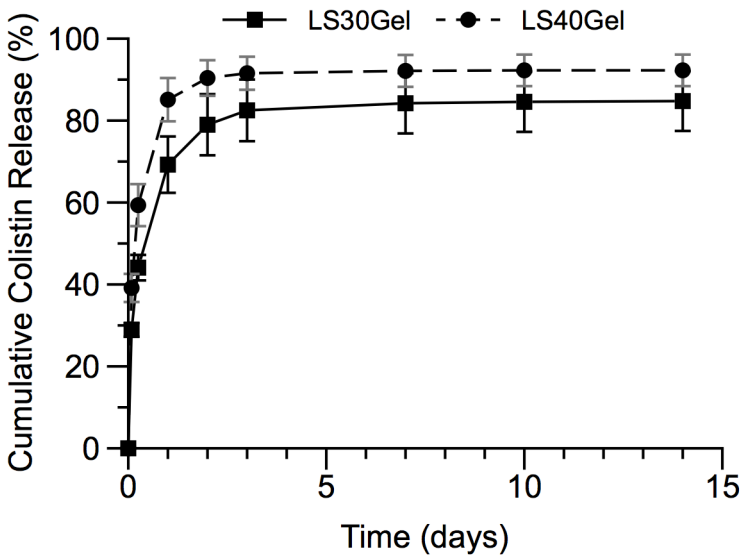

Figure 6.4. Cumulative release of colistin from constructs (n = 3) where colistin was loaded into the gelatin matrix at 30 and 40 wt%. There were significant differences between the LS40Gel and LS30Gel groups at 1 and 6 hours ($p < 0.05$).

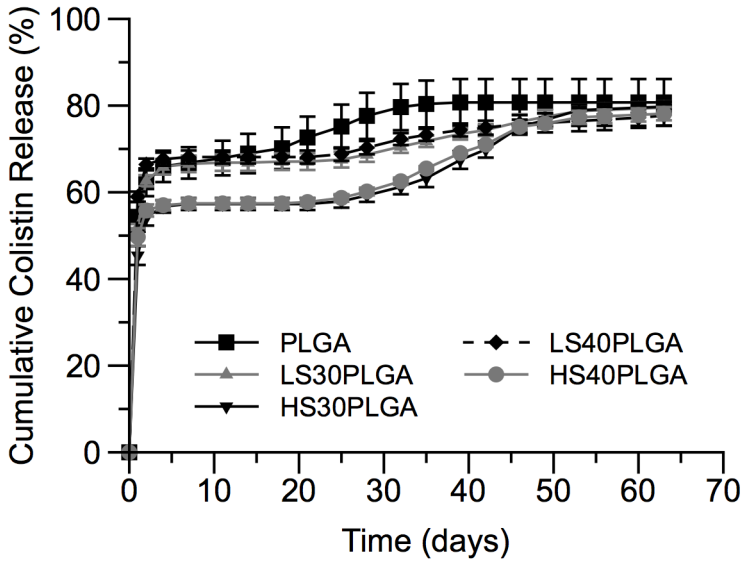

Figure 6.5. Cumulative release of colistin from constructs (n =3) where colistin was loaded into PLGA microparticles. There was a significant difference between the LS30PLGA and HS40PLGA groups at day 1. Additionally, there were significant differences between HS30PLGA and HS40PLGA groups and LS30PLGA and LS40PLGA groups from day 2 to day 39. Also, there was a significant difference between the HS30PLGA and the LS30PLGA and LS40PLGA groups, and a significant difference between LS40PLGA and HS40PLGA at day 42 ($p < 0.05$).

Chapter 7

Evaluation of Antibiotic-releasing Porous Polymethylmethacrylate Space Maintainers in an Infected Composite Tissue Defect Model

Non-porous space maintainers have been previously shown to enhance restoration of the craniofacial complex by maintaining the bony structure during craniofacial reconstruciton [199]. Current materials fail typically as a result of infection or by wound dehiscence. There has been some modifications of materials to release antibiotics to help mitigate infection [190, 200-203], but the release of antibiotics from these materials is on a very short timescale (< 3 days) and the majority of the encapsulated drug remains in the implant, reducing their efficacy [190].

Previous work from our laboratory has investigated gelatin and poly(DL-lactic-*co*-glycolic acid) (PLGA) microparticles to affect the controlled release of antibiotics from constructs [145, 157]. Additionally, these constructs are porous by the inclusion of a carboxymethylcellulose or gelatin hydrogel [50, 52, 145, 157]. This porosity enhanced

the tissue integration and allowed for greater cumulative release of antibiotic [50, 52, 145, 157]. In these studies, colistin, a polypeptide antibiotic, was selected for inclusion into these particulate delivery systems due to decreased resistance of *Acinetobacter baumannii* to the antibiotic [204]. *A. baumannii* has been observed to have increased incidence of infection in traumatic combat wounds [205-208].

This study investigated porous PMMA/PLGA/gelatin/colistin constructs serving as antibiotic-releasing space maintainers and evaluated their efficacy *in vivo* in a rabbit infected composite tissue defect model. It asked the following question: What are the effects of antibiotic-releasing space maintainer fabrication parameters on wound healing, infection clearance, kidney function, and tissue response to the construct?

7.1. Material and Methods

7.1.1. Materials

Surgiflo Hemostatic Matrix (Somerville, NJ) was used as a source of gelatin. Bone cement was obtained from Depuy Orthopaedics (Smartset HV, Warsaw, IN). Colistin sulfate salt was purchased from Sigma-Aldrich (St. Louis, MO). Poly(vinyl alcohol) (PVA) was 88% hydrolyzed with a nominal molecular weight of 22 kDA and was purchased from Acros Organics (Geel, Belgium). Poly(DL-lactic-co-glycolic acid) (PLGA) was obtained from Lakeshore Biomaterials (Birmingham, AL) and had a copolymer ratio of 50:50, a weight average molecular weight of 61.1 kDa, and a number average molecular weight of 37.3 kDa as measured by gel permeation chromatography [145].

7.1.2. Microparticle Fabrication

PLGA microparticles containing colistin were fabricated as previously described [145]. Briefly, a water-in-oil-in-water double emulsion solvent extraction technique was used, where colistin was dissolved in a solution of 0.4 wt% PVA at a concentration of 325 mg/mL as the internal phase. The oil phase comprised PLGA in methylene chloride at a concentration of 50 mg/mL. This oil phased was added to the internal phase in a ratio of 20:1 oil:internal phase, and homogenized. The external phase consisted of 0.4 wt% PVA with 0.5 M NaCl. The emulsion created by the homogenization was added to the external phase in a ratio of 10:1 external phase:oil. After 4 hours, allowing for solvent extraction, the particles were washed, dried, and stored at -20°C. Additionally, blank microparticles were fabricated with an internal phase of 0.4 wt% of PVA alone. The entrapment of colistin-loaded microparticles was determined as previously described [145].

7.1.3. Space Maintainer Fabrication

The gelatin matrix was swollen in a 1:1.9 ratio of solution weight to gelatin weight. The swollen gelatin matrix was used in 30 wt% of the total space maintainer mass. Bone cement was used for all samples in a ratio of 2.11:1 of powder phase to monomer phase as supplied by the manufacturer. To fabricate the space maintainers, the powder phase of the bone cement was first dispersed into the gelatin matrix. The monomer phase of the bone cement was added and mixed, and the space maintainer was molded and allowed to cure.

For colistin release, space maintainers were fabricated with the antibiotic-loaded in PLGA microparticles or in the gelatin matrix. For groups with colistin loaded into the gelatin matrix, the gelatin matrix was swollen with ddH_2O with a colistin concentration of 150 mg/mL. For groups with colistin loaded into the PLGA microparticles, PLGA microparticles in 11 wt% of the total mass were added to the powder phase of the bone cement. For the PLGA High group this 11% consisted entirely of colistin-loaded microparticles, while for the PLGA Low group approximately half was replaced with blank PLGA microparticles. Table 7.1 summarizes the groups used for all analyses including the drug content based on the entrapment efficiency for the PLGA groups and the concentration for the Gelatin group. Each sample was sterilely aliquoted in sterile containers for intraoperative fabrication and cured *in situ*.

7.1.4. Bacterial Culture

Acinetobacter baumannii (Isolate # 170) was obtained from Brook Army Medical Center as a cultured specimen from a deep wound of a soldier returning from Operation Iraqi Freedom. For the *in vivo* inoculum, *A. baumannii* was cultured in tryptic soy broth (BD, Franklin Lakes, NJ). Colony forming unit (CFU) concentration for inoculation was determined by absorption the morning of each surgery, diluted by sterile tryptic soy broth to 2×10^7 CFU/mL, and stored on ice until inoculation. Control defects were inoculated with the sterile tryptic soy broth.

7.1.5. Surgical Procedure

All procedures followed protocols approved by the Rice University and University of Texas Health Science Center at Houston Institutional Animal Care and Use

Committees. Four groups were selected for evaluation in an infected composite tissue defect model with 10 implants per group. *A. baumannii* was inoculated into defects filled with three different formulations: Gelatin, and two PLGA groups, PLGA High and an approximately half dose of colistin, called PLGA Low, where approximately half of the microparticles loaded were blank. The fourth group, Uninfected, served as a control, which was uninfected and had the same formulation as the PLGA High. The surgical procedure was completed as previously described [50-52]. Briefly, a midline incision extending posteriorly from the mentum was used to expose the inferior border of the right hemimandible. The soft tissue and periosteum were lifted from the body of the mandible and a 10 mm diameter bicortical defect was made in the body of the mandible with a dental trephine (Ace Surgical, Brockton, MA) powered by a micromotor handpiece (NSK, Kanuma, Japan) with copious irrigation. A crosscut bur (Stryker, Kalamazoo, MI) was used to cut a 2-3 mm notch in the superior aspect of the defect. The overlying crown was removed, creating an oral mucosal defect with intraoral communication. The defect was inoculated with 100 μL of the bacterial suspension, amounting to 2×10^7 CFU/mL of bacteria, or sterile broth by pipette on the defect walls. The implant was fabricated by first mixing the powder phase into the swollen gelatin until evenly mixed. The monomer phase was added and mixed until doughy, then shaped by hand and packed into the defect. The time from inoculation to packing was maintained at 7 min. A titanium plate was placed over the defect to prevent iatrogenic fracture. The defect was closed in layers with 4-0 Vicryl suture (Ethicon, Somerville, NJ) in running and subcuticular stitch patterns for the muscle and fascia, and skin, respectively. Each rabbit received a fentanyl

patch and carprofen subcutaneously for pain management and inflammation, respectively, for 48 hours postoperatively.

7.1.6. Kidney Function

The kidney function of the rabbits was analyzed at 0, 1 and 5 weeks by measuring plasma creatinine and blood urea nitrogen from blood drawn from the ear vein. The plasma concentrations were measured using an IDEXX Vet Test 8008 (IDEXX Laboratories, Westbrook, ME).

7.1.7. Sample Culture

At 12 weeks postoperatively, the rabbits were euthanized by barbiturate overdose. A blood sample was taken sterilely from cardiac puncture with 3.8% sodium citrate. The anterior edge of the defect was exposed by sterile dissection. Sterile cotton swabs were used to collect samples from saliva, the anterior edge of the defect, and any abscesses in the craniofacial region. The swabs were cultured at 37°C on tryptic soy agar (BD, Franklin Lakes, NJ) and tryptic soy agar with 5% sheep blood (BD, Franklin Lakes, NJ) for blood samples. Individual colonies were tested for oxidase activity by oxidase reagent (PML Microbiologicals, Wilsonville, OR). The same colonies were smeared on glass slides and stained with Gram's stain. All gram negative oxidase negative colonies were further identified by the API 20 NE kit (bioMerieux, Marcy l'Etoile, France).

7.1.8. Gross Observation

At the time of euthanasia, the right hemimandible was explanted. The mucosa over the defect was classified as healed or non-healed and the other oral mucosa was

classified as dehisced or non-dehisced. The mandibles were then placed in 10% neutral buffered formalin for fixation for 72 hours. After 72 hours, the mandibles were transferred to 70% ethanol.

7.1.9. Histology

The mandibles were dehydrated by serial solutions of ethanol (70-100%) and embedded in methylmethacrylate. After complete polymerization, 10 μm sections were cut coronally using an inner circle diamond microtome (Leica, Wetzlar, Germany) and stained with methylene blue and basic fuchsin. Three blinded reviewers scored each specimen according to the scoring system shown in Table 7.2 to assess the tissue response around the implant and within the pores of the implant [92]. Images were obtained using an AxioImager Z.2 microscope (Zeiss, Oberkochen, Germany).

7.1.10. Statistical Analysis

The creatinine, and the blood urea nitrogen values were compared using ANOVA with post-hoc analysis by Tukey's honestly significant difference. The classifications of oral mucosae were compared using the Fisher-Freeman-Halton test with post-hoc analysis by Fisher's exact test. The histological scores of the space maintainers were compared using the Kruskal-Wallis test with post-hoc analysis by the Mann-Whitney U test. An *a priori* level of significance was set a α=0.05. All analyses were performed using MATLAB (Version R2011B, Natick, MA).

7.2. Results

7.2.1. Microparticle Fabrication

The entrapment of colistin into the PLGA microparticles was 6.1 ± 0.9 wt%. This value was used to determine the drug content of PLGA-loaded implants shown in Table 7.1.

7.2.2. Animal Care

Surgery was performed on 45 rabbits with 5 prematurely euthanized animals. All prematurely euthanized animals had complications unrelated to the treatment but rather due to general problems including unresolved postoperative diarrhea, neurological deficits due to spinal fracture, and unresolved foot wounds. The remaining 40 animals were healthy and were euthanized at 12 weeks postoperatively.

7.2.3. Kidney Function

All mean values for creatinine and BUN were within normal range (creatinine: 0.8-1.8 mg/dL; BUN: 10-24 mg/dL) and there were no significant differences between groups at each time point (Figure 7.1). Creatinine and BUN remained below the threshold that would indicate acute tubular necrosis due to the use of nephrotoxic levels of colistin.

7.2.4. Gross Observation

In addition to healed (Figure 7.2A) and non-healed (Figure 7.2B) mucosal defects, some rabbits exhibited a separate medial mucosal dehiscence as seen in Figure 7.2C. Figure 7.3A shows the number of healed mucosae in each group and Figure 7.3B shows

the number of dehisced mucosae in each group. There was a significantly greater number of healed mucosae in the PLGA High group compared to the Gelatin; however, there were no significant differences between groups for the dehiscences.

7.2.5. Sample Culture

All saliva swabs and 3 defect swabs grew bacteria; however, none of these bacteria were proven to be *A. baumannii*. Colonies grown from saliva swabs were excluded based on gram stain, oxidase presence, or with the API 20NE kit. No blood swabs grew bacteria. Two defects had abscesses; however, only one grew bacteria, which were gram positive.

7.2.6. Histology

Histological assessment of the space maintainers in the mandible confirmed the presence of non-healed (Figure 7.4A) and healed (Figure 7.4B) oral mucosae in various samples. PLGA had significantly higher histological score than the Uninfected group at the tissue implant interface. As seen in Figure 7.5A, this is shown by all PLGA High samples receiving a score of 2, representative of a highly organized fibrous capsule. The Uninfected group had scores of 0, 1, and 2, indicating an abundance of inflammatory cells (Figure 7.4D), a poorly organized fibrous capsule and highly organized fibrous capsule, respectively. Although there were instances of direct bone implant contact (Figure 7.4C) this did not comprise the majority of the interface and thus could not receive a score of 3 or 4. No other significant differences were found for the tissue implant interface. None of the histological scores for the pore tissue were significantly different including scores of 0, 1, 2, and 3, representing exclusively inflammatory cells, a

majority of inflammatory cells, immature fibrous tissue, and fibrous tissue and bone, respectively, as indicated in Table 7.2.

7.3. Discussion

In the infected composite tissue defect, implants from the PLGA High group showed increased soft tissue healing over the Gelatin group. While this is an indirect measurement of infection clearing, previous studies have shown decreased healing in the presence of infection [210, 211]. Previous studies in non-porous PMMA based materials showed similar results in that the duration of release impacted reduction in bacterial load [190, 202, 212]. This may be due to some bacteria entering a sessile state as biofilm, thereby increasing the effective concentration necessary for clearance of the infection. These bacteria may then proliferate and colonize the wound after the short duration of antibiotic delivery, whereas they remain sessile with continued delivery of antibiotics in the extended release groups [213].

For the first time using this model, a dehiscence separate from the intentional mucosal defect was observed. As seen in Figure 7.2C, these dehiscences were located on the lingual aspect of the mucosa overlying the implant. Due to the presence of these dehiscences in the Uninfected group, the differences in formulation between these samples and previous studies is the use of gelatin matrix as the porogen and the delivery of antibiotics. Previous studies have shown that antibiotics, while targeted at bacteria, have detrimental effects on viability and function of host cells [214, 215]. This effect could lead to breakdown of the soft tissue, fenestration, and dehiscence.

In addition to efficacy in infection clearance, safety was measured through the analysis of kidney function by plasma concentration of BUN and creatinine. The early discovery of nephrotoxicity with colistin has led to increased research into local delivery of the drug for increased local concentration with decreased systemic exposure [209, 216-218]. This study showed that with high local delivery to the wound site, the negative systemic effects of colistin administration were avoided. Local delivery strategies may allow for increased application of powerful antibiotics that were previously underused clinically due to severe systemic adverse effects.

Clearance of the infection was also evaluated by cultures of the saliva, blood, and defect at 12 weeks. While a few of the defects and all of the saliva swabs grew bacteria, none were identified to be *A. baumannii*. In the normal rabbit, saliva swabs would culture many different bacteria due to mucosal colonization. In addition, these bacteria could inoculate and colonize the porosity of the implant through the mucosal defect. This is corroborated by the few defect swabs that did culture bacteria, but were not identified as *A. baumannii*. This finding is consistent with previous studies where increased inflammation in highly porous space maintainers was attributed to colonization of the implant by oral flora [50]. Additionally, a recent study showed that 37% of traumatic injuries resulted in polymicrobial infections [219]. Thus, while the delivery of a single antibiotic is likely inadequate alone to treat such polymicrobial wound infections, the animal model used in this study presents a complex environment very similar to the targeted problem area.

Although there were significant differences in gross wound healing, the histological response was similar for the tissue-implant interface and the tissue within the

pores. As seen in Figure 7.5A, many of the samples received scores of 2 for a mature fibrous capsule; however, for several of these samples, there was a layer of inflammatory cells between the fibrous capsule and the implant as shown in Figure 7.4D. This has been previously demonstrated to be due to continued release of proinflammatory molecules being released from the implant resulting in the invasion by inflammatory cells [220]. Inflammatory molecules from bacterial colonization or the degradation products of PLGA or gelatin may be released from the implant at late time points, resulting in the recruitment of inflammatory cells. Finally, there are several instances of direct bone-implant contact either at the interface or in the pores of the implant as shown in Figure 7.4C, illustrating that after 12 weeks, there is some growth of bone around and in the implant.

Considering the results, there are a few areas from this study that could receive further investigation. While this study elucidated the role of colistin release from the space maintainer against *A. baumannii* in this defect, the expansion of this study to include various antibiotics, bacterial strains and combinations thereof is important to address the clinical nature of many traumatic facial injuries. Additionally, further study into the mechanisms and relationships of the tissue regeneration with respect to infection clearance and delivery of the antibiotic is important. Finally, as traditional pharmacology focuses on the distribution of drug delivered systemically, adequate investigation into dose and duration on local concentrations of antibiotic and clearance of infection is warranted.

7.4. Conclusion

The loading parameters for the implants affected the gross soft tissue healing in an infected composite tissue defect model over a period of 12 weeks. Also, local delivery did not result in systemic effects, specifically nephrotoxicity. The results from this study indicate that the local delivery of antibiotic released from PLGA may increase soft tissue healing around an infected defect. Finally, the polymicrobial nature of this animal model allows for complex study, simulating the clinical problem seen in infected wounds.

Tables and Figures

Table 7.1. The composition of PMMA/PLGA/gelatin/colistin implants evaluated.

	Gelatin matrix parameters		Implant composition				
Group	Swelling Ratio	Drug in gelatin matrix (wt%)	Gelatin matrix incorporation (wt%)	Powder phase of bone cement (wt%)	Monomer phase of bone cement (wt%)	Colistin loaded PLGA (wt%)	Drug content (wt%)
Uninfected	1:1.9	0	26.7	42.3	20.0	11.0	0.67
Gelatin	1:1.9	4.9	30	47.5	22.5	0.0	1.55
PLGA Low	1:1.9	0	26.7	42.3	20.0	5.5*	0.36
PLGA High	1:1.9	0	26.7	42.3	20.0	11.0	0.67

* in the PLGA Low groups there is an additional 5.5 wt% of blank PLGA microparticles.

Table 7.2. Histological scoring system for the implant tissue interface and the tissue in the pores of the implant [92].

Hard tissue response at the implant-bone interface	Score
Direct bone-to-implant contact without soft interlayer	4
Remodeling lacuna with osteoblasts and/or osteoclasts at surface	3
Majority of implant is surrounded by fibrous tissue capsule	2
Unorganized fibrous tissue (majority of tissue is not arranged as capsule)	1
Inflammation marked by an abundance of inflammatory cells and poorly organized tissue	0
Hard tissue response within the pores of the scaffold	
Tissue in pores is mostly bone	4
Tissue in pores consists of some bone within mature, dense fibrous tissue and/or a few inflammatory response elements	3
Tissue in pores is mostly immature fibrous tissue (with or without bone) with blood vessels and young fibroblasts invading the space with few macrophages present	2
Tissue in pores consists mostly of inflammatory cells and connective tissue components in between (with or without bone) or the majority of the pores are empty or filled with fluid	1
Tissue in pores is dense and exclusively of inflammatory type (no bone present)	0

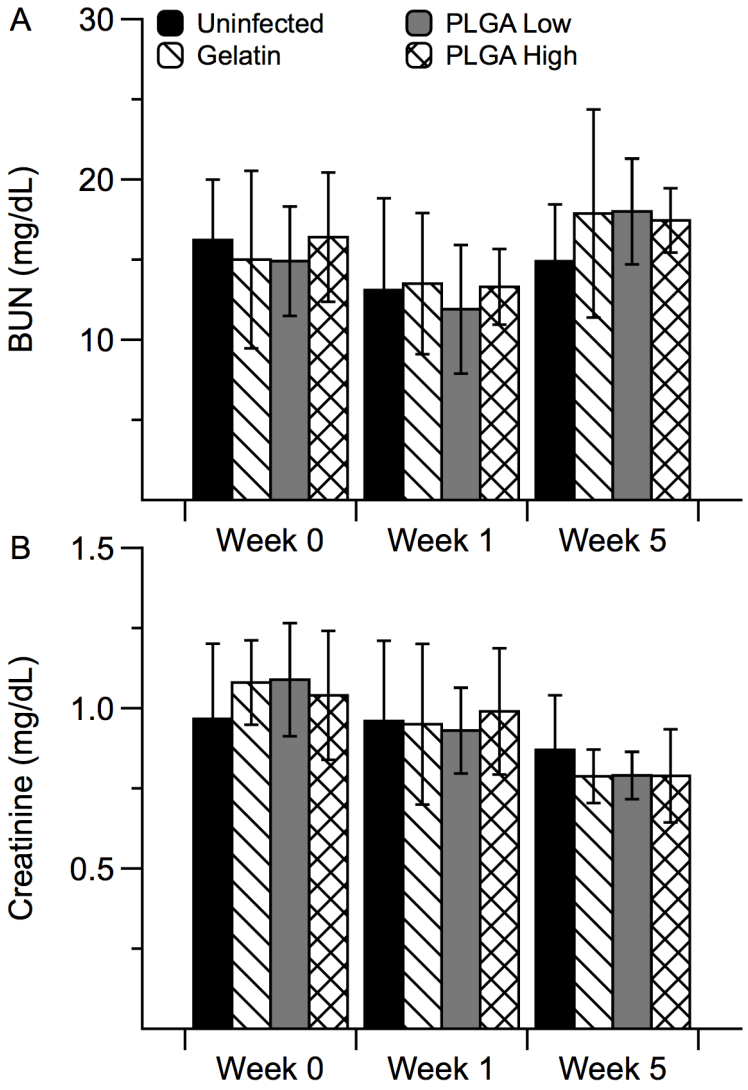

Figure 7.1. Plasma concentrations of (A) BUN and (B) creatinine taken preoperatively (week 0) and 1 and 5 weeks postoperatively as measures of kidney function. Data are presented as means ± the standard deviation for n = 10. Normal ranges: BUN: 10-24 mg/dL and creatinine: 0.8-1.8 mg/dL. There were no significant differences between groups for BUN or creatinine plasma concentrations.

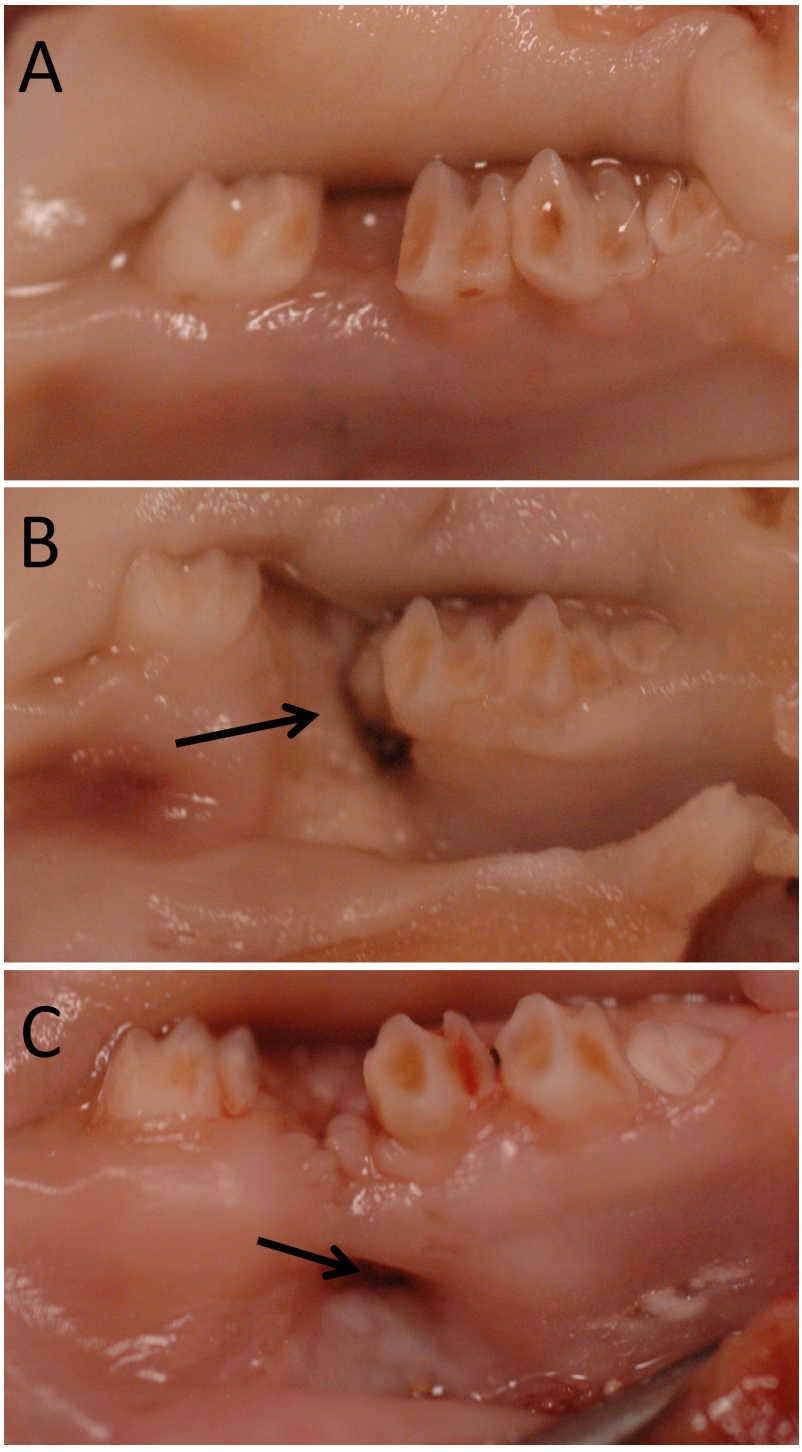

Figure 7.2. Gross photographs of oral mucosae 12 weeks postoperatively. Images show (A) well-healed, (B) non-healed, and (C) medially dehisced mucosae. Black arrows in (B) and (C) indicate exposed implant through non-healed and dehisced mucosae, respectively.

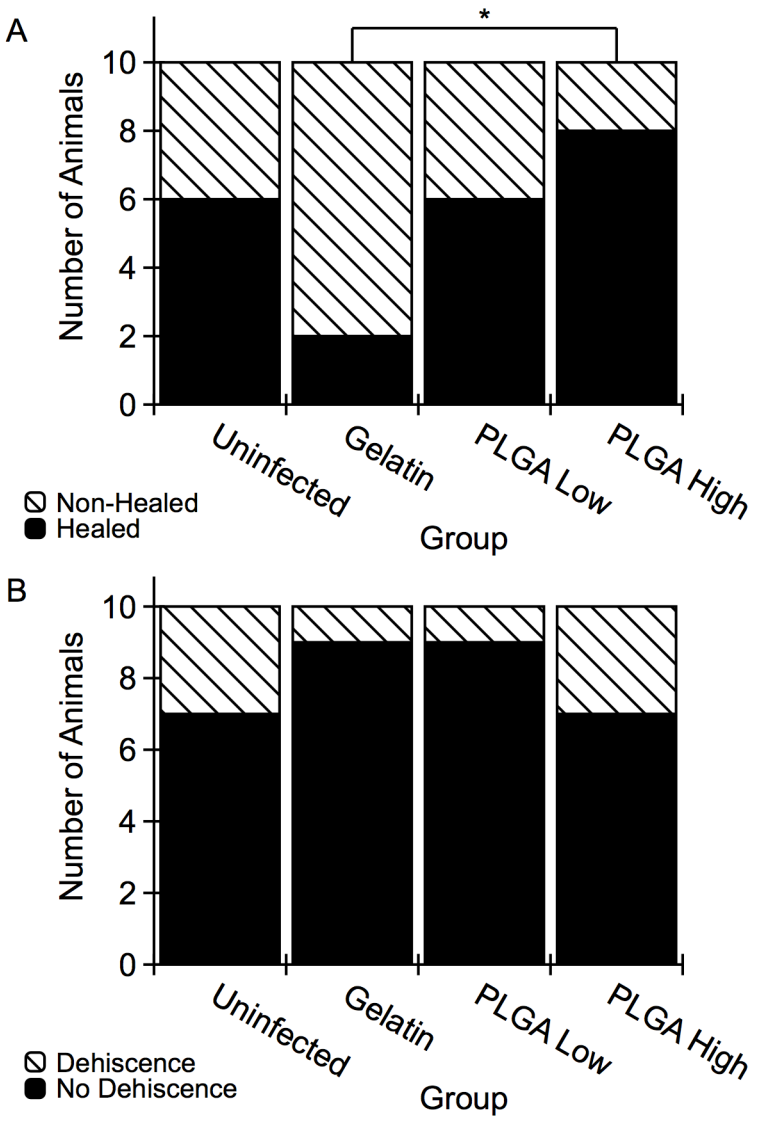

Figure 7.3. (A) Number of healed versus non-healed mucosal defects as well as (B) dehisced and non-dehisced mucosae for each group. * indicates a significant difference between the LS30PLGA and the LS30Gel groups ($p < 0.05$).

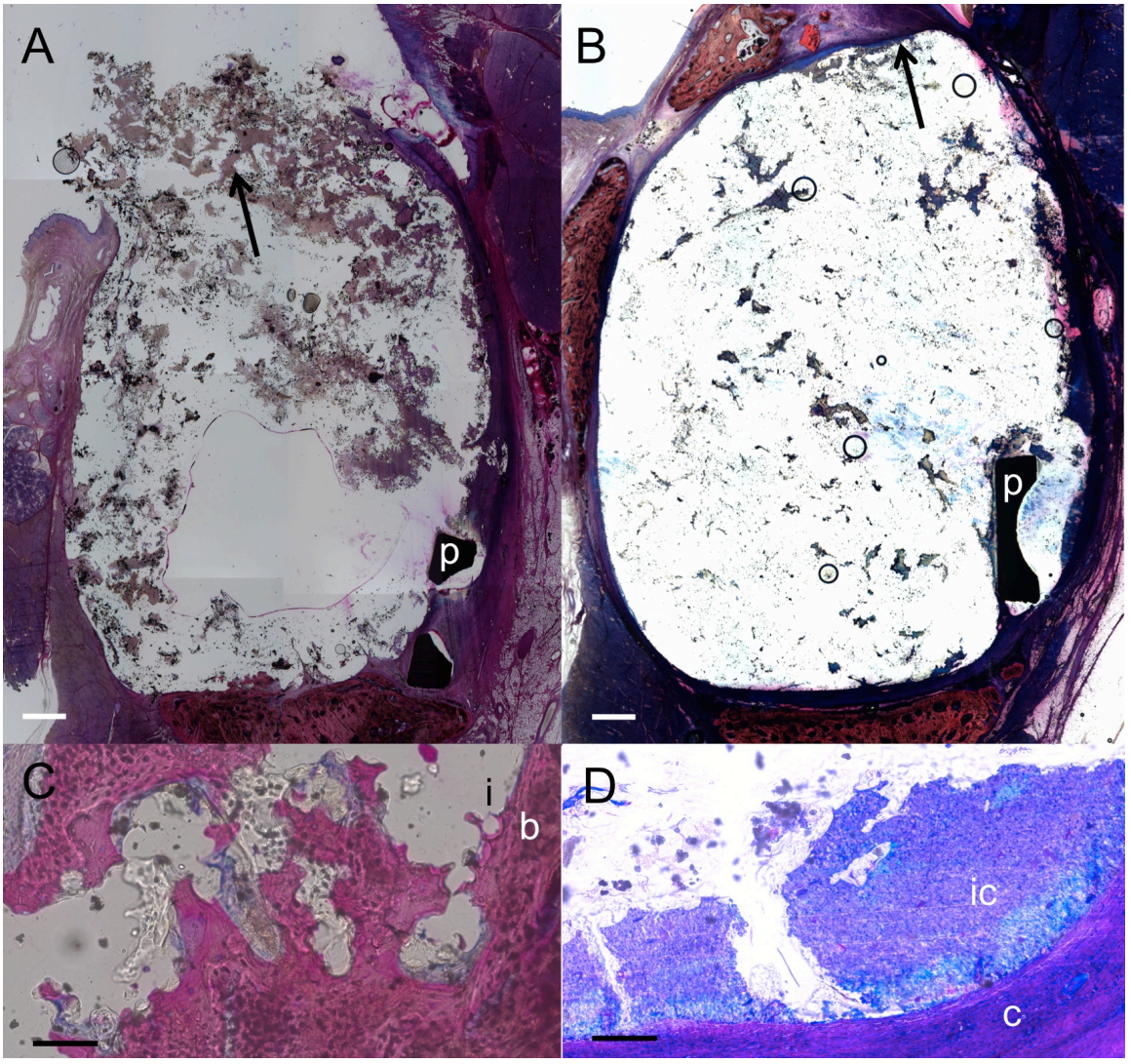

Figure 7.4. Representative histological images of (A-B) low and (C-F) high magnification stained with methylene blue and basic fuchsin. The low magnification images show a non-healed (A) and healed (B) mucosal defect with the titanium plate indicated with a (p). The exposure of the implant in (A) is indicated with a black arrow. The healed mucosa over the implant in (B) is indicated with a black arrow. Bone (b) can be seen in direct contact with the implant (i) in (C) at the tissue implant interface. (D) shows an abundance of inflammatory cells (ic) inside a thick fibrous capsule (c) at the tissue implant interface. Scale bars indicate 1 mm and 100 µm for the low (A and B) and high (C and D) magnifications, respectively.

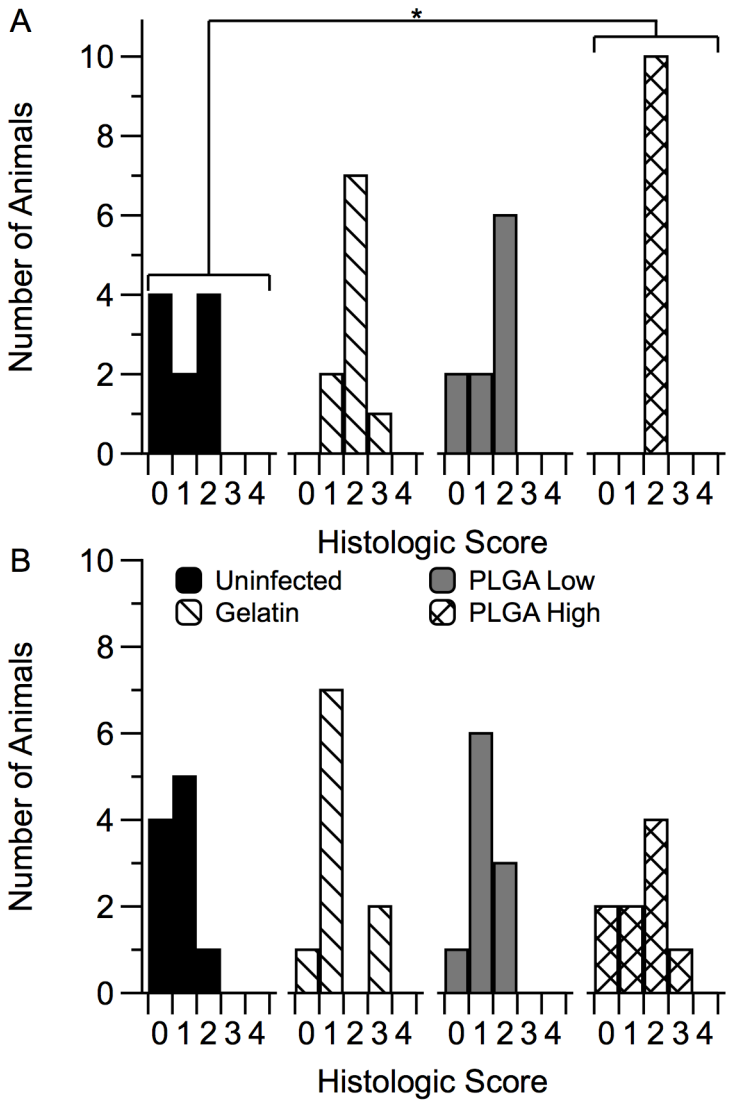

Figure 7.5. Distribution of histological scores of the (A) tissue-implant interface and the (B) tissue within the pores of the implants using the scoring system described in Table 2. * indicates a significant difference between the Uninfected and the LS30PLGA groups for the tissue-implant interface score ($p < 0.05$).

Chapter 8

Biodegradable Composite Scaffolds Incorporating an Intramedullary Rod and Delivering Bone Morphogenetic Protein-2 for Stabilization and Bone Regeneration in Segmental Long Bone Defects[‡]

Despite the inherent healing capacity of bone tissue, segmental defects remain a significant clinical challenge and often result in non-union [221]. Current standard of care relies on the use of stabilization with plates or rods and bone regeneration through the use of bone grafts or flaps. However, this strategy has inherent disadvantages with

[‡] This chapter was published as Henslee AM*, Spicer PP*, Yoon DM, Nair MB, Meretoja VV, Witherel KE, Jansen JA, Mikos AG, Kasper FK. "Biodegradable Composite Scaffold Incorporating an Intramedullary Rod and Delivering Bone Morphogenetic Protein-2 for Stabilization and Bone Regeneration in Segmental Long Bone Defects." *Acta Biomater.* **7**, 3627-3637 (2011). * indicates co-first authors.

donor site morbidity and subsequent removal of stabilization hardware or lifetime placement [222]. While many other bone regeneration strategies have been investigated, many do not consider stabilization of segmental long bone defects in combination with regeneration and thus still require fixation. However, there are strategies in tissue engineering aiming to address these two issues simultaneously, and commonly include the use of a strong scaffold material with or without cells and/or growth factors to promote osteogenesis [223-226].

In these strategies, the solid scaffold serves as the stabilization of the defect until the regenerated bone can sufficiently support the load. Loading of long bones varies by location but can be as much as 45 MPa with simple movements [227]. To support such loads mechanically strong materials must be used such as ceramics and polymers [224-226, 228-231]. Among those investigated, poly(propylene fumarate) (PPF) is a biodegradable linear polyester with many unsaturated double bonds capable of crosslinking and has been shown to be biocompatible[48, 232-234] and osteoconductive [225, 232-235]. Design issues such as scaffold porosity, shape, and architecture can all play a significant role in the tissue response, such that porosity is necessary for bone-scaffold integration and has significant effects on osteoconductivity [236-238]. Studies have previously shown that while solid PPF has mechanical characteristics similar to those of bone, porous PPF, commonly used in tissue engineering strategies, decreases the mechanical strength of the scaffold with increasing porosity [224, 228]. Strategies to address stabilization and bone regeneration have typically employed a solid and porous composite structure or a solid structure with degradable porogens to become porous [51, 239]. In a study by Kempen et al., a solid PPF intramedullary rod embedded with

poly(DL-lactic-*co*-glycolic acid) (PLGA) microparticles for growth factor delivery was used [239]. Intramedullary rods are used clinically to stabilize segmental defects and allow for bone growth and eventual union over the surface while maintaining mechanical support. Traditional metal intramedullary rods are non-degradable and thus remain in the body for the patient's lifetime but biodegradable systems allow for non-permanent fixation of these types of defects and could potentially mechanically stabilize segmental defects while allowing regeneration around them. For this stabilization to be sufficient, the mechanical properties of the intramedullary rod would be required to sustain the loads of the bone and be fixed to each segment of bone to prevent defect collapse and increase torsional stability.

In addition to scaffold design, delivery of drugs or bone healing promoting factors is commonly employed in tissue engineering strategies to accomplish several functions required for tissue regeneration [240-245]. A group of growth factors known as bone morphogenetic proteins (BMPs) have been studied extensively for applications related to bone regeneration. They have been shown to increase bone formation and are osteoinductive when delivered in a controlled manner [243, 246, 247]. Controlled release of BMPs has been studied with various release mechanisms, such as microparticle delivery systems [92, 93, 179, 239, 244, 247-253]. Specifically PLGA microparticles have been studied with recombinant human bone morphogenetic protein-2 (rhBMP-2) entrapped and adsorbed onto the surface [253]. Protein adsorption presents an alternative delivery method, which maximizes control of the factors at the time of scaffold fabrication, as the rhBMP-2 or other factor is not entrapped and therefore fabricated with the microparticles.

In this study, a long intramedullary rod of solid PPF was used to meet these mechanical requirements in a rat segmental femoral defect with additional internal fixation. Surrounding this rod, a porous PPF sleeve was used to increase bone integration and osteoconductivity and provide a structure for the delivery of rhBMP-2 adsorbed on PLGA microparticles. The solid intramedullary rod was hypothesized to enhance the mechanical stability with further enhancement by bone integration into the porous sleeve when present. Additionally, bone regeneration was hypothesized to be significantly affected by the delivery and dose of rhBMP-2.

8.1. Materials and Methods

8.1.1. PPF Synthesis and Scaffold Fabrication

PPF was synthesized according to established methods [254, 255]. Molecular weight was confirmed via gel permeation chromatography (GPC) (Waters, Milford, MA) using polystyrene standards (Fluka, Switzerland). For this study, PPF with a number average molecular weight of 2900 and a polydispersity index of 1.4 was used. To make the solid PPF rods, a solution of PPF and N-vinyl pyrrolidone (N-VP, Sigma-Aldrich, St. Louis, MO) was combined in a 4:1 mass ratio and benzoyl peroxide (BP, Sigma-Aldrich, St. Louis, MO) was added in 2 wt% of the total PPF/N-VP solution. The solution was poured into 1.6 mm diameter poly(tetrafluoroethylene) (PTFE) molds and allowed to crosslink for 24 hr at 60°C. The rods were removed, cut to 8.5 mm in length and sterilized by ethylene oxide gas. For fabrication of porous scaffolds, the same PPF/N-VP/BP solution was prepared as above and combined with 80% w/w NaCl (300-500 μm).

The resultant slurry was packed around a 1.6 mm diameter glass rod concentrically placed in a 3.5 mm diameter x 25 mm cylindrical PTFE mold. After packing the slurry to remove void spaces, the glass rod was removed and the resulting hollow cylinders were allowed to crosslink within the PTFE mold for 24 hr at 60°C. Subsequently, the NaCl/polymer cylinders were removed and cut with a diamond saw into 5 mm long sections. The salt porogen of the scaffolds was then leached in ddH_2O for 1 week with daily water changes, freeze-dried, and sterilized with ethylene oxide gas.

8.1.2. Scanning Electron Microscopy

Scanning electron microscopy samples were prepared by placing longitudinally cut scaffolds on sample holders and sputter coating with approximately 20 nm of gold using a CrC-150 Sputter Coater (Torr International, New Windsor, NY). The top surfaces of scaffolds were viewed using a Quanta 400 Electron Microscope (FEI, Hillsboro, OR) operated at 30kV.

8.1.3. PLGA Microparticle Fabrication and rhBMP-2 Adsorption

PLGA microparticles were fabricated by solvent extraction in a water in oil in water emulsion as previously described [256]. Briefly, 1 g of PLGA (52 mol% DL-lactide:48 mol% glycolide, ~ 50,000 MW, Purac Biomaterials, Gorinchem, The Netherlands) was dissolved in 4 mL of methylene chloride. 500 µL of 0.1 wt% bovine serum albumin (BSA) in phosphate-buffered saline (PBS) was injected into the PLGA solution and vortexed for 60 s. Six mL of 0.3 wt% aqueous poly(vinyl alcohol) (PVA) solution was added and vortexed for 60 s. This solution was added to a stirring solution of 394 mL 0.3 wt% aqueous PVA solution and 400 mL of 0.2 vol% aqueous isopropanol

solution. The extraction took place over 1 hr, when the microparticles were collected by centrifugation, rinsed with ddH_2O three times, frozen and freeze-dried. Microparticles were sterilized with ethylene oxide gas, stored at -20°C and handled thereafter with aseptic techniques.

To create PLGA microparticles with rhBMP-2 (PeproTech, Rocky Hill, NJ), PLGA microparticles were allowed warm to room temperature and a sterile rhBMP-2 solution (0.65 mg rhBMP-2/mL PBS/BSA[0.1 wt%]) was adsorbed onto unloaded PLGA microparticles in a fluid:particle ratio of 0.8 mL/mg. This ratio provided complete wetting of the PLGA microparticles without fluid surplus. After 30 min adsorption time, microparticles were frozen at -20˚C and lyophilized. Thereafter, microparticles were transferred into a new vial.

8.1.4. Composite Scaffold Preparation

Four PPF based scaffold groups and one empty group were included in the *in vivo* study. The groups are described in Table 8.1 and include: Group E: empty defect; Group R: solid PPF intramedullary rod; Group RSB: solid PPF intramedullary rod and porous PPF sleeve filled with 30 μL of 24% w/v Pluronic F-127 with 16.67 mg of blank PLGA microparticles; Group RSLo: solid PPF intramedullary rod and porous PPF sleeve filled with 30 μL of 24% w/v Pluronic F-127 with 12.5 mg of blank PLGA microparticles and 4.17 mg of rhBMP-2 adsorbed PLGA microparticles (corresponding to 2 μg of rhBMP-2 per scaffold based off of previous studies [93, 239, 253, 257] and scaled to the volume of the defect); and Group RSHi: solid PPF intramedullary rod and porous PPF sleeve filled with 30 μL of 24% w/v Pluronic F-127 with 16.67 mg of loaded PLGA microparticles

(corresponding to 8 μg of rhBMP-2 per scaffold based off of previous studies [93, 239, 257] and scaled to the volume of the defect). To fabricate the scaffolds prior to the surgical procedure, the porous sleeves were prewetted with an ethanol gradient and loaded with the Pluronic F-127 and PLGA suspension described above with a vacuum loading process by pipetting 15 μL of the mixture into the center of the sleeve and applying 100 mbar of vacuum, which was held for 15 s. This was repeated with an additional 15 μL of the Pluronic F-127 and PLGA suspension. The resultant 30 μL solution penetrated the scaffold. Each sleeve was incubated at 37°C for 10 min after the addition of the Pluronic F-127, to gel the solution within the pores. Figure 8.1 shows the assembled composite scaffold.

8.1.5. Surgical Procedure

Scaffolds were placed in a critical sized segmental femoral defect in a rat as previously described [239, 258, 259]. Fifty-three Lewis rats between 325 and 350 grams were purchased from Harlan Laboratories (Indianapolis, IN). All procedures complied with protocols approved by the Institutional Animal Care and Use Committee at Rice University.

Briefly, anesthesia was induced using 4% isoflurane in oxygen then maintained on 2% isoflurane in oxygen at 0.5 L/min using a nosecone. The rats were administered buprenorphine at 0.05 mg/kg intraperitoneally for perioperative analgesia and enrofloxacin at 10 mg/kg, subcutaneously for perioperative antimicrobial activity. The right hind leg of the rat was clipped free of hair and 100 μL of 0.25% bupivicaine with 1:200 of epinephrine were administered subcutaneously along the incision line. The rat

was placed on a warming plate and the right leg was prepared sterilely. A 2.5 cm incision was made on the lateral side of the right leg centered between the hip and knee. The femur was exposed by blunt dissection and a polyethylene plate (22x3x4 mm) was fixed to the anterolateral side of the femur with 4 threaded Kirschner wires (Zimmer, Warsaw, IN). A 5 mm defect was created in the diaphysis of the femur using a cutting bur under irrigation of saline. The defect was irrigated to remove any residual bone dust and bone marrow contents. The two wires immediately adjacent to the defect were removed from the bone but remained in the plate. The segments of bone were rotated to allow placement of the scaffold, where one side of the rod, with or without the porous sleeve, was placed in the intramedullary canal of the proximal end of the defect and the opposite end was placed in the intramedullary canal of the distal end while simultaneously rotating the segments of bone back into alignment. This procedure allowed the placement of an 8.5 mm rod into the 5 mm defect. Once in place, the two wires were screwed back into the bone and the wound closed in two layers, muscle and skin, with 5-0 Vicryl sutures (Ethicon, Somerville, NJ). Each rat was given normal saline intraperitoneally at 10 mg/kg per hour of surgery and received a radiograph immediately post-operatively to ensure placement of the plate and alignment of the femur segments. Finally, each rat recovered in an elevated oxygen and warming environment until responsive and ambulating. All rats received buprenorphine every 12 hr at 0.05 mg/kg for 48 hr postoperatively and at 0.025 mg/kg for the next 48 hr. Additionally, each rat received radiographs every 3 weeks to assess bone formation throughout the study.

All rats recovered immediately postoperatively and returned to ambulation. Of the 53 rats operated on, 9 rats experienced loosening of the plate more than 3 days post-

operatively. These animals were euthanized at the discretion of the institutional veterinarian due to difficult ambulation. The remaining 44 rats experienced no altered ambulation.

8.1.6. Radiographic Analysis

Radiographs were taken using an X-ray machine (Faxitron, Lincolnshire, IL), immediately after the surgery (Day 0) and periodically (3, 6, 9 and 12 weeks) after anesthetizing the animal with 2% isoflurane. The percentage of bone formation within the defect was evaluated blindly and independently by three observers (A.M.H., M.B.N., and V.V.M.). Images were scored according to a modified system described previously[260] and shown in Figure 8.2.

8.1.7. Microcomputed Tomography (Micro-CT) Analysis

8.1.7.1. Porous PPF Sleeve:

Three porous PPF sleeves were scanned using a SkyScan1172 micro-CT (SkyScan, Aartsellar, Belgium). A voltage of 40 kV and current of 250 μA were set for the x-ray using a nominal resolution of 5.5 μm/pixel. The scanned image slices were reconstructed with the NRecon program provided by Skyscan, which used a Feldkamp 3D cone beam reconstruction algorithm [261]. The reconstructed images were oriented so that a cylindrical region of interest (ROI) could be created with the CT-Analyzer software provided by Skyscan. A binary threshold of 60-255 was chosen when determining porosity and pore interconnectivity. Scaffold porosity was determined by the following equation:

Equation 8.1. Porosity equation for microcomputed tomography.

$$\% \text{ Porosity} = (1 - V/V_{total\ VOI}) \times 100\%$$

where V is the object volume composed of the polymer and $V_{total\ VOI}$ is the total volume that was selected to encompass the whole scaffold. Pore interconnectivity was quantified by the following equation, which is based on previous reports [93, 228]

Equation 8.2. Interconnectivity equation for microcomputed tomography.

$$\% \text{ Pore Interconnectivity} = (V_{total\ VOI} - V_{post})/(V_{total\ VOI} - V) \times 100\%$$

where V_{post} is the object volume that is present for the defined cube size. Briefly, the pore interconnectivity percentage was determined by how much volume a pre-defined 3D cube can migrate through the void spaces within a scaffold from the outside to the inside as a percentage of the total void volume of the scaffold.

8.1.7.2. Rat Femurs:

All rat femurs (n=8-10) were scanned using the SkyScan 1172 micro-CT imaging system prior to histology and mechanical testing. A voltage of 80 kV and current of 125 μA with a nominal resolution of 10 μm/pixel with a 0.5 mm aluminum filter were chosen based on previous reports [34, 48]. A binary threshold of 70-255 was chosen to accurately represent the bone as a grayscale image. Three-dimensional images were created using the CT-Analyzer software for all samples and blindly reviewed by three individuals (A.M.H., M.B.N., and V.V.M.). Percentage of guided bone growth within the defect area at 12 weeks was assessed using the same scoring system as previously described for radiographic analysis.

The percentage of bone formation was quantitatively determined by creating a volume of interest that incorporates the defect and all regenerated bone, with a height of 5 mm, length of 8.1 mm and depth of 8 mm. The ROI height was located equidistant from the two K-wires adjacent to the defect. The data are reported as the percentage of bone volume found within the created ROI within the CT-Analyzer software.

8.1.8. Biomechanical Testing

Femurs from 5 rats from each group were excised after euthanasia at 12 weeks postsurgery. Excess soft tissue was removed and the femurs were wrapped in PBS-soaked gauze and stored at -20°C until testing. Prior to mechanical testing, micro-CT scans were taken. Briefly, samples were thawed at room temperature and the inner two K-wires were removed to prevent interference with the x-rays. After micro-CT scans were taken, femur ends were potted in acrylic cement (Great Lakes Orthodontics, Tonowanda, NY) in custom made stainless steel holders up to the fixation plate while wrapped in PBS-soaked gauze to prevent dehydration. After sufficient polymerization of the cement; gauze, the remaining outer two K-wires, and fixation plates were carefully removed and each sample was mounted in an MTS 858 Mini Bionix II testing system (MTS, Eden Prairie, MN) with the bones coaxially aligned to the system axis of rotation. Each femur was rotated at 6°/s until failure or for 20 s. Maximum torque (N-mm) and torsional stiffness (N-mm/°) were recorded for each specimen, with the stiffness being measured as the slope of the linear portion of the torque–angular displacement curve [262, 263]. Mechanically unstable bones were not tested, and their values were considered to be zero in the statistical analysis.

8.1.9. Histological Processing

After the rat femurs were excised, the femurs were placed in 10% neutral buffered formalin for at least three days (n=3-4). After micro-CT scanning, the femurs were dehydrated in increasing concentrations of ethanol (70-100%) and then embedded in methylmethacrylate. All samples were initially hemi-sectioned through the center of the defect and each section was cut in the longitudinal direction parallel to the polyethylene fixation plate using a microtome with an inner circular diamond blade (Leica Microsystems, Nussloch, Germany). Sections were stained with methylene blue/basic fuchsin (n=3).

8.1.10. Light Microscopy and Histological Scoring

All sections were observed using an upright AxioImager.Z1and AxioCam MRc 5 (Carl Zeiss AG, Oberkochen, Germany) and were reviewed by three blinded observers (A.M.H., M.B.N., and V.V.M.) using a quantitative scoring system (Table 8.2). Samples were observed for tissue response at the implant surfaces (rod and sleeve), within the pores of the sleeve, as well as the presence of cartilage surrounding the implant (rod and sleeve).

8.1.11. Statistical Analysis

Mechanical testing values were analyzed using a one-way ANOVA and any significance was analyzed with a *post-hoc* unpaired t-test. Radiographic and histologic scores were analyzed using nonparametric statistical tests. For both radiograph and histology scores of hard tissues, the Kruskal-Wallis one-way analysis of variance was

used and *post-hoc* analysis with the Dwass-Steel-Critchlow-Fligner test. For histology scores of cartilage tissues, the Fisher-Freeman-Halton analysis of variance was used and *post-hoc* analysis with Fisher's exact test. For all statistical methods, an *a priori* level of significance was set at α=0.05.

8.2. Results

8.2.1. Characterization of PPF Scaffolds

Scanning electron micrographs as seen in Figure 8.1 revealed a porous network within the PPF sleeve, with pores ranging in size from 50 to 500 μm. The pores were distributed evenly throughout the scaffold (both outer and inner surface) and were roughly cubical in shape. Micro-CT analysis demonstrated a total porosity of 74.5 ± 2.1%, where a larger minimum interconnection size (352 μm) from leached NaCl crystals resulted in 45.0 ± 3.1% interconnected porosity, whereas a smaller minimum interconnection size (44 μm) resulted in 93.2 ± 2.5% interconnected porosity.

8.2.2. Radiographic Analysis at weeks 3, 6, 9, and 12

Representative images of bone formation shown by radiography for each group at week 12 are shown in Figure 8.3. The scores resulting from the level of bone formation from each radiograph are depicted in Figure 8.4. Groups E, R, and RSLo showed an increasing trend in bone formation throughout the duration of the experiment. However, only group E showed that bone formation was significantly higher at week 12 compared to that observed by weeks 3, 6, and 9 ($p < 0.05$). While there was no significant bone formation between any of the groups at weeks 3 and 6, by week 9 differences were

observed. The highest bone formation at week 9 was for groups R and RSLo compared to groups E, RSB, and RSHi ($p < 0.05$). The significant differences were similar to week 12; however, group E was also significantly higher than RSB and RSHi ($p < 0.05$).

8.2.3. Micro-CT Analysis

The amount of bone formed within the defect was evaluated both qualitatively and quantitatively at 12 weeks with micro-CT. Complete bone union was not observed in any sample as evaluated by observing three-dimensional images of the femurs as shown in Figure 8.5. Bone formed along the outside edges of the defect area. The majority of samples showed that the bone formation occurred along the polyethylene plate, which can be seen in the representative images. The scores given to all the groups for bridging within the defect were not significantly different at 12 weeks as shown in Figure 8.6.

Figure 8.7 shows the percentage of bone volume for intact femurs (C) and all experimental groups. The percentage of bone volume for the intact femurs was significantly higher by approximately 2-fold compared to the experimental groups ($p < 0.05$). Additionally, the RSHi group had more bone formation at 12 weeks compared to the E and RSB groups ($p < 0.05$).

8.2.4. Histological Analysis

At the 12 week time point, a fibrous capsule or immature/mature bone was most commonly found surrounding the PPF rod and/or PPF porous sleeve for each group. However, no bone union was observed. When there was a presence of immature/mature bone around the scaffolds, it always surrounded the outer periphery of the PPF rod and/or

PPF porous sleeve for each group. Immature cartilage was also observed in the samples, which was often near the presence of osteoids containing osteoblasts and osteoclasts. Pores within the sleeve were mainly filled with fibrous tissue. The RSLo and RSHi groups had some samples that contained bone within the outer pores of the porous sleeve versus the RSB group, which contained a layer of bone that did not penetrate the pores as shown in Figure 8.8. For each group, at least one rod was broken by the end of the study at 12 weeks. Whenever this occurred, one end of the rod within the intramedullary canal was always surrounded by bone.

The tissue response was evaluated for all the groups (n=3-4) at the bone-rod interface, bone-sleeve interface, and within the pores of the sleeve at 12 weeks as shown in Figure 8.9A-C. Figure 8.9A shows tissue response scores at the rod interface within the intramedullary canal (IM) and the defect area. The RSLo and RSHi groups showed significantly lower scores compared to the R and RSB group within the intramedullary canal ($p < 0.05$). However, within the defect area, no differences were observed.

The scoring of the hard tissue response at the porous sleeve interface can be seen in Figure 8.9B. Two different locations were evaluated at the porous sleeve interface: adjacent to the original defect and within the central defect area. No significant differences were observed for either of the interface areas at week 12. Tissue response scores within the pores of the PPF porous sleeve were given for the RSB, RSLo, and RSHi groups as shown in Figure 8.9C. The results showed that no significant differences were observed between all the groups.

The presence of cartilage was also evaluated at the rod interface, within the intramedullary canal and defect area, as well as within the pores of the porous sleeve as shown in Figure 8.9 with a representative image shown in Figure 8.10. The rod interface created significantly more immature cartilage tissue compared to the RSHi group within the intramedullary canal ($p < 0.05$). The R group also showed more cartilage formation than the rest of the other groups along the rod interface within the defect area ($p < 0.05$). Cartilage was not found for the RSB group at the rod-defect area. The pores within the sleeve were also evaluated for cartilage tissue formation and no significant differences were found.

8.2.5. Biomechanical Analysis

Torsional mechanical testing was performed to assess the functional recovery of sample femurs. All experimental groups exhibited significantly greater maximum torque (N-mm) and torsional stiffness (N-mm/°) when compared to empty defects ($p < 0.01$) as shown in Figure 8.11. Additionally, the femurs of animals receiving low dose rhBMP-2 exhibited significantly greater maximum torque than those with a rod alone ($p < 0.05$). For torsional stiffness, both groups receiving rhBMP-2 performed significantly better than the group with only the rod ($p < 0.05$). Contralateral control femurs from each rat were also tested and exhibited significantly higher torque and stiffness for each sample ($p < 0.05$).

8.3. Discussion

To address the mechanical as well as regenerative requirements of segmental defects, structural components of tissue engineering strategies must be considered. Clinically used intramedullary rods or internally fixed plates provide mechanical support, but require lifetime placement or subsequent surgical removal. Considering the scaffold requirements for stabilization and tissue engineering two conflicting principles must be addressed, decreased porosity for strength and increased porosity for tissue ingrowth and remodeling. A composite scaffold provides potential for these principles to be addressed.

In this study, a composite scaffold design was hypothesized to increase mechanical stabilization through incorporation of a solid PPF intramedullary rod and bone tissue integration through a porous PPF sleeve in a critical size rat femoral defect. Additionally, increased bone regeneration was hypothesized in groups with increased levels of rhBMP-2. The study results indicate that mechanical properties were enhanced by the presence of the scaffolds as shown in Figure 8.11 and the quantity of bone regeneration increased with rhBMP-2 delivery.

The scaffold clearly impacted the results through all analyses, including bone regeneration, mechanical stability and tissue response. Presence of a scaffold increased mechanical stability in all groups and was further increased with rhBMP-2 as in the RSLo group. The relationship between bone regeneration and mechanical strength has been previously reported in both ceramic and polymeric materials in calvaria [32, 264, 265] and long bones [225, 262]. Consistent with the studies in long bones, increased

bone formation increased the mechanical stability of implants, even when bridging did not occur.

Additionally, the radiographic scores showed that group R regenerated more bone than the RSB group at weeks 9 and 12. In the group with only the rod, there was no direct apposition of the scaffold to the cut bone surface, which prevented direct growth of bone from the cut plane of bone. In all groups with the porous sleeve, the scaffold was in immediate apposition to the cut surface of bone, filling the space of potential bone growth. As indicated in Figure 8.8, there was not significant PPF degradation over the 12 weeks, such that the potential space for bone growth was not created by degradation and bone regeneration was limited to the pores of the scaffold and the outer surface as seen in the radiograph (Figure 8.3) and micro-CT images (Figure 8.5). This limited the majority of bone growth in groups with the porous sleeve to the surface, which has been previously described [237, 239, 266]. In a study by Woodard et al., growth into the scaffold was dependent upon the presence of micropores (2-8 μm) and limited to surface growth when only larger pores were present as is in this study [237]. Another study by Aronin et al. similarly found that smaller pore sizes (100 μm) had increased tissue infiltration compared to larger pore sizes (500 μm) in rat critical-sized cranial defects [267]. In addition to pore size, pore and scaffold architecture have also been shown to play a critical role in tissue response [236, 268-270]. For example, Kim et al. showed that scaffolds fabricated by stereolithography with a highly permeable and porous architecture induced upregulation of osteogenic signal expression with rat bone marrow stromal cells *in vitro* when compared to random porous architecture as in this study [270]. Another interesting study found that scaffold architectures that mimic the structure of native bone

have exhibited up to a 500% increase in bone volume when compared to defined architectures [271].

Decreased bone formation as a result of the porous sleeve can also be attributed to isolation of cell sources. The osteoprogenitor cells responsible for regenerating the bone in these acellular scaffolds would likely be cells from the periosteum or the bone marrow. As the porous sleeve separates these two populations with an open but tortuous route, the impact of both cell types on bone regeneration could be diminished.

Scaffold design also had a significant impact on the cartilage tissue response. Within the defect area, group R showed significantly more cartilage formation than any other group. Cartilage formation in bone defects has been previously reported by Sarkar et al. [272]. This immature cartilage formation could lead to bone regeneration through hypertrophy of the chondrocytes and ossification. Additionally, other factors could contribute to the chondrogenesis present in the defect, such as low oxygen tension due to removal of vasculature present in the defect previously.

Delivery of rhBMP-2 also affected the bone regeneration, mechanical stability and tissue response. While radiography indicated group RSLo to have the greatest bone regeneration at 12 weeks, micro-CT indicated the most bone formation in group RSHi. As micro-CT is a quantifiable technique opposed to a viewer scored system, it is more reliable at accurately measuring bone formation although radiography may indicate density of bone growth in greater detail. This hypothesis is supported by the mechanical data, which showed the group RSLo had increased mechanical stability of it over the R group. Integration between the regenerated bone and the scaffold was not significant as

shown through the histological scores for the tissue present within the pores of the scaffold. Therefore, the transmittance of load between the regenerated bone and the scaffold imparted in the group RSLo is attributed to the strength of bone surrounding the scaffold. Previous studies have shown there can be a lack of correlation between the bone regeneration in a scaffold and the resultant mechanical properties at the interface as was seen with groups RSLo and RSHi [32, 264].

The tissue response showed decreased scores (more fibrous tissue and/or inflammatory cells present) adjacent to the rod in the intramedullary canal when there was rhBMP-2 present. Recently, with the increased clinical use of rhBMP-2, case reports and studies have shown inflammatory processes likely caused by the release of rhBMP-2 [273, 274]. While the mechanism has not been directly identified, the phenomenon has caused reconsideration of use of rhBMP-2 near swelling sensitive tissues such as airways. This same process could explain the increased inflammation present in the groups with rhBMP-2.

Finally, there was increased cartilage formation against the rod in the intramedullary canal when higher doses of rhBMP-2 were delivered compared to the rod alone. Previous studies have shown that that mesenchymal stem cells can be induced down a chondrogenic lineage when in low oxygen tension environments and in the presence of rhBMP-2 [275]. This result also suggests higher concentration of rhBMP-2 in the intramedullary canal in the RSHi group versus the RSLo group. This observation is consistent with the decreased mechanical strength in the RSHi group versus RSLo group. An increase in microparticle placement in the intramedullary canal could be due to scaffold loading parameters. As is described above, rhBMP-2 was adsorbed onto a

subset of PLGA microparticles and these two groups of microparticles were used in ratios to create groups with 0, 2, and 8 μg of rhBMP-2 per defect. This meant that for the RSHi group all microparticles had adsorbed proteins. This adsorption could have increased electrostatic interactions between particles creating aggregates, that when loaded into the porous sleeve did not penetrate the scaffold due to size. A lack of penetration of particles would increase the number of particles transferred to the rod as it slid into the sleeve during the surgical procedure. As the cartilage formed could be well vascularized if given enough time this would be expected to undergo hypertrophy and ossification creating bone tissue, although that was not seen in the 12 weeks of this study.

Several conclusions can be drawn from the model system described above regarding bone regeneration with rhBMP-2 with porous scaffolds in the defect, but to further understand the relationship between these two components more groups would be necessary. Primarily, a group with the porous sleeve without the rod, while contrary to the objective of increased stability, could allow for more investigation into the role of bone marrow stromal cells in the regenerative process. Additionally, including groups which deliver rhBMP-2 without the porous scaffold, could show the degree of effect of the porous scaffold has on bone regeneration. Finally, a larger animal model would be necessary to further investigate the role of mechanical stability as this model describes a load-bearing bone, off-loaded by internal fixation. While the majority of the defect load is supported by the polyethylene plate, the results indicate some degree of load transfer to the scaffold, indicated by the breaking of the rod in scaffolds where the rod was surrounded by new bone within the intramedullary canal. Nevertheless, this study clearly indicates the increased stabilization effect of composite scaffolds utilizing both porous

and solid structures as shown by the increase in mechanical strength of group R over group E and group RSLo over group R. Additionally, rhBMP-2 increased bone formation as hypothesized.

8.4. Conclusion

The presented study analyzed the effects of composite scaffold construction, which aimed to address the bone regeneration and stabilization concerns of non-union fractures. While in no experimental groups was the segmental femoral defect in the rat bridged, many conclusions can be drawn concerning scaffold design from this model system. These conclusions address issues regarding the source of stem cell populations in an acellular construct, factors associated with stabilization of non-unions, and environmental factors present in a defect driving cell differentiation. Results showed increased bone formation in groups without the porous sleeve, suggesting the role of the sleeve as a physical barrier to both bone growth and to the migration of regenerative cells present in the bone marrow and periosteal regions. Conversely, while the scaffold was shown to be hinder bone bridging, it did impart significant mechanical strength to the defect, a critical objective to non-union therapy. Lastly, environmental factors, such as low oxygen tension or micromotion could contribute to the tissue formed and the control of these factors would be necessary to elucidate the causal effects of parameters tested.

8.5. Tables and Figures

Table 8.1. Abbreviations for all the groups in the study.

Group	Description
C	Femur with no defect
E	Empty
R	Rod
RS	Rod + sleeve
RSLo	Rod + sleeve loaded with 2 μg BMP-2
RSHi	Rod + sleeve loaded with 8 μg BMP-2

Table 8.2. Quantitative histological analysis of the hard tissue response at the PPF rod and porous PPF sleeve interface within the intramedullary canal and adjacent to the initial defect margin, respectively. Also, the hard tissue response for the PPF rod and porous PPF sleeve interfaces were evaluated in the defect. For the porous PPF sleeve the hard tissue response within the pores was also investigated. Additionally, the presence of cartilage tissue formation was observed within the intramedullary canal for the PPF rod, around or within the PPF porous sleeve, and within the defect for both the PPF rod and porous PPF sleeve.

Hard tissue response at PPF rod/porous sleeve interface

Description	Score
Direct bone to implant contact without soft interlayer	4
Remodeling lacuna with osteoblasts and/or osteoclasts at surface	3
Majority of implant is surrounded by fibrous tissue capsule	2
Unorganized fibrous tissue (majority of tissue is not arranged as a capsule)	1
Inflammation marked by an abundance of inflammatory cells and poorly organized tissue	0

Hard tissue response within the pores of the PPF sleeve

Description	Score
Tissue in pores is mostly bone	4
Tissue in pores consists of some bone within mature, dense fibrous tissue and/or few inflammatory response elements	3
Tissue in pores is mostly immature fibrous tissue (with or without bone) with blood vessels and young fibroblasts invading the space with few macrophages present	2
Tissue in pores consists mostly of inflammatory cells and connective tissue components in between (with or without bone) OR the majority of the pores are empty or filled with fluid	1
Tissue in pores is dense and exclusively of inflammatory type (no bone present)	0

Presence of cartilage tissue formation at the PPF rod/porous sleeve interface

Description	Score
Yes	1
No	0

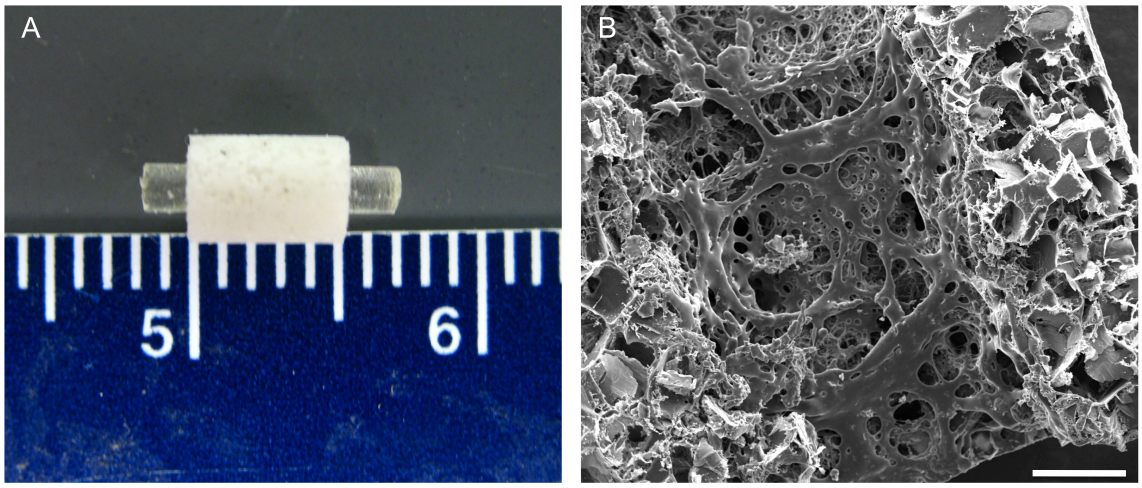

Figure 8.1. Structure of the PFF scaffold shown grossly in (A) where the rod is placed in the porous sleeve and microscopically through scanning electron microscopy shown in (B). Scale bar in (B) represents 500 µm.

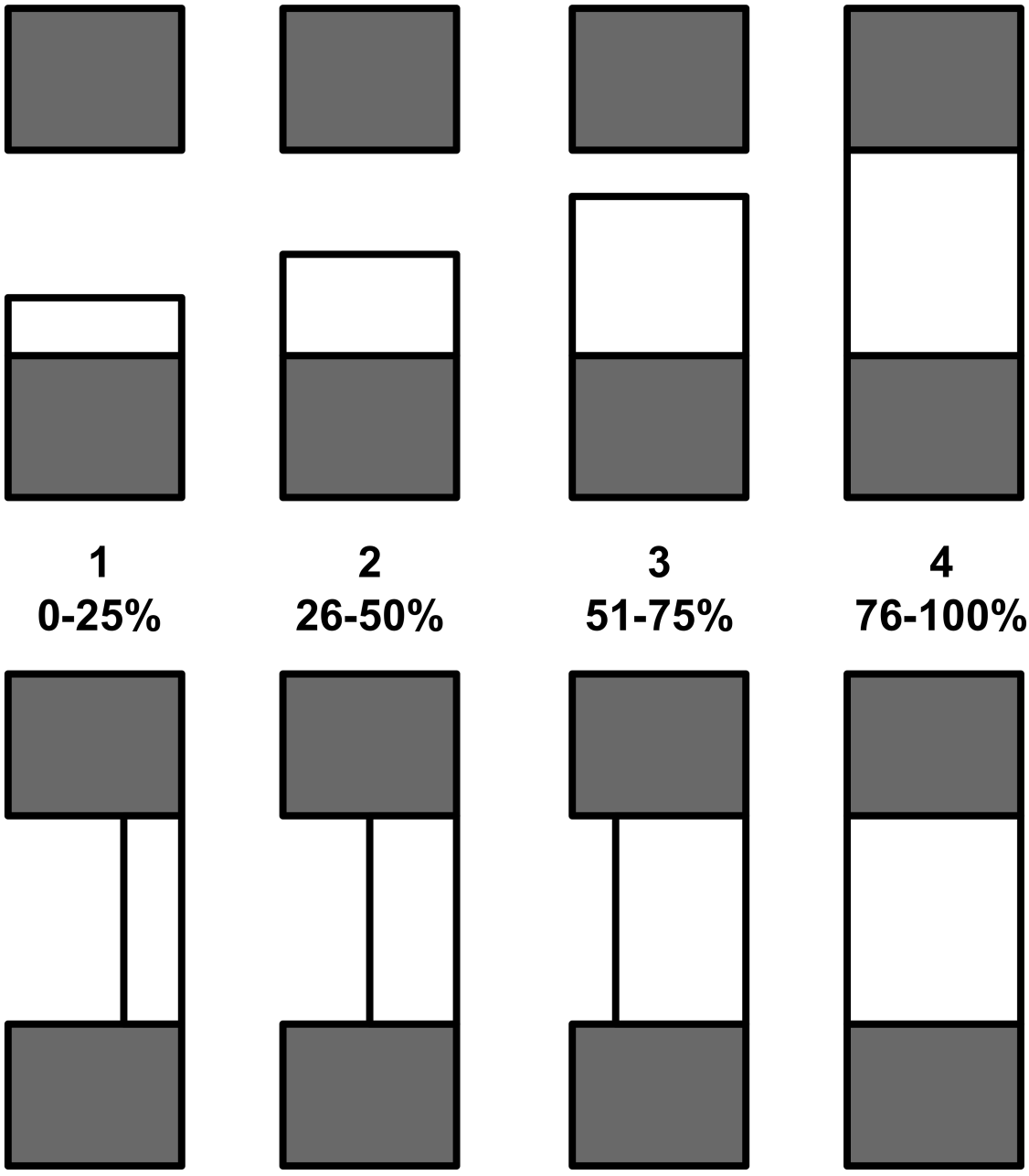

Figure 8.2. Schematic representation of the scoring system used for evaluation of radiographic and micro-CT images [260].

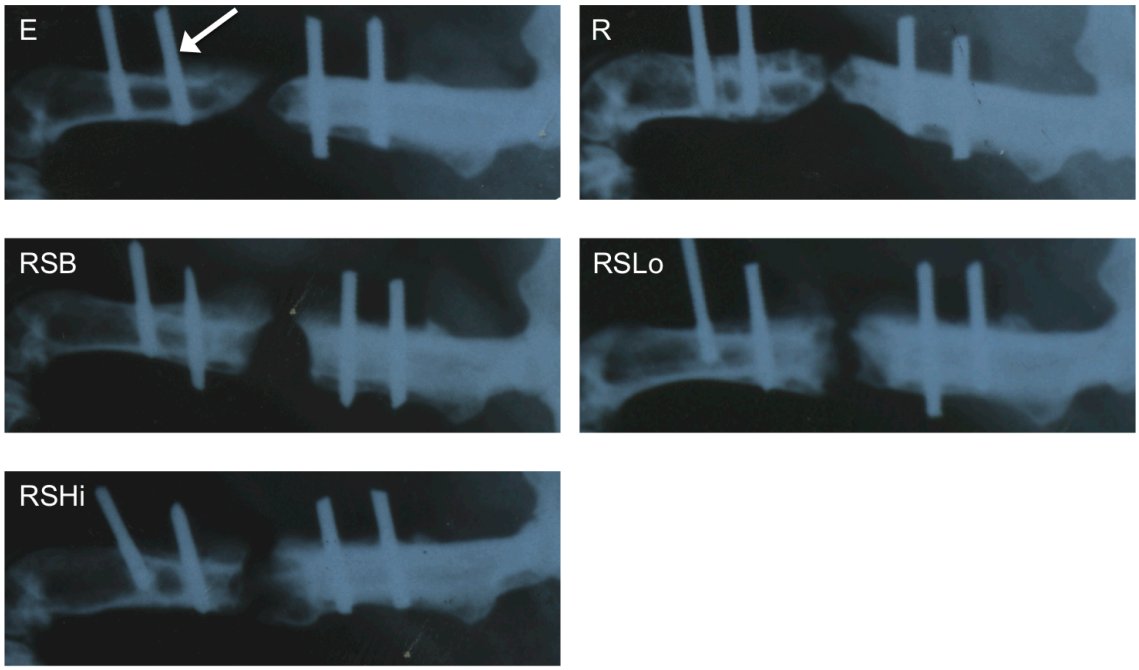

Figure 8.3. Representative x-ray micrographs of the rat femoral segmental defect at 12 weeks (refer to groups described in Table 8.1). The distal side (knee) is located on the left and the proximal end (hip) of the femur is on the right of each radiograph. The white arrow is pointing to the location of a K-wire. The original defect (5 mm) is centered between the two inner K-wires. Although bridging is close in several groups (R, RSLo), complete bone union was not observed in any groups at this time point.

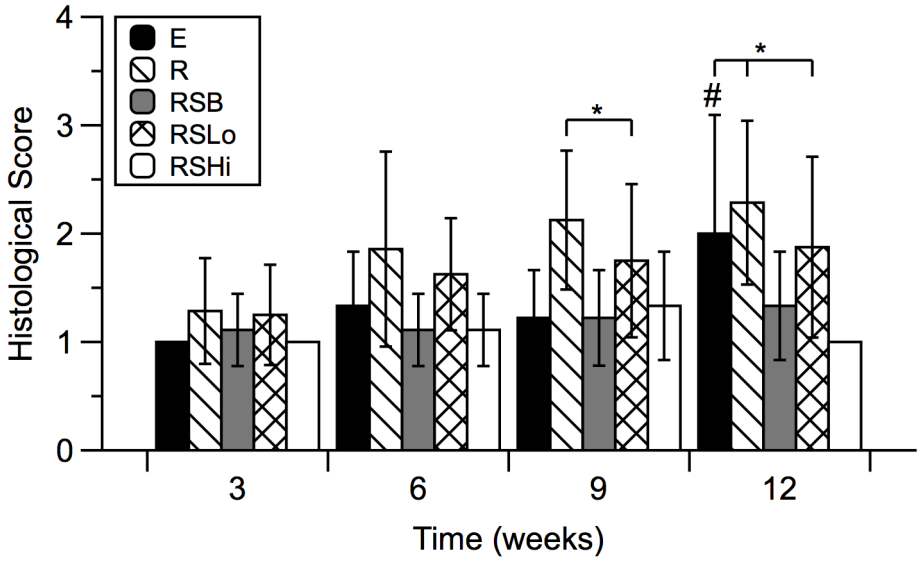

Figure 8.4. Radiographic scores for bone formation within the defect at 3, 6, 9, and 12 weeks. Data are reported as means with standard deviations (n = 6-9). * indicates significant differences with other groups at the same timepoint ($p < 0.05$). # denotes that group E at week 12 is significantly different from weeks 3, 6, and 9 ($p < 0.05$).

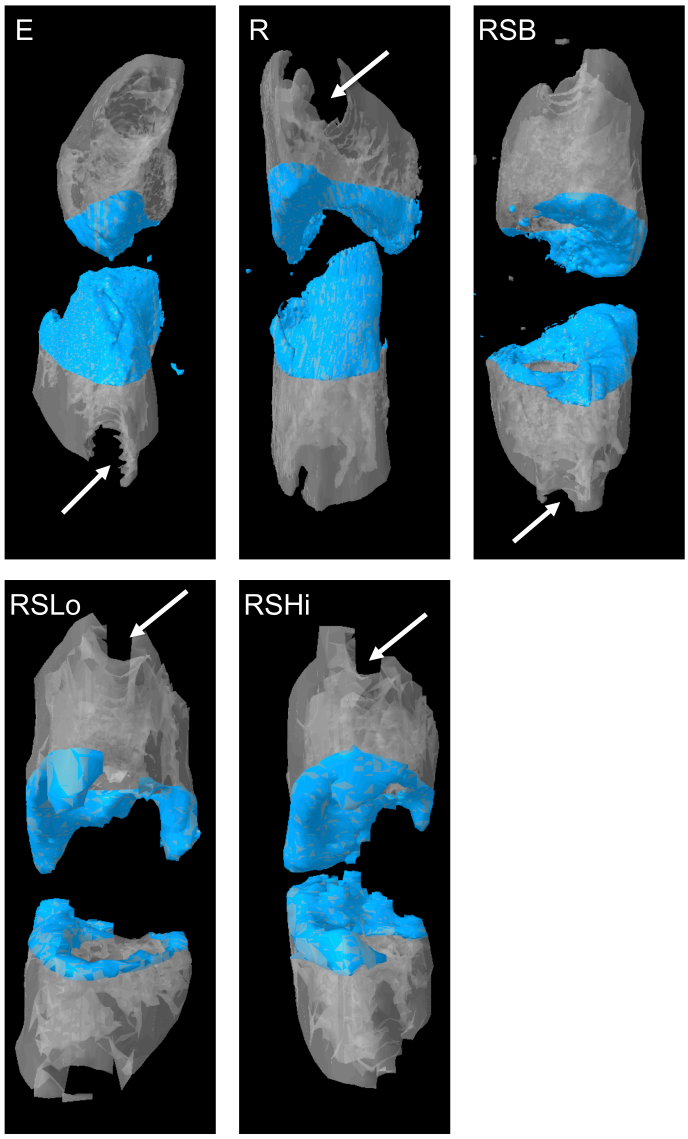

Figure 8.5. Representative micro-CT images for each group at 12 weeks. The shaded area represents the defect space with a height of 5 mm with the polyethylene plate (not-visible) being located behind the bone images. The arrow indicates the location of a removed K-wire. Bone formation occurred along the periphery of the defect area for the groups that contained a PPF rod and/or sleeve.

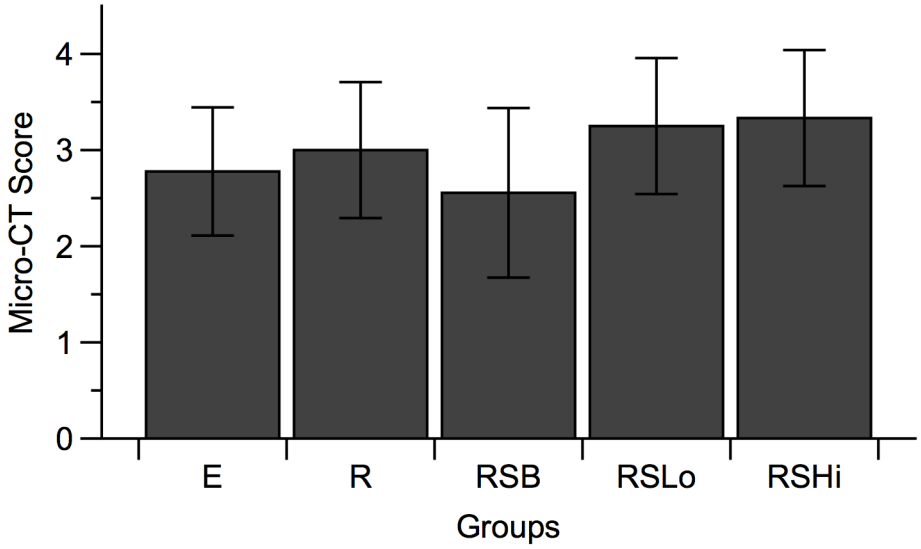

Figure 8.6. Micro-CT scores for bone formation within the defect at 12 weeks. Data are reported as means with standard deviations (n = 8-9).

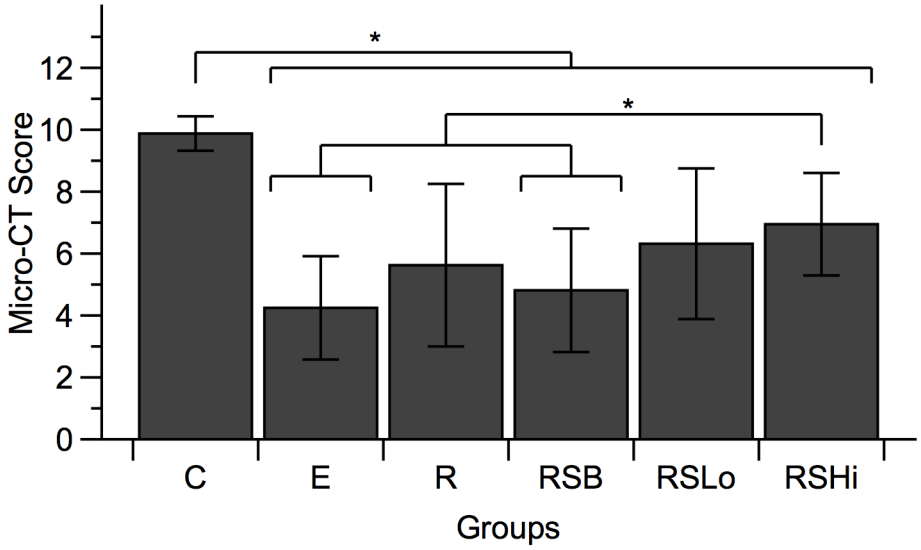

Figure 8.7. Percentage of bone volume formed at 12 weeks within the 5 mm femoral defect calculated by micro-CT for all groups. Data are reported as the means with standard deviations (n = 8-9). * indicates statistical differences compared between the groups denoted ($p < 0.05$).

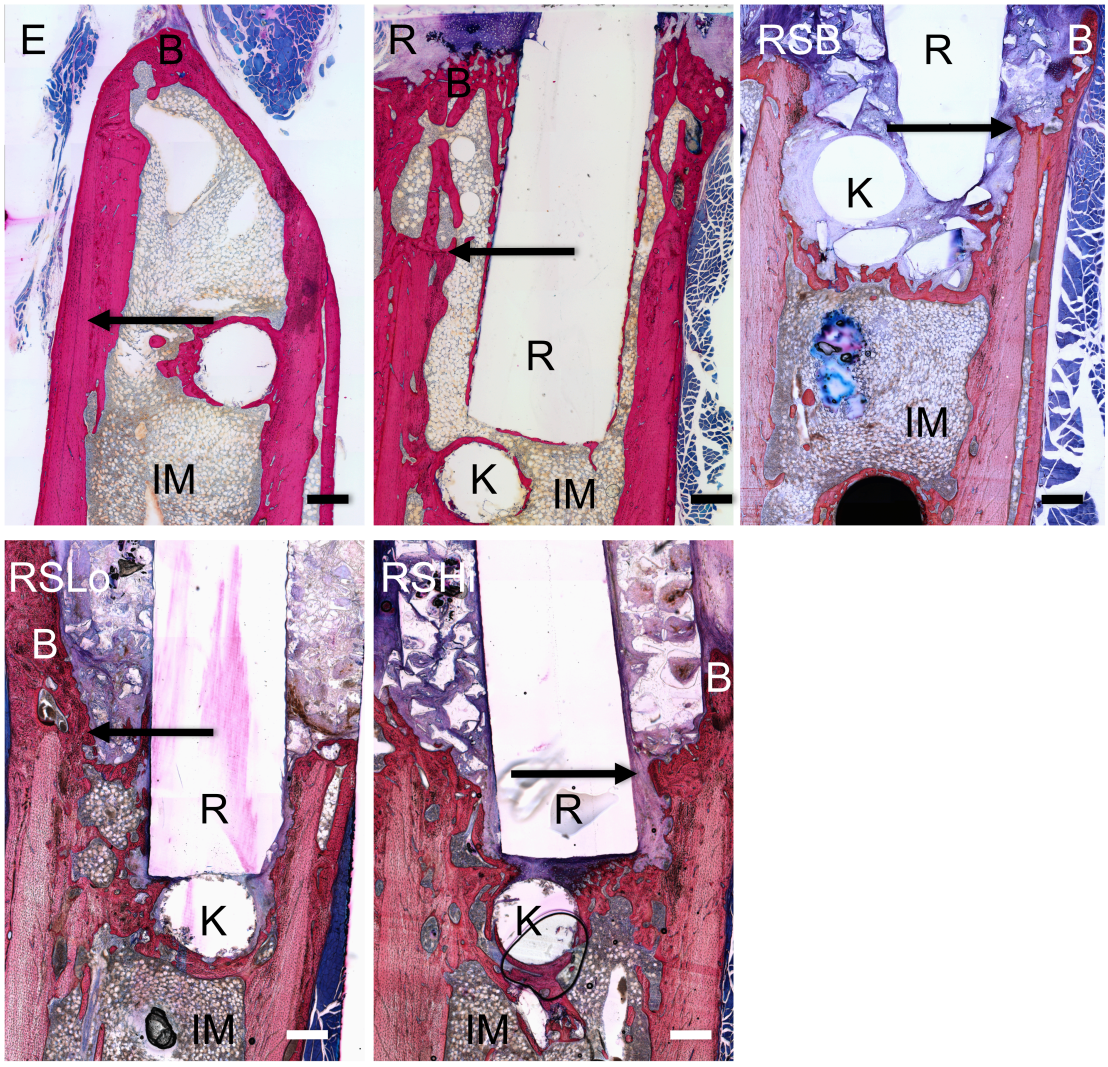

Figure 8.8. Representative histological images for each group at 12 weeks. Bone formation readily occurred at the PPF rod interface or on the periphery of the PPF porous sleeve. IM – intramedullary canal with bone marrow, R: PPF rod, B: newly formed bone, S: remaining porous scaffold, K: location of removed K-wire, arrows indicate the initial defect margin. Scale bars represent 500 µm.

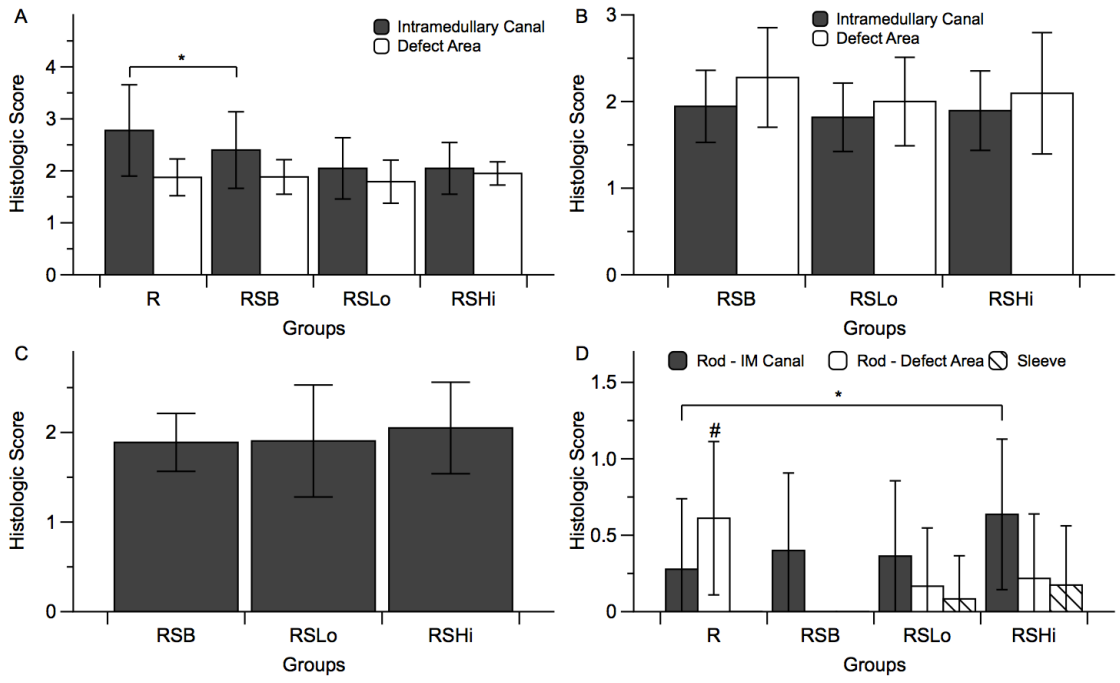

Figure 8.9. Histological scores for the hard tissue response at week 12 (A) at the rod interface within the intramedullary canal and within the 5 mm defect area, (B) at the porous PPF sleeve interface along the initial defect margin and within the defect area and (C) within the pores of the porous PPF sleeve; as well as (D) for the presence of cartilage formation against the solid PPF rod within the intramedullary canal and within the defect area, and against the porous PPF sleeve. Data are reported as means with standard deviations (n=3-4). * indicates statistical differences compared to other groups ($p < 0.05$).

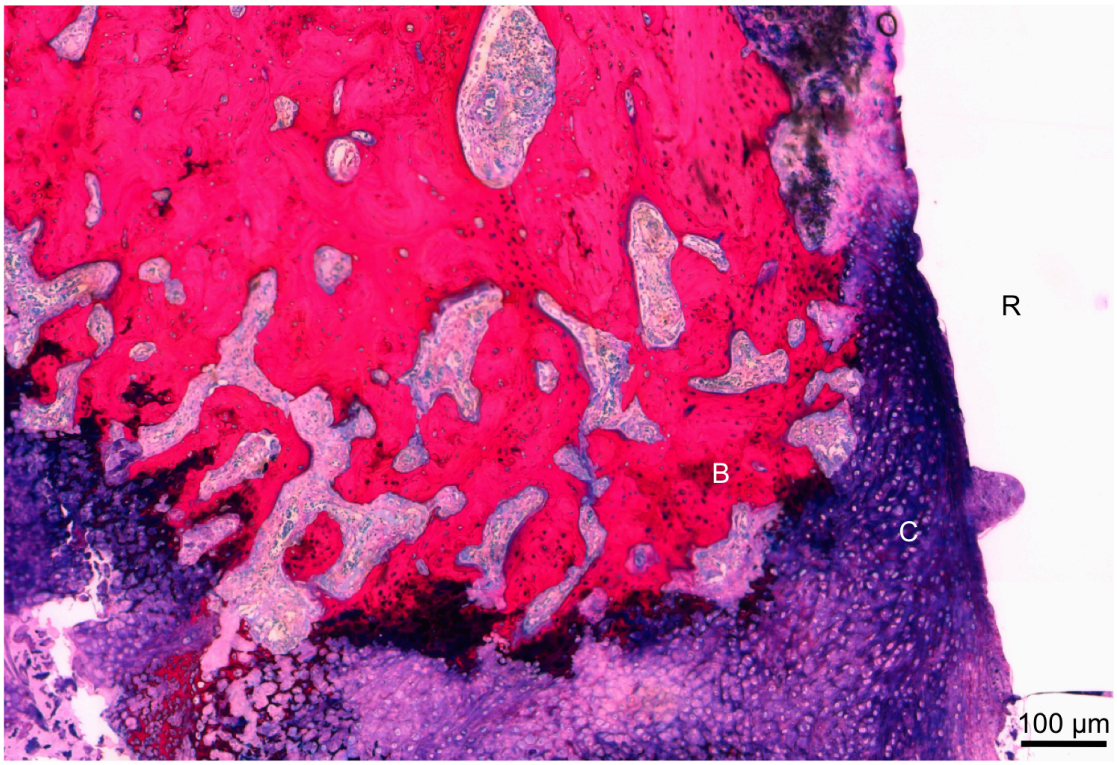

Figure 8.10. Representative histological section of group R at 12 weeks. Immature cartilage formation (C), noted by the dark purple matrix with blue cells, was found along the PPF rod surface (R). Newly formed bone (B) was found along the cartilage. Scale bar represents 100 µm.

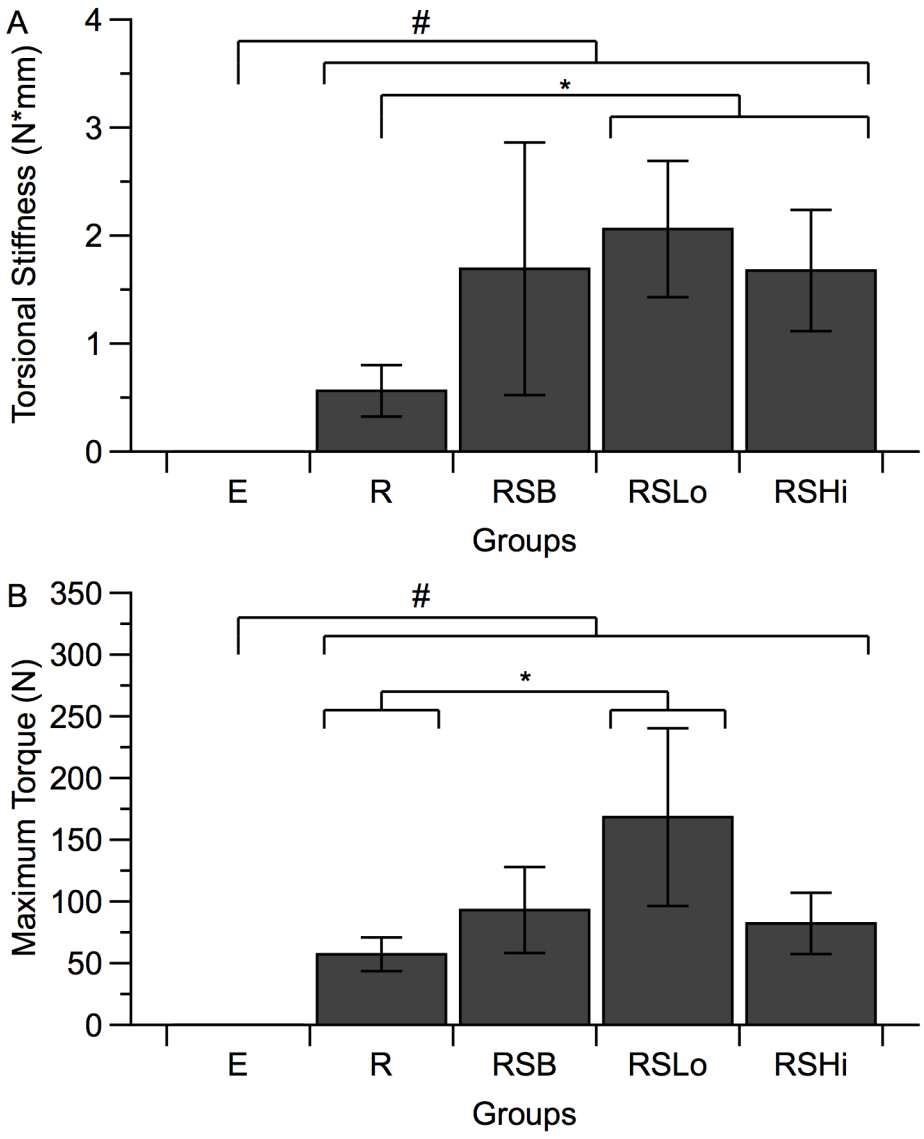

Figure 8.11. Torsional stiffness (A) and maximum torque (B) for harvested specimens from each group at 12 weeks. Data are reported as means with standard deviation (n=6). # indicates significant differences between all experimental groups and empty defects ($p < 0.01$). * indicates significant differences between groups marked ($p < 0.05$).

Chapter 9

Summary

The goals of this work were to evaluate aspects of the two stage strategy to craniofacial repair. The first objective was to evaluate porous space maintenance. In this first study, prefabricated implants were characterized for porosity and evaluated for soft tissue healing and tissue response in a composite tissue defect model of the rabbit mandible. This study indicated that porous implants may have enhanced soft tissue regeneration over them and that low porosity implants reduced the amount of inflammation present around and in the implant at 12 weeks. Study 2 evaluated the solid and low porosity implants in the same model using implants fabricated *in situ*. This differences allowed for the evaluation of the curing of the construct on the soft tissue healing and tissue response.

The second objective was to characterize and evaluate antibiotic-releasing scaffolds for their physicochemical characteristics, release kinetics, *in vitro* efficacy and *in vivo* efficacy. Study 1 characterized porous space maintainers fabricated with PMMA-

based bone cement and gelatin microparticles for their mechanical strength, porosity, interconnectivity and release kinetics. The release of colistin from porous PMMA-based space maintainers could be tuned with fabrication and loading parameters. Similarly, study 2 characterized the physical properties and release kinetics of porous space maintainers fabricated with PMMA-based bone cement and a gelatin matrix from a clinical product. This study showed similar results in that fabrication parameters could control release kinetics and furthered the idea of rapid translation of these strategies considering the clinical products used. Finally, study 3 evaluated these antibiotic releasing porous space maintainers in an infected composite tissue defect model of the rabbit mandible. Extended release of antibiotics increased soft tissue healing over that of more burst release and that no inoculum was detected at the end of the 12 week study.

Objective 3 investigated the regeneration of bone in large defects where stabilization of the defect ends may be necessary and vascularization of the implant preimplantation may be necessary. Study 1 illustrated value of mechanically stabilizing structures in bone regeneration strategies to enhance biomechanical properties of the defect.

The three objectives investigated in this work strengthen the strategy employed utilizing two stages of regeneration, isolating the regeneration of soft tissues around a bone defect from that of the bone itself. Overall, this work provides evidence that while tissue engineering strategies with degradable scaffolds obviating the need for multiple surgeries is ideal, the principles of tissue engineering can be applied to clinical material in new strategies to enhance craniofacial reconstruction with more rapid clinical translation.

References

[1] Rowlands RP, Turner P. The Operations of Surgery. New York: MacMillan; 1915.

[2] Christensen LV, McKay DC. Rotational and translational loading of the temporomandibular joint. Cranio : the journal of craniomandibular practice 2000;18:47-57.

[3] van Eijden TM. Biomechanics of the Mandible. Critical Reviews in Oral Biology & Medicine 2000;11:123-36.

[4] Seper L, Piffko J, Joos U, Meyer U. Treatment of fractures of the atrophic mandible in the elderly. J Am Geriatr Soc 2004;52:1583-4.

[5] Hidalgo DA. Fibula free flap mandibular reconstruction. Clinics in plastic surgery 1994;21:25-35.

[6] Mao JJ, Giannobile WV, Helms JA, Hollister SJ, Krebsbach PH, Longaker MT, et al. Craniofacial tissue engineering by stem cells. J Dent Res 2006;85:966-79.

[7] Smolka W, Iizuka T. Surgical reconstruction of maxilla and midface: Clinical outcome and factors relating to postoperative complications. J Cranio Maxill Surg 2005;33:1-7.

[8] Marx RE. Clinical application of bone biology to mandibular and maxillary reconstruction. Clinics in plastic surgery 1994;21:377-92.

[9] Bernhart BJ, Huryn JM, Disa J, Shah JP, Zlotolow IM. Hard palate resection, microvascular reconstruction, and prosthetic restoration: a 14-year retrospective analysis. Head & Neck 2003;25:671-80.

[10] Sharma AB, Beumer J. Reconstruction of maxillary defects: the case for prosthetic rehabilitation. Journal of oral and maxillofacial surgery : official journal of the American Association of Oral and Maxillofacial Surgeons 2005;63:1770-3.

[11] Eppley BL, Sadove AM. Management of alveolar cleft bone grafting--state of the art. The Cleft palate-craniofacial journal : official publication of the American Cleft Palate-Craniofacial Association 2000;37:229-33.

[12] Kretlow JD, Young S, Klouda L, Wong M, Mikos AG. Injectable Biomaterials for Regenerating Complex Craniofacial Tissues. Adv Mater 2009;21:3368-93.

[13] Poshusta AK, Anseth KS. Photopolymerized biomaterials for application in the temporomandibular joint. Cells Tissues Organs 2001;169:272-8.

[14] Kasper FK, Young S, Tanahashi K, Barry MA, Tabata Y, Jansen JA, et al. Evaluation of bone regeneration by DNA release from composites of oligo(poly(ethylene glycol) fumarate) and cationized gelatin microspheres in a critical-sized calvarial defect. J Biomed Mater Res B 2006;78:335-42.

[15] Klouda L, Hacker MC, Kretlow JD, Mikos AG. Cytocompatibility evaluation of amphiphilic, thermally responsive and chemically crosslinkable macromers for in situ forming hydrogels. Biomaterials 2009;30:4558-66.

[16] Bleich NK, Kallai I, Lieberman JR, Schwarz EM, Pelled G, Gazit D. Gene therapy approaches to regenerating bone. Advanced Drug Delivery Reviews 2012:1-11.

[17] Lieberman JR, Daluiski A, Einhorn TA. The role of growth factors in the repair of bone. Biology and clinical applications. Journal Of Bone And Joint Surgery-American Volume 2002;84-A:1032-44.

[18] Seto I, Marukawa E, Asahina I. Mandibular reconstruction using a combination graft of rhBMP-2 with bone marrow cells expanded in vitro. Plast Reconstr Surg 2006;117:902-8.

[19] Dumas JE, Brownbaer PB, Prieto EM, Guda T, Hale RG, Wenke JC, et al. Injectable reactive biocomposites for bone healing in critical-size rabbit calvarial defects. Biomed Mater 2012;7:024112.

[20] Dean D, Wolfe MS, Ahmad Y, Totonchi A, Chen JE, Fisher JP, et al. Effect of transforming growth factor beta2 on marrow-infused foam poly(propylene fumarate) tissue-engineered constructs for the repair of critical-size cranial defects in rabbits. Tissue Eng 2005;11:923-39.

[21] Kawaguchi H, Kurokawa T, Hanada K, Hiyama Y, Tamura M, Ogata E, et al. Stimulation of fracture repair by recombinant human basic fibroblast growth factor in normal and streptozotocin-diabetic rats. Endocrinology 1994;135:774-81.

[22] Srouji S, Rachmiel A, Blumenfeld I, Livne E. Mandibular defect repair by TGF-beta and IGF-1 released from a biodegradable osteoconductive hydrogel. Journal of cranio-maxillo-facial surgery : official publication of the European Association for Cranio-Maxillo-Facial Surgery 2005;33:79-84.

[23] Vikjaer D, Blom S, Hjorting-Hansen E, Pinholt EM. Effect of platelet-derived growth factor-BB on bone formation in calvarial defects: an experimental study in rabbits. Eur J Oral Sci 1997;105:59-66.

[24] Nussenbaum B, Teknos TN, Chepeha DB. Tissue engineering: the current status of this futuristic modality in head neck reconstruction. Current opinion in otolaryngology & head and neck surgery 2004;12:311-5.

[25] Jung RE, Glauser R, Scharer P, Hammerle CH, Sailer HF, Weber FE. Effect of rhBMP-2 on guided bone regeneration in humans. Clin Oral Implants Res 2003;14:556-68.

[26] Boyne PJ, Lilly LC, Marx RE, Moy PK, Nevins M, Spagnoli DB, et al. De novo bone induction by recombinant human bone morphogenetic protein-2 (rhBMP-2) in maxillary sinus floor augmentation. Journal of oral and maxillofacial surgery : official journal of the American Association of Oral and Maxillofacial Surgeons 2005;63:1693-707.

[27] Moghadam HG, Urist MR, Sandor GK, Clokie CM. Successful mandibular reconstruction using a BMP bioimplant. Journal of Craniofacial Surgery 2001;12:119-27; discussion 28.

[28] Carstens MH, Chin M, Ng T, Tom WK. Reconstruction of #7 facial cleft with distraction-assisted in situ osteogenesis (DISO): role of recombinant human bone morphogenetic protein-2 with Helistat-activated collagen implant. Journal of Craniofacial Surgery 2005;16:1023-32.

[29] Herford AS, Stoffella E, Tandon R. Reconstruction of Mandibular Defects Using Bone Morphogenic Protein: Can Growth Factors Replace the Need for Autologous Bone Grafts? A Systematic Review of the Literature. Plast Surg Int 2011;2011:1-7.

[30] Warnke PH, Springer IN, Wiltfang J, Acil Y, Eufinger H, Wehmoller M, et al. Growth and transplantation of a custom vascularised bone graft in a man. Lancet 2004;364:766-70.

[31] Mesimäki K, Lindroos B, Törnwall J, Mauno J, Lindqvist C, Kontio R, et al. Novel maxillary reconstruction with ectopic bone formation by GMP adipose stem cells. Int J Oral Max Surg 2009;38:201-9.

[32] Kretlow JD, Spicer PP, Jansen JA, Vacanti CA, Kasper FK, Mikos AG. Uncultured marrow mononuclear cells delivered within fibrin glue hydrogels to porous scaffolds enhance bone regeneration within critical size rat cranial defects. Tissue Eng Part A 2010;16:3555-68.

[33] Pieri F, Lucarelli E, Corinaldesi G, Iezzi G, Piattelli A, Giardino R, et al. Mesenchymal stem cells and platelet-rich plasma enhance bone formation in sinus grafting: a histomorphometric study in minipigs. J Clin Periodontol 2008;35:539-46.

[34] Hannallah D, Peterson B, Lieberman JR, Fu FH, Huard J. Gene therapy in orthopaedic surgery. Instructional course lectures 2003;52:753-68.

[35] Alden TD, Beres EJ, Laurent JS, Engh JA, Das S, London SD, et al. The use of bone morphogenetic protein gene therapy in craniofacial bone repair. Journal of Craniofacial Surgery 2000;11:24-30.

[36] Dunn CA, Jin Q, Taba M, Franceschi RT, Bruce Rutherford R, Giannobile WV. BMP gene delivery for alveolar bone engineering at dental implant defects. Molecular therapy : the journal of the American Society of Gene Therapy 2005;11:294-9.

[37] Huang YC, Simmons C, Kaigler D, Rice KG, Mooney DJ. Bone regeneration in a rat cranial defect with delivery of PEI-condensed plasmid DNA encoding for bone morphogenetic protein-4 (BMP-4). Gene Ther 2005;12:418-26.

[38] Warren SM, Fong KD, Chen CM, Loboa EG, Cowan CM, Lorenz HP, et al. Tools and techniques for craniofacial tissue engineering. Tissue Engineering 2003;9:187-200.

[39] Ono I, Yamashita T, Jin HY, Ito Y, Hamada H, Akasaka Y, et al. Combination of porous hydroxyapatite and cationic liposomes as a vector for BMP-2 gene therapy. Biomaterials 2004;25:4709-18.

[40] Blum JS, Barry MA, Mikos AG, Jansen JA. In vivo evaluation of gene therapy vectors in ex vivo-derived marrow stromal cells for bone regeneration in a rat critical-size calvarial defect model. Hum Gene Ther 2003;14:1689-701.

[41] Levi B, Glotzbach JP, Wong VW, Nelson ER, Hyun J, Wan DC, et al. Stem Cells. J Craniofac Surg 2012;23:319-23.

[42] Shang Q, Wang Z, Liu W, Shi Y, Cui L, Cao Y. Tissue-engineered bone repair of sheep cranial defects with autologous bone marrow stromal cells. J Craniofac Surg 2001;12:586-95.

[43] Dudas JR, Marra KG, Cooper GM, Penascino VM, Mooney MP, Jiang S, et al. The Osteogenic Potential of Adipose-Derived Stem Cells for the Repair of Rabbit Calvarial Defects. Ann Plas Surg 2006;56:543-8.

[44] Smith DM, Cooper GM, Afifi AM, Mooney MP, Cray J, Rubin JP, et al. Regenerative Surgery in Cranioplasty Revisited. Plast Reconstr Surg 2011;128:1053-60.

[45] Herring SW, Ochareon P. Bone--special problems of the craniofacial region. Orthodontics & craniofacial research 2005;8:174-82.

[46] Hollister SJ, Lin CY, Saito E, Lin CY, Schek RD, Taboas JM, et al. Engineering craniofacial scaffolds. Orthod Craniofac Res 2005;8:162-73.

[47] Smith MH, Flanagan CL, Kemppainen JM, Sack JA, Chung H, Das S, et al. Computed tomography-based tissue-engineered scaffolds in craniomaxillofacial surgery. Int J Med Robot Comp 2007;3:207-16.

[48] Fisher JP, Lalani Z, Bossano CM, Brey EM, Demian N, Johnston CM, et al. Effect of biomaterial properties on bone healing in a rabbit tooth extraction socket model. J Biomed Mater Res A 2004;68A:428-38.

[49] Shin H, Zygourakis K, Farach-Carson MC, Yaszemski MJ, Mikos AG. Attachment, proliferation, and migration of marrow stromal osteoblasts cultured on biomimetic hydrogels modified with an osteopontin-derived peptide. Biomaterials 2004;25:895-906.

[50] Kretlow JD, Shi M, Young S, Spicer PP, Demian N, Jansen JA, et al. Evaluation of soft tissue coverage over porous polymethylmethacrylate space maintainers within nonhealing alveolar bone defects. Tissue Eng Part C: Methods 2010;16:1427-38.

[51] Nguyen C, Young S, Kretlow JD, Mikos AG, Wong ME. Surface characteristics of biomaterials used for space maintenance in a mandibular defect: a pilot animal study. J Oral Maxillofac Surg 2011;69:11-8.

[52] Spicer PP, Kretlow JD, Henslee AM, Shi M, Young S, Demian N, et al. In situ formation of porous space maintainers in a composite tissue defect. J Biomed Mater Res A 2012;100:827-33.

[53] Moharamzadeh K, Brook IM, Van Noort R, Scutt AM, Thornhill MH. Tissue-engineered oral mucosa: a review of the scientific literature. Journal of Dental Research 2007;86:115-24.

[54] Kinikoglu B, Auxenfans C, Pierrillas P, Justin V, Breton P, Burillon C, et al. Reconstruction of a full-thickness collagen-based human oral mucosal equivalent. Biomaterials 2009;30:6418-25.

[55] Luitaud C, Laflamme C, Semlali A, Saidi S, Grenier G, Zakrzewski A, et al. Development of an engineering autologous palatal mucosa-like tissue for potential clinical applications. J Biomed Mater Res B 2007;83B:554-61.

[56] Rouabhia M, Allaire P. Gingival mucosa regeneration in athymic mice using in vitro engineered human oral mucosa. Biomaterials 2010;31:5798-804.

[57] Song J, Izumi K, Lanigan T, Feinberg SE. Development and characterization of a canine oral mucosa equivalent in a serum-free environment. J Biomed Mater Res B 2004;71A:143-53.

[58] Yoshizawa M, Feinberg SE, Marcelo CL, Elner VM. Ex vivo produced human conjunctiva and oral mucosa equivalents grown in a serum-free culture system. J Oral Maxillofac Surg 2004;62:980-8.

[59] Izumi K, Feinberg SE, Iida A, Yoshizawa M. Intraoral grafting of an ex vivo produced oral mucosa equivalent: a preliminary report. Int J Oral Max Surg 2003;32:188-97.

[60] Peramo A, Marcelo CL, Feinberg SE. Tissue engineering of lips and muco-cutaneous junctions: in vitro development of tissue engineered constructs of oral mucosa and skin for lip reconstruction. Tissue Eng C-Meth 2012;18:273-82.

[61] Rahaman MN, Mao JJ. Stem cell-based composite tissue constructs for regenerative medicine. Biotechnology and bioengineering 2005;91:261-84.

[62] Alhadlaq A, Elisseeff JH, Hong L, Williams CG, Caplan AI, Sharma B, et al. Adult stem cell driven genesis of human-shaped articular condyle. Annals of biomedical engineering 2004;32:911-23.

[63] Dormer NH, Busaidy K, Berkland CJ, Detamore MS. Osteochondral Interface Regeneration of Rabbit Mandibular Condyle With Bioactive Signal Gradients. J Oral Maxillofac Surg 2011;69:e50-e7.

[64] Owens BD, Kragh Jr JF, Wenke JC, Macaitis J, Wade CE, Holcomb JB. Combat Wounds in Operation Iraqi Freedom and Operation Enduring Freedom. J Trauma 2008;64:295-9.

[65] Wade A, Dye J, Mohrle C. Head, face, and neck injuries during Operation Iraqi Freedom II: results from the US navy-marine corps combat trauma registry. … Journal of Trauma 2007.

[66] Champion HR, Bellamy RF, Roberts CP, Leppaniemi A. A profile of combat injury. Journal of Trauma 2003;54:S13-9.

[67] Kummoona R. Posttraumatic missile injuries of the orofacial region. Journal of Craniofacial Surgery 2008;19:300-5.

[68] Koshima I, Nanba Y, Tsutsui T, Itoh S. Sequential vascularized iliac bone graft and a superficial circumflex iliac artery perforator flap with a single source vessel for established mandibular defects. Plast Reconstr Surg 2004;113:101-6.

[69] Rodriguez ED, Martin M, Bluebond-Langner R, Manson PN. Multiplanar distraction osteogenesis of fibula free flaps used for secondary reconstruction of traumatic maxillary defects. Journal of Craniofacial Surgery 2006;17:883-8.

[70] Thorne CH. Gunshot wounds to the face. Current concepts. Clinics in Plastic Surgery 1992;19:233-44.

[71] Gruss JS, Antonyshyn O, Phillips JH. Early definitive bone and soft-tissue reconstruction of major gunshot wounds of the face. Plast Reconstr Surg 1991;87:436-50.

[72] Kihtir T, Ivatury RR, Simon RJ, Nassoura Z, Leban S. Early management of civilian gunshot wounds to the face. Journal of Trauma 1993;35:569-75; discussion 75-7.

[73] Suominen E, Tukiainen E. Close-range shotgun and rifle injuries to the face. Clinics in Plastic Surgery 2001;28:323-37.

[74] Futran ND, Farwell DG, Smith RB, Johnson PE, Funk GF. Definitive management of severe facial trauma utilizing free tissue transfer. Otolaryngology--head and neck surgery : official journal of American Academy of Otolaryngology-Head and Neck Surgery 2005;132:75-85.

[75] Goodger NM, Wang J, Smagalski GW, Hepworth B. Methylmethacrylate as a space maintainer in mandibular reconstruction. J Oral Maxillofac Surg 2005;63:1048-51.

[76] Wright S, Bekiroglu F, Whear NM, Grew NR. Use of Palacos R-40 with gentamicin to reconstruct temporal defects after maxillofacial reconstructions with temporalis flaps. Br J Oral Maxillofac Surg 2006;44:531-3.

[77] Goode RL, Reynolds BN. Tobramycin-impregnated methylmethacrylate for mandible reconstruction. Archives of Otolaryngology -- Head and Neck Surgery 1992;118:201-4.

[78] Brody HJ. Complications of expanded polytetrafluoroethylene (e-PTFE) facial implant. Dermatologic Surgery 2001;27:792-4.

[79] Shields CL, Shields JA, De Potter P, Singh AD. Problems with the hydroxyapatite orbital implant: experience with 250 consecutive cases. British Journal of Ophthalmology 1994;78:702-6.

[80] Brown AE, Banks P. Late extrusion of alloplastic orbital floor implants. British Journal of Oral and Maxillofacial Surgery 1993;31:154-7.

[81] Hartman EH, Vehof JW, de Ruijter JE, Spauwen PH, Jansen J. Ectopic bone formation in rats: the importance of vascularity of the acceptor site. Biomaterials 2004;25:5831-7.

[82] Baran CN, Celebioglu S, Sensöz O, Ulusoy G, Civelek B, Ortak T. The behavior of fat grafts in recipient areas with enhanced vascularity. Plast Reconstr Surg 2002;109:1646-51; 52.

[83] Wang H, Chen T, Chow L, Cheng T, Chen J. Recipient bed vascularity and the survival of ischaemic flaps. British Journal of Plastic Surgery 1997;50:266-71.

[84] van Gemert JTM, van Es RJJ, Van Cann EM, Koole R. Nonvascularized Bone Grafts for Segmental Reconstruction of the Mandible– A Reappraisal. Journal of Oral and Maxillofacial Surgery 2009;67:1446-52.

[85] August M, Tompach P, Chang Y, Kaban L. Factors influencing the long-term outcome of mandibular reconstruction. Journal of Oral and Maxillofacial Surgery 2000;58:731-7.

[86] Vaandrager JM, van Mullem PJ, de Wijn JR. Porous acrylic cement for the correction of craniofacial deformities and repair of defects, animal experimentation and two years of clinical application. Biomaterials 1983;4:128-30.

[87] Zhang SM, Chen JD. PMMA based foams made via surfactant-free high internal phase emulsion templates. Chem Commun 2009:2217-9.

[88] van Mullem PJ, de Wijn JR, Vaandrager JM. Porous acrylic cement: evaluation of a novel implant material. Ann Plast Surg 1988;21:576-82.

[89] Boger A, Bisig A, Bohner M, Heini P, Schneider E. Variation of the mechanical properties of PMMA to suit osteoporotic cancellous bone. Journal of Biomaterials Science, Polymer Edition 2008;19:1125-42.

[90] van Mullem PJ, Vaandrager JM, Nicolai JPA, de Wijn JR. Implantation of porous acrylic cement in soft tissues: an animal and human biopsy histological study. Biomaterials 1990;11:299-304.

[91] Hautamäki MP, Aho AJ, Alander P, Rekola J, Gunn J, Strandberg N, et al. Repair of bone segment defects with surface porous fiber-reinforced polymethyl methacrylate (PMMA) composite prosthesis: histomorphometric incorporation model and characterization by SEM. Acta orthopaedica 2008;79:555-64.

[92] Patel ZS, Young S, Tabata Y, Jansen JA, Wong MEK, Mikos AG. Dual delivery of an angiogenic and an osteogenic growth factor for bone regeneration in a critical size defect model. Bone 2008;43:931-40.

[93] Young S, Patel ZS, Kretlow JD, Murphy MB, Mountziaris PM, Baggett LS, et al. Dose effect of dual delivery of vascular endothelial growth factor and bone morphogenetic protein-2 on bone regeneration in a rat critical-size defect model. Tissue Eng Part A 2009;15:2347-62.

[94] Young S, Bashoura AG, Borden T, Baggett LS, Jansen JA, Wong M, et al. Development and characterization of a rabbit alveolar bone nonhealing defect model. J Biomed Mater Res A 2008;86:182-94.

[95] van der Lubbe HBM, Klein CPAT, de Groot K. A simple method for preparing thin (10 μm) histological sections of undecalcified plastic embedded bone with implants. Biotech Histochem 1988;63:171-6.

[96] Mellonig JT, Nevins M. Guided bone regeneration of bone defects associated with implants: an evidence-based outcome assessment. The International journal of periodontics & restorative dentistry 1995;15:168-85.

[97] Behnia H, Motamedi MH. Reconstruction and rehabilitation of short-range, high-velocity gunshot injury to the lower face: a case report. Journal of Cranio-Maxillo-Facial Surgery 1997;25:220-7.

[98] Gasparini G, Boniello R, Moro A, Tamburrini G, Di Rocco C, Pelo S. Cranial Reshaping Using Methyl Methacrylate: Technical Note. Journal of Craniofacial Surgery 2009;20:184.

[99] Tan BH, Grijpma DW, Nabuurs T, Feijen J. Crosslinkable surfactants based on linoleic acid-functionalized block copolymers of ethylene oxide and epsilon-caprolactone for the preparation of stable PMMA latices. Polymer 2005;46:1347-57.

[100] Nathanson D, Gettleman L, Schnitman P, Shklar G. Histologic response to porous PMMA implant materials. J Biomed Mater Res B: App Biom 1978;12:13-33.

[101] McLaren AC, McLaren SG, Hickmon MK. Sucrose, xylitol, and erythritol increase PMMA permeability for depot antibiotics. Clinical Orthopaedics and Related Research 2007;461:60-3.

[102] McLaren AC, McLaren SG, McLemore R, Vernon BL. Particle size of fillers affects permeability of polymethylmethacrylate. Clinical Orthopaedics and Related Research 2007;461:64-7.

[103] De Wijn JR. Poly(methyl methacrylate)--aqueous phase blends: in situ curing porous materials. Journal of Biomedical Materials Research 1976;10:625-35.

[104] Bruens ML, Pieterman H, de Wijn JR, Vaandrager JM. Porous polymethylmethacrylate as bone substitute in the craniofacial area. J Craniofac Surg 2003;14:63-8.

[105] Meng T, Shi B, Lu D, Li Y, Wu M. Roles of palatine bone denudation repairing with free buccal or palatal mucosal graft on maxillary growth: an experimental study in rabbits. Annals of Plastic Surgery 2007;59:323.

[106] Al-Asfour A, Al-Melh M, Andersson L, Joseph B. Healing pattern of experimental soft tissue lacerations after application of novel topical anesthetic agents - an experimental study in rabbits. Dental Traumatology 2008;24:27-31.

[107] Bronson RE, Treat JA, Bertolami CN. Fibroblastic subpopulations in uninjured and wounded rabbit oral mucosa. Journal of Dental Research 1989;68:51-8.

[108] Elshal EE, Inokuchi T, Yoshida S, Sekine J, Sano K, Ninomiya H, et al. A comparative study of epithelialization of subcutaneous fascial flaps and muscle-only flaps in the oral cavity. A rabbit model. International Journal of Oral and Maxillofacial Surgery 1998;27:141-8.

[109] Fujisawa K, Miyamoto Y, Nagayama M. Basic fibroblast growth factor and epidermal growth factor reverse impaired ulcer healing of the rabbit oral mucosa. Journal of Oral Pathology and Medicine 2003;32:358-66.

[110] Onerci M. The effects of lyophilized homograft amniotic membrane on wound healing on rabbits. Acta Otorhinolaryngologica Italica 1991;11:491-6.

[111] Levin MP, Tsaknis PJ, Cutright DE. Healing of the oral mucosa with the use of collagen artificial skin. Journal of Periodontology 1979;50:250-3.

[112] Figueiredo JA, Pesce HF, Gioso MA, Figueiredo MA. The histological effects of four endodontic sealers implanted in the oral mucosa: submucous injection versus implant in polyethylene tubes. International Endodontic Journal 2001;34:377-85.

[113] Bertolami CN, Ellis DG, Donoff RB. Healing of cutaneous and mucosal wounds grafted with collagen-glycosaminoglycan/silastic bilayer membranes: a preliminary report. Journal of Oral and Maxillofacial Surgery 1988;46:971-8.

[114] Al Ruhaimi KA. Closure of palatal defects without a surgical flap: an experimental study in rabbits. Journal of Oral and Maxillofacial Surgery 2001;59:1319-25.

[115] Ueda M, Ebata K, Kaneda T. In vitro fabrication of bioartificial mucosa for reconstruction of oral mucosa: Basic research and clinical application. Annals of Plastic Surgery 1991;27:540.

[116] Williams DF. Introduction: Implantable materials and infection. Injury 1996;27:1-4.

[117] Depprich RA, Handschel JG, Meyer U, Meissner G. Comparison of prevalence of microorganisms on titanium and silicone/polymethyl methacrylate obturators used for rehabilitation of maxillary defects. Journal of Prosthetic Dentistry 2008;99:400-5.

[118] Cordero J, Munuera L, Folgueira MD. The influence of the chemical composition and surface of the implant on infection. Injury 1996;27:34-7.

[119] Pelissier P, Masquelet AC, Bareille R, Pelissier SM, Amedee J. Induced membranes secrete growth factors including vascular and osteoinductive factors and could stimulate bone regeneration. Journal of Orthopaedic Research 2004;22:73-9.

[120] Viateau V, Bensidhoum M, Guillemin G, Petite H, Hannouche D, Anagnostou F, et al. Use of the induced membrane technique for bone tissue engineering purposes: animal studies. Orthopedic Clinics of North America 2010;41:49-56.

[121] Masquelet AC, Begue T. The concept of induced membrane for reconstruction of long bone defects. Orthopedic Clinics of North America 2010;41:27-37.

[122] Lenton KA, Nacamuli RP, Longaker MT. Porous polymethylmethacrylate as bone substitute in the craniofacial area. Bruens ML, Pieterman H, de Wijn JR, et al. J Craniofac Surg 2003; 14:63-68. Journal of Craniofacial Surgery 2003;14:596-8.

[123] de Jong WC, Koolstra JH, Korfage JA, van Ruijven LJ, Langenbach GE. The daily habitual in vivo strain history of a non-weight-bearing bone. Bone 2009.

[124] Worley R. The experimental use of poly (methyl methacrylate) implants in mandibular defects. Journal of Oral Surgery 1973;31:170.

[125] Kangur TT, Tolman DE, Jowsey J. The use of methylmethacrylate in the fixation of mandibular fractures in dogs. Experimental results. Oral Surgery, Oral Medicine, and Oral Pathology 1976;41:578-87.

[126] Chiarini L, Figurelli S, Pollastri G, Torcia E. Cranioplasty using acrylic material: a new technical procedure. J Cranio Maxill Surg 2004;32:5-9.

[127] Lye KW, Tideman H, Merkx MA, Jansen J. Bone cements and their potential use in a mandibular endoprosthesis. Tissue engineering Part B, Reviews 2009.

[128] Vaandrager JM, van Mullem PJ, de Wijn JR. Craniofacial contouring and porous acrylic cement. Ann Plast Surg 1988;21:583-93.

[129] Romo Iii T, Morris L, Reitzen S, Ghossaini S, Wazen J, Kohan D. Reconstruction of Congenital Microtia-Atresia: Outcomes With the Medpor/Bone-Anchored Hearing Aid-Approach. Annals of Plastic Surgery 2009;62:384.

[130] Shirazi M, Marzo S, Leonetti J. Perioperative complications with the bone-anchored hearing aid. Otolaryngology - Head and Neck Surgery 2006;134:236-9.

[131] Kiechel SF, Rodeheaver GT, Klawitter JJ, Edgerton MT, Edlich RF. The role of implant porosity on the development of infection. Surgery, Gynecology and Obstetrics 1977;144:58-62.

[132] Sclafani AP, Romo TI, Silver L. Clinical and histologic behavior of exposed porous high-density polyethylene implants. Plast Reconstr Surg 1997;99:41-50.

[133] Padera RF, Colton CK. Time course of membrane microarchitecture-driven neovascularization. Biomaterials 1996;17:277-84.

[134] Beck S, Boger A. Evaluation of the particle release of porous PMMA cements during curing. Acta Biomater 2009;5:2503-7.

[135] Yaszay B, Trindade MC, Lind M, Goodman SB, Smith RL. Fibroblast expression of C-C chemokines in response to orthopaedic biomaterial particle challenge in vitro. Journal of Orthopaedic Research 2001;19:970-6.

[136] Takushima A, Harii K, Asato H, Nakatsuka T, Kimata Y. Mandibular reconstruction using microvascular free flaps: a statistical analysis of 178 cases. Plast Reconstr Surg 2001;108:1555-63.

[137] McLean JN, Moore CE, Yellin SA. Gunshot wounds to the face-acute management. Facial Plast Surg 2005;21:191-8.

[138] Vásconez HC, Shockley ME, Luce EA. High-energy gunshot wounds to the face. Ann Plas Surg 1996;36:18-25.

[139] Finch DR, Dibbell DG. Immediate reconstruction of gunshot injuries to the face. J Traum 1979;19:965-8.

[140] Becelli R, Renzi G, Perugini M, Iannetti G. Craniofacial traumas: immediate and delayed treatment. J Craniofac Surg 2000;11:265-9.

[141] Lawson W, Loscalzo LJ, Baek S, Biller HF, Krespi YP. Experience with immediate and delayed mandibular reconstruction. Laryngoscope 1982;92:5-10.

[142] Chaushu G, Mardinger O, Peleg M, Ghelfan O, Nissan J. Analysis of complications following augmentation with cancellous block allografts. J Periodontol 2010;81:1759-64.

[143] Gooch MR, Gin GE, Kenning TJ, German JW. Complications of cranioplasty following decompressive craniectomy: analysis of 62 cases. Neurosurg Focus 2009;26:E9.

[144] Lee S, Thiele C. Factors associated with free flap complications after head and neck reconstruction and the molecular basis of fibrotic tissue rearrangement in preirradiated soft tissue. J Oral Maxillofac Surg 2010;68:2169-78.

[145] Shi M, Kretlow JD, Nguyen A, Young S, Baggett LS, Wong ME, et al. Antibiotic-releasing porous polymethylmethacrylate constructs for osseous space maintenance and infection control. Biomaterials 2010;31:4146-56.

[146] Toksvig-Larsen S, Franzen H, Ryd L. Cement interface temperature in hip arthroplasty. Acta Orthop Scand 1991;62:102-5.

[147] Verlaan J, Oner FC, Verbout AJ, Dhert WJA. Temperature elevation after vertebroplasty with polymethylmethacrylate in the goat spine. J Biomed Mater Res B App Biomater 2003;67B:581-5.

[148] Saha S, Pal S. Mechanical properties of bone cement: a review. J Biomed Mater Res B App Biomater 1984;18:435-62.

[149] Santin M, Motta A, Borzachiello A, Nicolais L, Ambrosio L. Effect of PMMA cement radical polymerisation on the inflammatory response. J Mater Sci - Mater M 2004;15:1175-80.

[150] Petty W. Methyl methacrylate concentrations in tissues adjacent to bone cement. J Biomed Mater Res 1980;14:427-34.

[151] Kieswetter K, Schwartz Z, Dean DD, Boyan BD. The role of implant surface characteristics in the healing of bone. Crit Rev Oral Bio & Med 1996;7:329-45.

[152] Murray DW, Rae T, Rushton N. The influence of the surface energy and roughness of implants on bone resorption. J Bone Joint Surg - Br 1989;71:632-7.

[153] Gelb H, Schumacher HR, Cuckler J, Ducheyne P, Baker DG. In vivo inflammatory response to polymethylmethacrylate particulate debris: effect of size, morphology, and surface area. J Orthop Res 1994;12:83-92.

[154] González O, Smith RL, Goodman SB. Effect of size, concentration, surface area, and volume of polymethylmethacrylate particles on human macrophages in vitro. J Biomed Mater Res B App Biomater 1996;30:463-73.

[155] Ingham E. Production of TNF-α and bone resorbing activity by macrophages in response to different types of bone cement particles. Biomaterials 2000;21:1005-13.

[156] Mountziaris PM, Spicer PP, Kasper FK, Mikos AG. Harnessing and modulating inflammation in strategies for bone regeneration. Tissue Eng Part B Rev 2011;17:393-402.

[157] Shi M, Kretlow JD, Spicer PP, Tabata Y, Demian N, Wong ME, et al. Antibiotic-releasing porous polymethylmethacrylate/gelatin/antibiotic constructs for craniofacial tissue engineering. J Control Release 2011;152:195-205.

[158] Rodriguez ED, Bluebond-Langner R, Park JE, Manson PN. Preservation of contour in periorbital and midfacial craniofacial microsurgery: reconstruction of the soft-tissue elements and skeletal buttresses. Plast Reconstr Surg 2008;121:1738-47; discussion 48-9.

[159] Akhlaghi F, Aframian-Farnad F. Management of maxillofacial injuries in the Iran-Iraq War. J Oral Maxillofac Surg 1997;55:927-30;discussion 30-1.

[160] van Mullem PJ, de Wijn JR. Bone and soft connective tissue response to porous acrylic implants. A histokinetic study. J Craniomaxillofac Surg 1988;16:99-109.

[161] Hacking SA, Bobyn JD, Toh K, Tanzer M, Krygier JJ. Fibrous tissue ingrowth and attachment to porous tantalum. J Biomed Mater Res 2000;52:631-8.

[162] Bobyn JD, Wilson GJ, MacGregor DC, Pilliar RM, Weatherly GC. Effect of pore size on the peel strength of attachment of fibrous tissue to porous-surfaced implants. J Biomed Mater Res 1982;16:571-84.

[163] Siepmann J, Siepmann F. Mathematical modeling of drug delivery. Int J Pharm 2008;364:328-43.

[164] Hospenthal DR, Crouch HK. Infection control challenges in deployed US military treatment facilities. J Trauma 2009;66:S120-8.

[165] Sebeny PJ, Riddle MS, Petersen K. Acinetobacter baumannii skin and soft−tissue infection associated with war trauma. Clin Infect Dis 2008;47:444-9.

[166] Yun HC, Branstetter JG, Murray CK. Osteomyelitis in military personnel wounded in Iraq and Afghanistan. The Journal of Trauma 2008;64:S163-8- discussion S8.

[167] Olsen D, Yang C, Bodo M, Chang R, Leigh S, Baez J, et al. Recombinant collagen and gelatin for drug delivery. Adv Drug Deliv Rev 2003;55:1547-67.

[168] Young S, Wong M, Tabata Y, Mikos AG. Gelatin as a delivery vehicle for the controlled release of bioactive molecules. J Control Release 2005;109:256-74.

[169] Ikada Y, Tabata Y. Protein release from gelatin matrices. Adv Drug Deliv Rev 1998;31:287-301.

[170] Sutter M, Siepmann J, Hennink WE, Jiskoot W. Recombinant gelatin hydrogels for the sustained release of proteins. J Control Release 2007;119:301-12.

[171] Smartset HV Bone Cement K023012 approval letter. February 13, 2003 ed: U.S. Food and Drug Administration, Center for Devices and Radiologic Health; 2003.

[172] Cranioplastic K071791 approval letter. July 30, 2007 ed: U.S. Food and Drug Administration, Center for Devices and Radiologic Health; 2007.

[173] Gelatin Sponge ENT, Absorbable Gelatin Sponge, USP approval letter. December 9,2008 ed: U.S. Food and Drug Administration, Center for Devices and Radiologic Health; 2008.

[174] Surgifoam Absorbable Gelatin Sponge, USP approval letter. September 30, 1999 ed: U.S. Food and Drug Administration, Center for Devices and Radiologic Health; 1999.

[175] Li J, Nation RL, Turnidge JD, Milne RW, Coulthard K, Rayner CR, et al. Colistin: the re-emerging antibiotic for multidrug-resistant Gram-negative bacterial infections. Lancet Infect Dis 2006;6:589-601.

[176] Karageorgopoulos DE, Falagas ME. Current control and treatment of multidrug-resistant Acinetobacter baumannii infections. Lancet Infect Dis 2008;8:751-62.

[177] Scott P, Deye G, Srinivasan A, Murray C, Moran K, Hulten E, et al. An outbreak of multidrug-resistant Acinetobacter baumannii-calcoaceticus complex infection in the US military health care system associated with military operations in Iraq. Clin Infect Dis 2007;44:1577-84.

[178] Crane DP, Gromov K, Li D, Søballe K, Wahnes C, Büchner H, et al. Efficacy of colistin-impregnated beads to prevent multidrug-resistant A. baumannii implant-associated osteomyelitis. J Orthop Res 2009;27:1008-15.

[179] Patel ZS, Yamamoto M, Ueda H, Tabata Y, Mikos AG. Biodegradable gelatin microparticles as delivery systems for the controlled release of bone morphogenetic protein-2. Acta Biomaterialia 2008;4:1126-38.

[180] ISO. Implants for surgery - Acrylic resin cements. 58332002.

[181] Haralson MA, Hassell JR. Extracellular matrix: a practical approach. New York: Oxford University Press; 1995.

[182] Yoshihara Y, Nakamura H, Obata K, Yamada H, Hayakawa T, Fujikawa K, et al. Matrix metalloproteinases and tissue inhibitors of metalloproteinases in synovial fluids from patients with rheumatoid arthritis or osteoarthritis. Ann Rheum Dis 2000;59:455-61.

[183] Taakiran D, Taakiran E, Ozsoy H, Lok V. Effects of Surgical Trauma on Articular Cartilage. Tr J of Medical Sciences 1999;29:177-80.

[184] Holland TA, Tessmar JKA, Tabata Y, Mikos AG. Transforming growth factor-ß1 release from oligo(poly(ethylene glycol) fumarate) hydrogels in conditions that model the cartilage wound healing environment. J Control Release 2004;94:101-14.

[185] Siepmann J, Peppas NA. Modeling of drug release from delivery systems based on hydroxypropyl methylcellulose (HPMC). Adv Drug Deliv Rev 2001;48:139-57.

[186] Serra L, Domenech J, Peppas NA. Drug transport mechanisms and release kinetics from molecularly designed poly(acrylic acid-g-ethylene glycol) hydrogels. Biomaterials 2006;27:5440-51.

[187] Virto MR, Frutos P, Torrado S, Frutos G. Gentamicin release from modified acrylic bone cements with lactose and hydroxypropylmethylcellulose. Biomaterials 2003;24:79-87.

[188] Corry D, Moran J. Assessment of acrylic bone cement as a local delivery vehicle for the application of non-steroidal anti-inflammatory drugs. Biomaterials 1998;19:1295-301.

[189] Frutos Cabanillas P, Diez Pena E, Barrales-Rienda JM, Frutos G. Validation and in vitro characterization of antibiotic-loaded bone cement release. Int J Pharm 2000;209:15-26.

[190] van de Belt H, Neut D, Schenk W, van Horn JR, van der Mei HC, Busscher HJ. Gentamicin release from polymethylmethacrylate bone cements and Staphylococcus aureus biofilm formation. Acta Orthop Scand 2000;71:625-9.

[191] Webb JC, Spencer RF. The role of polymethylmethacrylate bone cement in modern orthopaedic surgery. J Bone Joint Surg Br 2007;89:851-7.

[192] Li J, Milne RW, Nation RL, Turnidge JD, Coulthard K. Stability of colistin and colistin methanesulfonate in aqueous media and plasma as determined by high-performance liquid chromatography. Antimicrob Agents Chemother 2003;47:1364-70.

[193] Perez-Lozano P, Garcia-Montoya E, Orriols A, Minarro M, Tico JR, Sune-Negre JM. Application of a validated method in the stability study of colistin sulfate and methylparaben in a veterinary suspension formulation by high-performance liquid chromatography with a diode array detector. J AOAC Int 2007;90:706-14.

[194] Dudhani RV, Nation RL, Li J. Evaluating the stability of colistin and colistin methanesulphonate in human plasma under different conditions of storage. J Antimicrob Chemother;65:1412-5.

[195] Galani I, Kontopidou F, Souli M, Rekatsina P. Colistin susceptibility testing by Etest and disk diffusion methods. … of antimicrobial agents 2008.

[196] Patel ZS, Ueda H, Yamamoto M, Tabata Y, Mikos AG. In vitro and in vivo release of vascular endothelial growth factor from gelatin microparticles and biodegradable composite scaffolds. Pharmaceutical Research 2008;25:2370-8.

[197] Park H, Temenoff JS, Holland TA, Tabata Y, Mikos AG. Delivery of TGF-beta1 and chondrocytes via injectable, biodegradable hydrogels for cartilage tissue engineering applications. Biomaterials 2005;26:7095-103.

[198] Holland TA, Tabata Y, Mikos AG. In vitro release of transforming growth factor-beta 1 from gelatin microparticles encapsulated in biodegradable, injectable oligo(poly(ethylene glycol) fumarate) hydrogels. J Control Release 2003;91:299-313.

[199] Wolff D, Hassfeld S, Hofele C. The outcome of various cements in combination with titanium reconstruction plates after segmental resection of the mandible. Br J Oral Maxillofac Surg 2005;43:303-8.

[200] Meyer J, Piller G, Spiegel CA, Hetzel S, Squire M. Vacuum-Mixing Significantly Changes Antibiotic Elution Characteristics of Commercially Available Antibiotic-Impregnated Bone Cements. J Bone Joint Surg Am 2011;93:2049-56.

[201] Chang CC, Merritt K. Effect of Staphylococcus epidermidis on adherence of Pseudomonas aeruginosa and Proteus mirabilis to polymethyl methacrylate (PMMA) and gentamicin−containing PMMA. J Orthop Res 1991;9:284-8.

[202] Dunne N, Hill J, McAfee P, Todd K, Kirkpatrick R, Tunney M, et al. In vitro study of the efficacy of acrylic bone cement loaded with supplementary amounts of gentamicin: effect on mechanical properties, antibiotic release, and biofilm formation. Acta Orthop Scand 2007;78:774-85.

[203] Dunne NJ, Hill J, McAfee P, Kirkpatrick R, Patrick S, Tunney M. Incorporation of large amounts of gentamicin sulphate into acrylic bone cement: effect on handling and mechanical properties, antibiotic release, and biofilm formation. Proc Inst Mech Eng H 2008;222:2041-3033.

[204] Hawley JS, Murray CK, Griffith ME, McElmeel ML, Fulcher LC, Hospenthal DR, et al. Susceptibility of acinetobacter strains isolated from deployed U.S. military personnel. Antimicrob Agents Ch 2007;51:376-8.

[205] Davis KA, Moran KA, McAllister CK, Gray PJ. Multidrug-resistant Acinetobacter extremity infections in soldiers. Emerg Infect Dis 2005;11:1218-24.

[206] Berlana D, Llop JM, Fort E, Badia AB, Jodar R. Use of colistin in the treatment of multiple-drug-resistant gram-negative infections. Am J Health-Syst Ph 2005;62:39-47.

[207] Keen EF, Robinson BJ, Hospenthal DR, Aldous WK, Wolf SE, Chung KK, et al. Incidence and bacteriology of burn infections at a military burn center. Burns 2010;36:461-8.

[208] Keen EF, Robinson BJ, Hospenthal DR, Aldous WK, Wolf SE, Chung KK, et al. Prevalence of multidrug-resistant organisms recovered at a military burn center. Burns 2010;36:819-25.

[209] Falagas M, Fragoulis KN, Kasiakou S, Sermaidis GJ, Michalopoulos A. Nephrotoxicity of intravenous colistin: a prospective evaluation. Int J Antimicrob Ag 2005;26:504-7.

[210] Wenke JC, Guelcher SA. Dual delivery of an antibiotic and a growth factor addresses both the microbiological and biological challenges of contaminated bone fractures. Expert Opin Drug Del 2011;8:1555-69.

[211] Nair MB, Kretlow JD, Mikos AG, Kasper FK. Infection and tissue engineering in segmental bone defects—a mini review. Curr Opin Biotech 2011;22:721-5.

[212] van de Belt H, Neut D, Schenk W, van Horn JR, van der Mei HC, Busscher HJ. Staphylococcus aureus biofilm formation on different gentamicin-loaded polymethylmethacrylate bone cements. Biomaterials 2001;22:1607-11.

[213] Brady RA, Leid JG, Calhoun JH, Costerton JW, Shirtliff ME. Osteomyelitis and the role of biofilms in chronic infection. FEMS Immunol Med Mic 2008;52:13-22.

[214] Rathbone CR, Cross JD, Brown KV, Murray CK, Wenke JC. Effect of various concentrations of antibiotics on osteogenic cell viability and activity. J Orthop Res 2011;29:1070-4.

[215] Duewelhenke N, Krut O, Eysel P. Influence on mitochondria and cytotoxicity of different antibiotics administered in high concentrations on primary human osteoblasts and cell lines. Antimicrob Agents Ch 2007;51:54-63.

[216] Falagas ME, Kasiakou SK, Tsiodras S, Michalopoulos A. The use of intravenous and aerosolized polymyxins for the treatment of infections …. Clin Med Res 2006;4:138-46.

[217] Falagas ME, Rizos M, Bliziotis IA, Rellos K, Kasiakou SK, Michalopoulos A. Toxicity after prolonged (more than four weeks) administration of intravenous colistin. BMC Infect Dis 2005;5:1-8.

[218] Falagas ME, Kasiakou SK. Toxicity of polymyxins: a systematic review of the evidence from old and recent studies. Crit Care 2006;10:R27-39.

[219] Johnson EN, Burns TC, Hayda RA, Hospenthal DR, Murray CK. Infectious complications of open type III tibial fractures among combat casualties. Clin Infect Dis 2007;45:409-15.

[220] Mainil-Varlet P, Gogolewski S, Nieuwenhuis P. Long-term soft tissue reaction to various polylactides and their in vivo degradation. J Mater Sci Mater Med 1996;7:713-21.

[221] Borrelli J, Prickett WD, Ricci WM. Treatment of nonunions and osseous defects with bone graft and calcium sulfate. Clin Orthop Relat Res 2003;411:245-54.

[222] Sawin PD, Traynelis VC, Menezes AH. A comparative analysis of fusion rates and donor-site morbidity for autogeneic rib and iliac crest bone grafts in posterior cervical fusions. J Neurosurg 1998;88:255-65.

[223] Sitharaman B, Shi X, Tran LA, Spicer PP, Rusakova I, Wilson LJ, et al. Injectable in situ cross-linkable nanocomposites of biodegradable polymers and carbon nanostructures for bone tissue engineering. J Biomater Sci Polym Ed 2007;18:655-71.

[224] Shi X, Hudson JL, Spicer PP, Tour JM, Krishnamoorti R, Mikos AG. Rheological behaviour and mechanical characterization of injectable poly (propylene fumarate)/single-walled carbon nanotube composites for bone tissue engineering. Nanotechnology 2005;16:S531-8.

[225] Chu TG, Warden SJ, Turner CH, Stewart RL. Segmental bone regeneration using a load-bearing biodegradable carrier of bone morphogenetic protein-2. Biomaterials 2007;28:459-67.

[226] Balçik C, Tokdemir T, Senköylü A, Koç N, Timuçin M, Akin S, et al. Early weight bearing of porous HA/TCP (60/40) ceramics in vivo: A longitudinal study in a segmental bone defect model of rabbit. Acta Biomater 2007;3:985-96.

[227] Rybicki EF, Simonen FA, Weis EB. On the mathematical analysis of stress in the human femur. J Biomech 1972;5:203-15.

[228] Shi X, Sitharaman B, Pham QP, Liang F, Wu K, Billups WE, et al. Fabrication of porous ultra-short single-walled carbon nanotube nanocomposite scaffolds for bone tissue engineering. Biomaterials 2007;28:4078-90.

[229] Bruder SP, Kraus KH, Goldberg VM, Kadiyala S. The Effect of Implants Loaded with Autologous Mesenchymal Stem Cells on the Healing of Canine Segmental Bone Defects. J Bone Joint Surg Am 1998;80:985-96.

[230] Guelcher SA. Biodegradable polyurethanes: synthesis and applications in regenerative medicine. Tissue Eng Pt B Rev 2008;14:3-17.

[231] Oest ME, Dupont KM, Kong HJ, Mooney DJ, Guldberg RE. Quantitative assessment of scaffold and growth factor-mediated repair of critically sized bone defects. J Orthop Res 2007;25:941-50.

[232] Fisher JP, Vehof JW, Dean D, van der Waerden JP, Holland TA, Mikos AG, et al. Soft and hard tissue response to photocrosslinked poly(propylene fumarate) scaffolds in a rabbit model. J Biomed Mater Res Part A 2002;59A:547-56.

[233] Mistry AS, Pham QP, Schouten C, Yeh T, Christenson EM, Mikos AG, et al. In vivo bone biocompatibility and degradation of porous fumarate-based polymer/alumoxane nanocomposites for bone tissue engineering. J Biomed Mater Res A 2010;92A:451-62.

[234] Yaszemski MJ, Payne RG, Hayes WC, Langer R, Aufdemorte TB, Mikos AG. The ingrowth of new bone tissue and initial mechanical properties of a degrading polymeric composite scaffold. Tissue Eng 1995;1:41-52.

[235] Peter SJ, Lu L, Kim DJ, Mikos AG. Marrow stromal osteoblast function on a poly(propylene fumarate)/beta-tricalcium phosphate biodegradable orthopaedic composite. Biomaterials 2000;21:1207-13.

[236] Kim K, Yeatts A, Dean D, Fisher JP. Stereolithographic Bone Scaffold Design Parameters: Osteogenic Differentiation and Signal Expression. Tissue Eng Pt B Rev 2010;16:523-39.

[237] Woodard JR, Hilldore AJ, Lan SK, Park CJ, Morgan AW, Eurell JC, et al. The mechanical properties and osteoconductivity of hydroxyapatite bone scaffolds with multi-scale porosity. Biomaterials 2007;28:45-54.

[238] Brown JL, Peach MS, Nair LS, Kumbar SG, Laurencin CT. Composite scaffolds: Bridging nanofiber and microsphere architectures to improve bioactivity of mechanically competent constructs. J Biomed Mater Res A 2010;95A:1150-8.

[239] Kempen DHR, Lu L, Heijink A, Hefferan TE, Creemers LB, Maran A, et al. Effect of local sequential VEGF and BMP-2 delivery on ectopic and orthotopic bone regeneration. Biomater 2009;30:2816-25.

[240] Ito Y. Tissue engineering by immobilized growth factors. Materials Science and Engineering: C 1998;6:267-74.

[241] Ahrendt G, Chickering DE, Ranieri JP. Angiogenic Growth Factors: A Review for Tissue Engineering. Tissue Eng 1998;4:117-30.

[242] Boden S. Bioactive factors for bone tissue engineering. Clin Orthop Relat R 1999:S84-94.

[243] Babensee JE, McIntire LV, Mikos AG. Growth Factor Delivery for Tissue Engineering. Pharm Res 2000;17:497-504.

[244] Tabata Y. Tissue regeneration based on growth factor release. Tissue Engineering 2003;9:S5-15.

[245] Rose FRAJ, Hou Q, Oreffo ROC. Delivery systems for bone growth factors—the new players in skeletal regeneration. J Pharm Pharmacol 2004;56:415-27.

[246] Chen D, Zhao M, Mundy GR. Bone Morphogenetic Proteins. Growth Factors 2004;22:233-41.

[247] Jeon O, Song SJ, Yang HS, Bhang S-H, Kang S-W, Sung MA, et al. Long-term delivery enhances in vivo osteogenic efficacy of bone morphogenetic protein-2 compared to short-term delivery. Biochem Biophys Res Commun 2008;369:774-80.

[248] Kempen DHR, Lu L, Hefferan TE, Creemers LB, Maran A, Classic KL, et al. Retention of in vitro and in vivo BMP-2 bioactivities in sustained delivery vehicles for bone tissue engineering. Biomater 2008;29:3245-52.

[249] Kempen DHR, Yaszemski MJ, Heijink A, Hefferan TE, Creemers LB, Britson J, et al. Non-invasive monitoring of BMP-2 retention and bone formation in composites for bone tissue engineering using SPECT/CT and scintillation probes. J Control Release 2009;134:169-76.

[250] Kim S, Gwak S, Kim B. Orthotopic bone formation by implantation of apatite-coated poly(lactide-co-glycolide)/hydroxyapatite composite particulates and bone morphogenetic protein-2. J Biomed Mater Res A 2008;87:245-53.

[251] Lane JM, Yasko AW, Tomin E, Cole BJ, Waller S, Browne M, et al. Bone marrow and recombinant human bone morphogenetic protein-2 in osseous repair. Clin Orthop Relat Res 1999:216-27.

[252] Ruhé PQ, Hedberg EL, Padron NT, Spauwen PHM, Jansen JA, Mikos AG. rhBMP-2 Release from Injectable Poly(DL-Lactic-co-glycolic Acid)/ Calcium-Phosphate Cement Composites. J Bone Joint Surg Am 2003;85:75-81.

[253] Ruhe PQ, Boerman OC, Russel FGM, Spauwen PHM, Mikos AG, Jansen JA. Controlled release of rhBMP-2 loaded poly(DL-lactic-co-glycolic acid)/calcium phosphate cement composites in vivo. J Control Release 2005;106:162-71.

[254] Shung AK, Timmer MD, Jo S, Engel PS, Mikos AG. Kinetics of poly (propylene fumarate) synthesis by step polymerization of diethyl fumarate and propylene glycol using zinc chloride as a catalyst. J Biomater Sci Polym Ed 2002;13:95-108.

[255] Kasper FK, Tanahashi K, Fisher JP, Mikos AG. Synthesis of poly (propylene fumarate). Nat Protoc 2009;4:518-25.

[256] Ruhé PQ, Boerman OC, Russel FGM, Spauwen PHM, Mikos AG, Jansen JA. Controlled release of rhBMP-2 loaded poly(dl-lactic-co-glycolic acid)/calcium phosphate cement composites in vivo. J Control Release 2005;106:162-71.

[257] Yasko AW, Lane JM, Fellinger EJ, Rosen V, Wozney JM, Wang EA. The healing of segmental bone defects, induced by recombinant human bone morphogenetic protein (rhBMP-2). A radiographic, histological, and biomechanical study in rats. J Bone Joint Surg Am 1992;74:659-70.

[258] Drosse I, Volkmer E, Seitz S, Seitz H, Penzkofer R, Zahn K, et al. Validation of a femoral critical size defect model for orthotopic evaluation of bone healing: a biomechanical, veterinary and trauma surgical perspective. Tissue Eng Pt C-Meth 2008;14:79-88.

[259] Einhorn TA, Lane JM, Burstein AH, Kopman CR, Vigorita VJ. The healing of segmental bone defects induced by demineralized bone matrix. A radiographic and biomechanical study. The Journal of bone and joint surgery American volume 1984;66:274-9.

[260] Hedberg EL, Kroese-Deutman HC, Shih CK, Lemoine JJ, Liebschner MAK, Miller MJ, et al. Methods: A Comparative Analysis of Radiography, Microcomputed Tomography, and Histology for Bone Tissue Engineering. Tissue Eng 2005;11:1356-67.

[261] Feldkamp LA, Davis LC, Kress JW. Practical cone-beam algorithm. J Opt Soc Am 1984;1:612-9.

[262] Rai B, Oest ME, Dupont KM, Ho KH, Teoh SH, Guldberg RE. Combination of platelet-rich plasma with polycaprolactone-tricalcium phosphate scaffolds for segmental bone defect repair. J Biomed Mater Res Pt A 2007;81A:888-99.

[263] Kokubu T, Hak DJ, Hazelwood SJ, Reddi AH. Development of an atrophic nonunion model and comparison to a closed healing fracture in rat femur. J Orthop Res 2003;21:503-10.

[264] Hing KA, Best SM, Tanner KE, Bonfield W, Revell PA. Mediation of bone ingrowth in porous hydroxyapatite bone graft substitutes. J Biomed Mater Res A 2004;68A:187-200.

[265] Schantz JT, Hutmacher DW, Lam CXF, Brinkmann M, Wong KM, Lim TC, et al. Repair of calvarial defects with customised tissue-engineered bone grafts - II. Evaluation of cellular efficiency and efficacy in vivo. Tissue Eng 2003;9:S127-S39.

[266] Hedberg EL, Kroese-Deutman HC, Shih CK, Crowther RS, Carney DH, Mikos AG, et al. Effect of varied release kinetics of the osteogenic thrombin peptide TP508 from biodegradable, polymeric scaffolds on bone formation in vivo. J Biomed Mater Res 2005;72:343-53.

[267] Petrie Aronin CE, Sadik KW, Lay AL, Rion DB, Tholpady SS, Ogle RC, et al. Comparative effects of scaffold pore size, pore volume, and total void volume on cranial

bone healing patterns using microsphere-based scaffolds. Journal of Biomedical Materials Research Part A 2009;89A:632-41.

[268] Lee JW, Lan PX, Kim B, Lim G, Cho D. Fabrication and characteristic analysis of a poly (propylene fumarate) scaffold using micro-stereolithography technology. J Biomed Mater Res B 2008;87B:1-9.

[269] Melchels FPW, Feijen J, Grijpma DW. A poly (d, l-lactide) resin for the preparation of tissue engineering scaffolds by stereolithography. Biomaterials 2009;30:3801-9.

[270] Kim K, Dean D, Wallace J, Breithaupt R, Mikos AG, Fisher JP. The Influence of Stereolithographic Scaffold Architecture and Composition on Osteogenic Signal Expression with Rat Bone Marrow Stromal Cells. Biomaterials, in press 2011.

[271] Geffre CP, Margolis DS, Ruth JT, DeYoung DW, Tellis BC, Szivek JA. A novel biomimetic polymer scaffold design enhances bone ingrowth. J Biomed Mater Res A 2009;91A:795-805.

[272] Sarkar MR, Augat P, Shefelbine SJ, Schorlemmer S, Huber-Lang M, Claes L, et al. Bone formation in a long bone defect model using a platelet-rich plasma-loaded collagen scaffold. Biomaterials 2006;27:1817-23.

[273] Shields LBE, Raque GH, Glassman SD, Campbell M, Vitaz T, Harpring J, et al. Adverse effects associated with high-dose recombinant human bone morphogenetic protein-2 use in anterior cervical spine fusion. Spine 2006;31:542-7.

[274] Perri B, Cooper M, Lauryssen C, Anand N. Adverse swelling associated with use of rh-BMP-2 in anterior cervical discectomy and fusion: a case study. Spine J 2007;7:235-9.

[275] Heng BC, Cao T, Lee EH. Directing stem cell differentiation into the chondrogenic lineage in vitro. Stem Cells 2004;22:1152-67.

Appendix A: List of Manuscripts Co-Authored by the Doctoral Candidate During the Course of this Thesis

Spicer PP, Mikos AG. "Fibrin glue as a drug delivery system." *J Control Release.* **148**, 49-55 (2010).

Kretlow JD, Spicer PP, Jansen JA, Vacanti CA, Kasper FK, Mikos AG. "Uncultured Marrow Mononuclear Cells Delivered Within Fibrin Glue Hydrogels to Porous Scaffolds Enhance Bone Regeneration Within Critical-Sized Rat Cranial Defects." *Tissue Eng Pt A.* **16**, 3555-3568 (2010).

Chew SA, Kretlow JD, Spicer PP, Edwards AW, Baggett LS, Tabata Y, Kasper FK, Mikos AG. "Delivery of Plasmid DNA Encoding Bone Morphogenetic Protein-2 with a Biodegradable Branched Polycationic Polymer in a Critical-Size Rat Cranial Defect Model." *Tissue Eng Pt A*. **17**, 751-763 (2011).

Mountziaris PM, Spicer PP, Kasper FK, Mikos AG. "Harnessing and Modulating Inflammation in Strategies for Bone Regeneration." *Tissue Eng Pt B Rev.* **17**, 393-402 (2011).

Appel AA, Larson JC, Somo S, Zhong Z, Spicer PP, Kasper FK, Garson AB, Zisk AM, Mikos AG, Anastasio MA, Brey EM. "Imaging of Poly(α-hydroxy-ester) Scaffolds with X-ray Phase Contrast Microcomputed Tomography." *Tissue Eng Pt C Methods*. **18**, 859-865 (2012).

Spicer PP*, Kretlow JD*, Young S, Jansen JA, Kasper FK, Mikos AG. "Evaluation of Bone Regeneration using the Rat Critical Size Calvarial Defect." *Nat Prot.* **7**, 1918-1929 (2012).

Wang L, Yoon DM, Spicer PP, Henslee AM, Scott DW, Wong ME, Kasper FK, Mikos AG. "Characterization of Porous Polymethylmethacrylate Space Maintainers for Craniofacial Reconstruction." *J Biomed Mater Res B Appl Biomater.* (2012, *submitted*)

Kim K, Lam J, Lu S, Spicer PP, Lueckgen A, Tabata Y, Wong ME, Jansen JA, Mikos AG, Kasper FK. "Osteochondral Tissue Regeneration using a Bilayered Composite Hydrogel with Modulating Dual Growth Factor Release Kinetics in a Rabbit Model." *J Control Release.* (2012, *submitted*)

* Co-First Authors